CHAPTER ONE

INTRODUCTION

This chapter contains a brief introduction of carbon nanotubes (CNT) and their important features, including brief historical development, unique properties and potential applications. The main objectives and research's scope of this study were also highlighted

1.1 Background

CNT are form of carbon made by rolling up graphite sheets into narrow but long tubes with cylindrical patterns. These unique allotropes of carbon were elucidated from the discovery of ball structure C60. The tubes were discovered to exist in various forms, Single-Walled Carbon Nanotubes (SWCNT), Multi-Walled Carbon Nanotubes (MWCNT) and Double-Walled Carbon Nanotubes (DWCNT). Due to unique structural characteristics, discovery of CNT creates a remarkably large impact on nanoscience and nanotechnology (Baughman *et al.* 2002). Many interesting properties of CNT have been discovered. Possessions of both metallic and semiconducting properties with high tensile strength have been popular topics among scholars (Klabunde *et al.* 2001; Endo *et al.* 2004). At the same time, the synthesizing processes of CNT have been optimized vigorously via various studies and investigations to overcome the limitations of high-cost and low production-yield (Little 2003). However, the discovery of CNT have arisen continuous historical and current arguments. The discovery of CNT is generally recognized as credited to a Japanese researcher, Sumio Iijima (Iijima *et al.* 1991). At the same time, arguments have been arisen about 40 years ~~ago~~ before the discovery by Iijima, but the characterization

was limited by the resolution of electronic microscope (Iijima, 1991; Monthioux, 2006). The unique properties of CNT have attracted many attentions for the last two decades on its high potential applications.

Due to the covalent sp^2 bonds present in hexagonal lattice of carbon atoms (Kiang *et al.* 1995), CNT possesses high moduli ranging from 0.32-1.47 TPa and tensile strength between 10-52 GPa (Files *et al.* 2000). Besides, CNT possesses unique electrical properties, where the conduction properties vary with its diameter, length and chirality (Mashreghi *et al.* 2011). Beside, metallic nanotubes can also carry much higher current density than conventional conductive materials such as copper (Hong *et al.* 2007). Carbon nanotubes exhibit good thermal conductivity along the tube due to ballistic conduction (Mayuyama *et al.* 2011). The main contribution of high thermal conductivity is due to scattering of conduction particles, where the thermal resistivity would be negligible. Measurements show that a SWCNT exhibits thermal conductivity of 3500 $W.m^{-1}.K^{-1}$ along its axis (Pop *et al.* 2005). Although CNT exhibits outstanding properties, the high-costs productions and complications in synthesizing CNT have limited its practical applications. Conventional methods of synthesizing CNT often involved high production costs, low production yield, and complicated synthesis steps. As these problems arise, studies have been carried out to overcome these limitations.

The first synthesis method of CNT is arc discharge (Iijima *et al.* 1991). Arc discharge method reported a yield of 30 wt% and it produced both SW- and MWCNT with lengths of up to 50 μm (Collins 2000). The quality of the tubes is highly dependant on the types of gas chambers used during synthesis process (Kim *et al.* 2006). A few years later, Smalley and co-workers had developed a synthesis method via laser ablation (Scott *et al.* 2001). This

method reported a higher yield of 60 % (Kokai *et al.* 1999) as compared to the arc discharge. However, the production cost is higher as compared to the arc-discharge and Chemical Vapor Deposition (CVD). The current most favorable synthesis method is CVD process, where CNT with well-controlled alignment and quality are produced with cheap production costs and high production yield (Balogh *et al.* 2008; Naha *et al.* 200). Nonetheless, a chemical method which doesn't ~~not~~ involved usage of machinery is still yet to be discovered and optimized.

The difficulties in synthesizing CNT have steered researchers to look for alternative substituent materials which possessing similar unique properties. Amorphous carbon nanotubes (a-CNT) have seen as a high potential substituent for fully crystalline CNT due to their unique defective and porous structures. This amorphous structured carbon allotrope is relatively easier to be synthesized in a large quantity (Banerjee *et al.* 2009; Jha *et al.* 2011). Apart from that, current researchers have discovered and justified the impressive field emission properties of a-CNT, which are compatible to the fully crystalline CNT (Ahmed *et al.* 2007).

In spite of unique properties of a-CNT, the self-agglomeration and hydrophobic properties of a-CNT have limited its usage in various applications (Xia *et al.* 2007). Addition of oxygen-containing functional group; -COOH group for instance, may increase CNT's dispersion in selected solvent, reduce overall length of CNT bodies, and creates open ends tubes which are favorable for attachment of particles and dispersion in solvent (Lim *et al.* 2004). CNT samples sonicated with nitric acids or citric acids create –COOH groups which will improve the hydrophilic properties of CNT body (Naseh *et al.* 2009). Besides dispersibility, addition of active functional groups upon CNT's body also acts as

starting points to further hybridize with foreign nanoparticles (Kasaliwal *et al.* 2010).

Attachments of foreign nanoparticles on CNT bodies introduce significant modifications on its properties. A hybrid of gold nanoparticles and CNT will be a compatible hetero-structure with many biological systems. The attachment of gold particles on pristine CNT shows remarkable improvements on electrical and optical properties, which enables direct applications in biosensors (Lim *et al.* 2004). As a-CNT has inferior properties compared to the fully crystalline CNT, attachment of foreign particles are important to improve its performance in various applications. Since a-CNT possesses porous and defective structures, it has added advantages in foreign particles attachments as compared to the fully crystalline CNT (Azamian *et al.* 2002).

In this work, a-CNT were synthesized via a simple chemical route. Purification, oxidation and solution treatments were performed to obtain different samples. As-synthesized, functionalized, and gold particles decorated a-CNT were synthesized respectively. The morphological, microstructural, elemental and thermal studies of the a-CNT were conducted. Both optical and electrical properties were also investigated by ultraviolet-visible (UV-Vis), Raman spectroscopy, Nyquist plots and transference number calculation.

1.2 Importance of Study

As CNT possessed numerous promising applications, synthesis steps of CNT often involved high production costs, complicated synthesis steps, but relatively low production yield. Therefore, low synthesis costs and relatively high production yield of a-CNT open

possibilities to be good substituent (Banerjee *et al.* 2009; Jha *et al.* 2011). At the same time, porous and defective structure of a-CNT provides high potential in gas storage applications (Orinakova *et al.* 2011). It was reported that a-CNT have 1.29 wt% of hydrogen up-take capacity at room temperature under pressure of 10 MPa (Ci *et al.* 2003). Besides gas storage applications, previous study reported outstanding Field Emission (FE) properties of a-CNT (Jha *et al.* 2011). The as prepared a-CNT sample showed good FE properties and ~~the FE properties were~~ significantly improved for the stearic acid functionalized a- CNT.

Besides pristine a-CNT, foreign particles decorated a-CNT exhibits outstanding properties which promise outstanding performances in various applications. For example, gold particles decorated a-CNT provides a wide range of applications in biomedical field including determination of cytochrome (Wu *et al.* 2005), glucose biosensing application (Li *et al.* 2009), antigen immunosensor (Gao *et al.* 2011), and choline sensors (Qin *et al.* 2010). In general, attachment of gold particles on CNT body would remarkably improve its electrical conductivity (Deepak *et al.* 2010). However, there are still limited exposures on the electrical properties of gold particles decorated a-CNT.

In this study, a-CNT was synthesized with an existing bottom-up method at low temperature and ambient air condition (Tan *et al.* 2012). At the same time, the attachment of gold particles on a-CNT was carried out by an existing solution treatment method (Lim *et al.* 2004). The novelty of this study was mainly divided into a few parts. By using zeta potential as an approach, the effectiveness as oxidation agents for various types of acids to functionalize a-CNT was investigated. As there are still limited researches on the electrical properties of a-CNT, the electrical conductivity and conduction properties of as-synthesized, functionalized, gold particles decorated a-CNT were studied. To study the

effect of re-agglomeration property on the overall electrical conductivity of a-CNT/Epoxy composites, electrical resistivities of composites cured in two different temperatures were compared.

1.3 Research Objectives

The objectives of this study are as follows:

- To synthesize a-CNT via simple chemical route.
- To determine the most effective functionalizing agent for a-CNT.
- To hybridized a-CNT with Au at different concentrations, and characterize the electrical, optical, and thermal properties of a-CNT.

1.4 Scope of Research Work

In this work, a-CNT were synthesized using a relatively simple chemical method that required only low temperature with ambient pressure and air flow conditions for a short processing period. The obtained and purified a-CNT from this method was named as "as-synthesized a-CNT". A simple study was carried out to compare the relative effectiveness of various acids in functionalizing a-CNT. Zeta potential was used as an approach to access to the samples' surface charges. FTIR shown the presence of carboxyl groups on samples functionalized with nitric acid, citric acid, hydrochloric acid and sulfuric acid. As nitric acid functionalized a-CNT exhibited highest zeta potential value, it was preliminarily determined to be the most effective oxidation agent for a-CNT. Therefore, nitric acid functionalized a-CNT was known as "functionalized a-CNT". After that, functionalizd a-CNT were solution treated with gold chloride solution at four different

concentrations. The six samples including as-synthesized a-CNT, functionalized a-CNT, and a-CNT solution treated at four different concentrations were characterized to investigate their respective properties.

The morphological, microstructural, elemental and thermal studies were conducted to all samples. Instruments such as transmission electron microscope (TEM), higher resolution transmission electron microscope (HRTEM), field emission scanning electron microscopy (FE-SEM), X-ray diffraction (XRD) spectrometer and energy-dispersive x-ray (EDX) spectrometer and thermogravimetric analyzer (TGA) were utilized. The optical tests were used to further characterize the samples. Fourier transform infrared (FTIR) to identify the organic bonds present in the samples, ultraviolet visible spectrometer (UV-Vis) to investigate the optical absorption and energy gap, and Raman spectrum to study the structural defects of all samples. The electrical resistivities of a-CNT/Epoxy composites cured in two different temperatures were compared to study the agglomeration properties of a-CNT and its effects on overall electrical conductivity. Electrical conduction properties of all samples are also investigated by measuring their respective electrical transference numbers. The obtained morphological, microstructural, elemental and thermal studies were then related to each other and correlated with both the optical and electrical conduction results. The pathway of the research work is summarized in Figure 1.1.

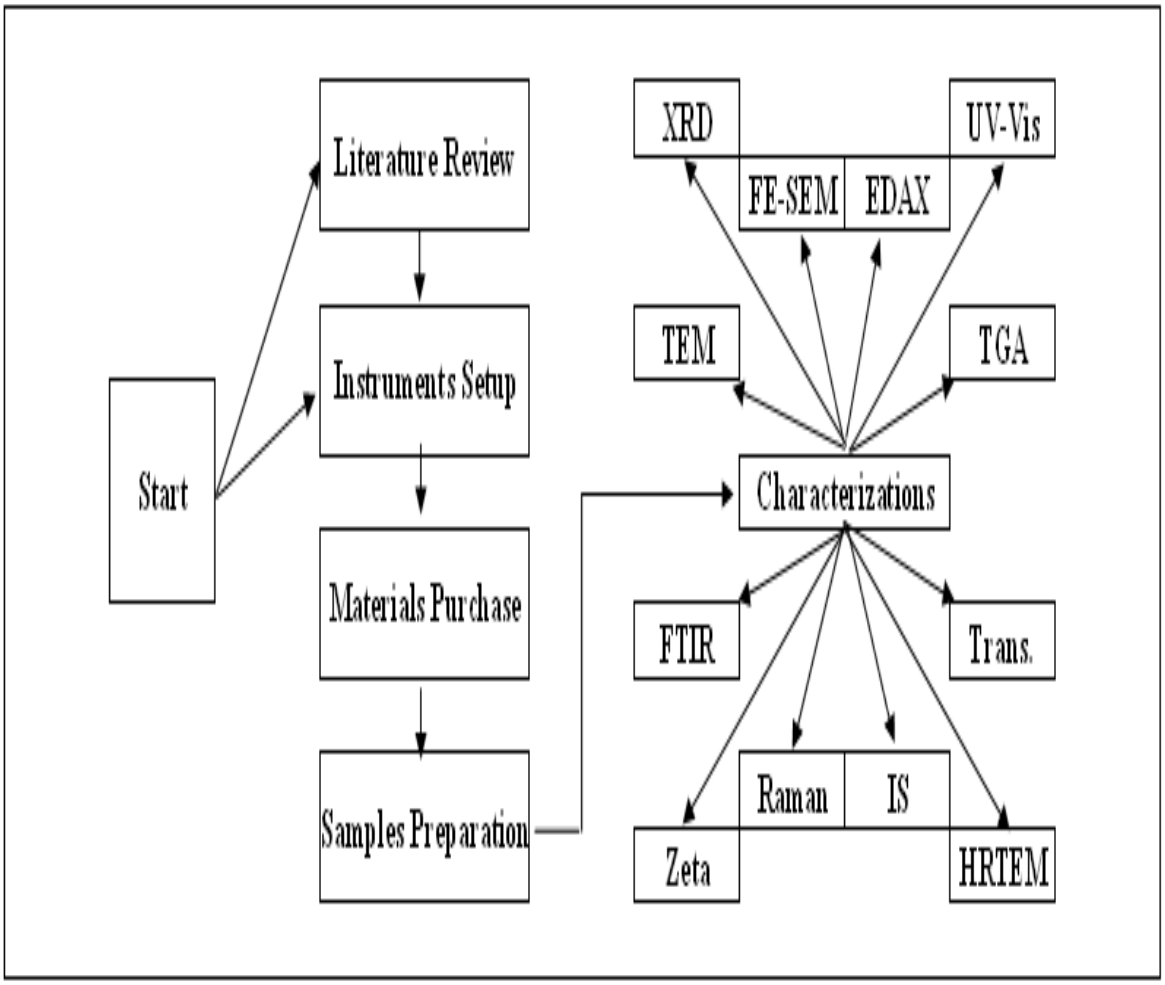

Figure 1.1: The pathway of the research work

CHAPTER TWO

LITERATURE REVIEW

This chapter introduced the types, structures, and properties of CNT by explained specifically in detail, from historical developments to current trends. Common synthesis techniques for both crystalline and amorphous nanotubes are also exposed and compared. Various properties of a-CNT which could be linked to their potential applications are included.

2.1 Carbon Nanotubes

The discovery of the soccer ball structure C60 has elucidated various forms of unusual carbon structures. It represents a starting point for discoveries of more forms of elemental carbons. A particularly high potential form of carbon structure is “nanotubes”. Nanotube structures are made up of graphite-like carbon composed by fusions of C6 and C5 rings to allow curvature into cylinders. These tubes can be single-walled (SWCNT) or multi-walled nanotubes (MWCNT), and can be closed at one end or both end (Klabunde *et al.* 2001). The schematic diagrams of types of carbon nanotubes are shown in Figure 2.1. Due to unparallel strength, high electrical and thermal conductivities (Bernhole *et al.* 2002) and specifically distinct properties possessed by SWCNT and MWCNT respectively, they introduced great impacts in nanoscience and nanotechnology (Baughman *et al.* 2002).

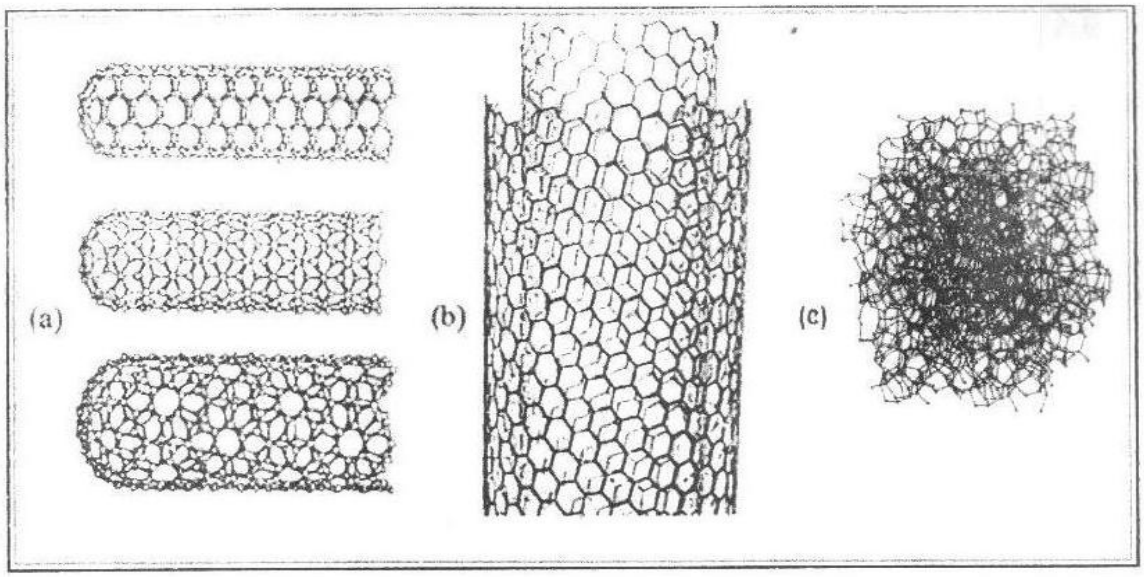

Figure 2.1: Types of Carbon Nanotubes: (a) SWCNT; (b) MWCNT; (c) a-CNT (Harns *et al.* 2009)

During the past ten years, many outstanding properties have been discovered on CNT (Klabunde *et al.* 2001; Endo *et al.* 2004). An example is that CNT could be semiconducting or conducting depending on the diameter of the nanotube. Besides, nanotubes can also be used as carbon fibers for reinforcing polymers or concrete (Klabunde *et al.* 2001). The outstanding performance of CNT in various properties gives potential applications in many aspects. The electronic and electrochemical applications of nanotubes, fabrication of lithium-ion secondary batteries, lead-acid batteries, electric double-layer capacitors, fuel cells, multifunctional fillers in polymer composites, and as templates for the creation of other nanostructures have been widely investigated and discussed (Endo *et al.* 2004).

Due to high potential of CNT in various applications, various synthesis methods have been developed to obtain a low-cost, high yield method. The first arc-discharge synthesis method was discovered by Iijima and coworkers (1991). The electrical energy in the process, as well as the energy associated with dangling bonds in a graphite sheet, seals and

rolled-up sheets as flawless nanotubes. They can be synthesized as SWCNT or concentrically layered MWCNT (Forro *et al.* 2001). The most conventional and commercial synthesis method is Chemical Vapor Deposition (CVD) method, where the production of carbon nanotubes at the rate of 300kg/day was reported (Little 2003). Various studies are still being carried out to optimize the synthesis efficiency of CNT.

2.1.1. General Properties of CNT

Due to the covalent sp^2 bonds present in hexagonal lattice of carbon atoms (Kiang *et al.* 1995), CNT possessed outstanding elastic modulus and tensile strength. The first mechanical properties measurements were made on MWCNT produced by the arc discharge process. By measuring the amplitude of intrinsic thermal vibrations observed in the TEM, the moduli of MWCNT was calculated to be 0.41-4.51TPa (Treacy *et al.* 1996). Three years later, Poncheral induced electromechanical resonant vibrations which give the resonant value between 0.7 and 1.3 TPa (Poncharal *et al.* 1999). The Young's modulus of MWCNT can be summarized ranging from 0.2-0.96 TPa (Yu *et al.* 2000) where tensile strength of MWCNT can be summarized ranging from 11-150 GPa (Demczyk *et al.* 2002). Measurements on SWCNT took longer due to the difficulties in handling them. The first measurements were carried out by Salvetat *et al.* using their AFM method (Salvetat *et al.* 1999). The experimental values of SWCNT's Young's modulus ranging from 0.32-1.47 TPa and tensile strength between 10-52 GPa (Files *et al.* 2000). The range of values is due to variations of mechanical properties with diameter and length of the tubes. Standard SWCNT possessed elastic limit of up to 24GPa. After plastic deformation, SWCNT would transform into a super hard phase nanotubes which would exhibits much higher modulus of 460 to 550 GPa. The deformation of CNT would favor the mechanical properties as it

would exponentially increases its modulus (Popov *et al.* 2002).

Besides mechanical properties, the interests in electrical properties of CNT have been sparked among researchers due to its highly tunable electrical properties. The unique electrical properties of CNT are mainly due to the symmetrical electronic structure of graphene. Chirality vector (n,m) strongly affects the overall properties of CNT (Mashreghi *et al.* 2011). Variation of chirality vectors can tune electrical conduction nature of CNT, to either metallic, semiconducting, or moderate semiconducting properties (Lu *et al.* 2005). Besides chirality, curvature orientations in CNT can significantly influence electrical properties, especially for CNT with relatively small diameter (Li *et al.* 2007). Therefore, a SWCNT that should be semiconducting in accordance to its chirality could be experimentally calculated as metallic due to curvature effects (Lu *et al.* 2005). Other than highly tunable electrical properties, the excellent electrical conductivity of metallic nanotubes is contributed by high current density. Metallic nanotubes can also carry much higher current density than conventional conductive materials such as copper (Hong *et al.* 2007). Due to their relatively small cross-sectional area (nano-scale), charge carrying electrons would only propagate along the tube's axis via hopping and tunneling mechanisms. Therefore, CNT conducts electricity in single direction, which better known as 1D conductor. The maximum electrical conductance of a SWCNT is limited as the conductance was based on single ballistic quantum channel (Charlier *et al.* 2007). In-spite of outstanding electrical properties, the intrinsic superconductivity in CNT still remains a subject of debate. Researches have been carried out to prove the high potential superconductivity of CNT in theory and computational approaches (Tang *et al.* 2001). However, the experimental proves for superconduction phenomenon of CNT is still yet to be developed (Bockrath 2006).

As mechanical and electrical properties of CNT are well-established and have immediate applications, the practical use of optical properties is yet unclear. However, optical tests on CNT lead to various structural and electrical properties studies. Ho *et al.* (2004) have related the electronic properties of CNT with optical properties, where the optical absorption spectra respond directly to the features of magnetoelectronic structures. This further develops a method in determining the double-walled geometric structures of CNT with optical absorption approach. Besides pure CNT, CNT doped with different kinds of doping such as alkali metal intercalations, covalent or non-covalent sidewall functionalization etc., the characteristic absorption peaks of the CNT can be easily diminished in UV-Visible spectra. This could be utilized to achieve superior optical limiting devices and could be useful for other applications like optical switch (Zhao *et al.* 2006). As optical absorption of CNT is due to relatively sharp transitions (Iakoubovskii *et al.* 2006), it is often used to identify nanotube types and qualities (Itkis *et al.* 2005). Due to highly tunable properties of CNT, it possessed high potential in various optical applications. Previous research reported applications of CNT in photodetectors and LED applications, where the narrow selectivity in wavelength emission and high sensitivity in light detection is possible to be achieved due to fine tuning of CNT structure (Freitag *et al.* 2003).

CNT exhibit good thermal conductivity along the tube due to ballistic conduction (Mayuyama *et al.* 2011). Previous study concluded that thermal conductivity in CNT is mainly due to phonons (Hone *et al.* 2000), where the phonon density that dictates the overall thermal conductivity of CNT can be calculated through band structure of isolated tubes (Sanchez *et al.* 2000).A SWCNT at room temperature exhibits thermal conductivity of 3500 $W.m^{-1}.K^{-1}$ along its axis (Pop *et al.* 2005). However,, SWCNT exhibits inferior thermal conductivity across its axis which is 1.52 $W.m^{-1}K^{-1}$ (Sinha *et al.* 2005). Besides

excellent thermal conductivity, CNT exhibits outstanding thermal stability. CNT can remain thermally stable above 2500 ℃ in vacuum and 700 ℃ in ambiet air condition (Thostenson *et al.* 2005).

As CNT exhibits impressive thermal and electrical conductivity, defective structures in CNT would affect the conduction properties of CNT. Crystallographic defects in CNT would affect the tube's electrical properties. Defects in SWCNT interrupt movements of electron charge carrier and gives semiconducting regions (Makarova *et al.* 2006). Besides electrical conductivity, crystallographic defects also affect the tube's thermal properties. Defects would lead to phonon scattering, which would increases the relaxation rate of the phonons. Upon increment of relaxation rate, the mean free path of phonons would be reduced and hence affects the thermal conductivity of nanotube structures. Primarily, defects would cause scattering of high-frequency optical phonons which favors both thermal and electrical conductions. However, large-scale defects in tube's structures would cause phonon scattering over a wide range of frequencies, causing tremendous reduction in thermal conductivity (Mingo *et al.* 2008).

2.1.2. Historical Developments of CNT

As the first CNT was discovered by a Japanese researcher, Sumio Iijima (Iijima, 1991), large interests have arisen among researchers on CNT due to its unique and outstanding properties. However, the first idea of CNT is actually developed from hollow graphitic carbon fibers. In year 1952, two researchers, Radushkevich and Lukyanovich first discovered a hollow graphitic carbon fibers which shows 50 nm of diameter, which they have published their findings in the Soviet Journal of Physical Chemistry (Monthioux,

2006). Arguments have been arisen on this issue where the credit in discovery of CNT should be given to Radushkevich and Lukyanovich. Researchers and scholars questioned that the 50 nm graphitic carbon fibers were actually the first carbon nanotubes. However, due to the constraints of electronic microscopes during that time, the tube structures were difficult to be verified. Eight years later, in year 1960, Bollman and Spreadborough discussed friction properties of carbon and related them to rolling sheets' mechanisms of graphene in Journal "Nature", where in their article, electronic microscope images clearly shown MWCNT (Monthioux *et al.* 1960). Arguments have been arisen that the first discovery of MWCNT should be credited to Radushkevich and Lukyanovich in 1952, which the graphitic carbon fibers that are 50 nm in diameter would possibly due to Multi-wall structures.

In year 1976, Oberlin, Endo and Koyama reported Chemical Vapor Deposition (CVD) synthesis of nano-sized carbon fibers (Oberlin *et al.* 1976), which is still the most preferable method of CNT synthesis until today. However, the tubular structures are still unseen. In year 1985, another allotrope of carbon, Fullerenes, was discovered (Kroto *et al.* 1985). The discovery of Fullerenes is seen to be a direct consequence of the interest in CNT. In year 1991, nanotubes were discovered in the soot of arc discharge at NEC, by Japanese researcher Sumio Iijima (Iijima 1991). On the same year itself, Al Harrington and Tom Maganas of Maganas Industries had discovered nanotubes in CVD, which initiates the first step in utilizing this low cost and high production yield method in synthesizing CNT (Maganas *et al.* 1992).

After the first tubular structure of CNT was observed by Iijima in 1991, researchers have been actively studied the unique properties and structures of CNT. From year 1992 to 1993, groups led by Donald S. Bethune at IBM and Sumio Iijima at NEC discovered SWCNT by producing them with transition-metal-based catalysts (Bethune *et al.* 1993). This discovery came after the first prediction of SWCNT's electronic properties by groups at Naval Research Laboratory, USA, Massachusetts Institute of Technology, and NEC Corporation (Saito *et al.* 1992). The structure of SWCNT was further exposed when Nature published a photo of individual 4 cm long single-wall nanotubes, which further justified the high aspect ratios of CNT (Zheng *et al.* 2004). Numerous unique properties of CNT have been discovered after the discovery of CNT in year 1991 by Iijima.

In year 1995, Swiss researchers first demonstrated the electron emission properties of CNT (Walt *et al.* 1995), which made an important contribution to the latter researches on the electron emission properties of CNT. The first CNT Field-Effect Transistor was demonstrated in year 1998 by research groups at Delft University and IBM (Martel *et al.* 1998). After years of research and development, IBM announced stable fabrication technology of CNT transistors in year 2003 (NEC 2003). Besides Field-Effect properties, various discoveries on the unique properties of CNT have been revealed through the years. In year 2000, Tombler and coworkers demonstrated that bending CNT would alternate their electrical resistance (Tombler *et al.* 2000). The following year, first report on semiconducting and metallic properties of nanotubes has been published (Collins *et al.* 2001), which prepared a good foundation for latter researches on semiconducting and metallic properties of nanotubes. At the same time, in year 2002, MWCNT demonstrated to be fastest known oscillators (> 50 GHz) as published in physical review letters (Minkel 2002). These important properties of CNT found in previous years have made a good

foundation for researchers to perform further, in-depth studies on CNT.

2.2 Synthesis for Crystalline CNT

As CNT possess a wide range of exceptional properties, explosion of interests especially on CNT's synthesis methods has been sparked. As mentioned in previous section, electric arc discharge method is the first method in synthesizing CNT, followed by laser ablation, only then the currently most efficient and effective method, Chemical Vapor Deposition (CVD) method, was developed. Minimizing costs and production time, maximizing production yield is the main priority in process optimizations. It was recognized that CNT was formed based on a general reaction mechanism. The growth of crystalline CNT during synthesis is believed to commence from the recombination of carbon atoms split by heat from their precursor. Although various methods such as pyrolysis, high temperature hydrothermal and low-, high-temperature solvothermal have been developed, the conventional methods in producing CNT, CVD, laser ablation, and arc discharge method are still preferred.

2.2.1. Arc Discharge

Nanotubes were observed in the carbon soot of graphite electrodes during an arc discharge by using a current of 100 A (Iijima *et al.* 1991). The method was initially designed for synthesis of fullerenes. A schematic diagram of the arc-discharge apparatus for producing CNT, a vacuum chamber, is shown in Figure 2.2 (Anyo *et al.* 2006). Two graphite electrodes are installed vertically, and the distance between the two rod tips is maintained in the range of 1-2mm. A current is run through an anode, or a positively charge piece of carbon. Then, these current jumps through a certain type of plasma material to a

cathode, or a negatively charged piece of carbon, where there is an evaporation and deposition of carbon particles in through the plasma (Ajayan *et al.* 1997). After the evacuation of chamber by a diffusion pump, rarefied ambient gas is introduced. When a dc arc discharge is applied between the two graphite rods, the anode is consumed, and CNT are formed in the chamber soot (Saito *et al.* 1992). The production yield for arc-discharge method is up to 30 wt%, which produces both SW- and MWCNT with lengths of up to 50 μm (Collins 2000).

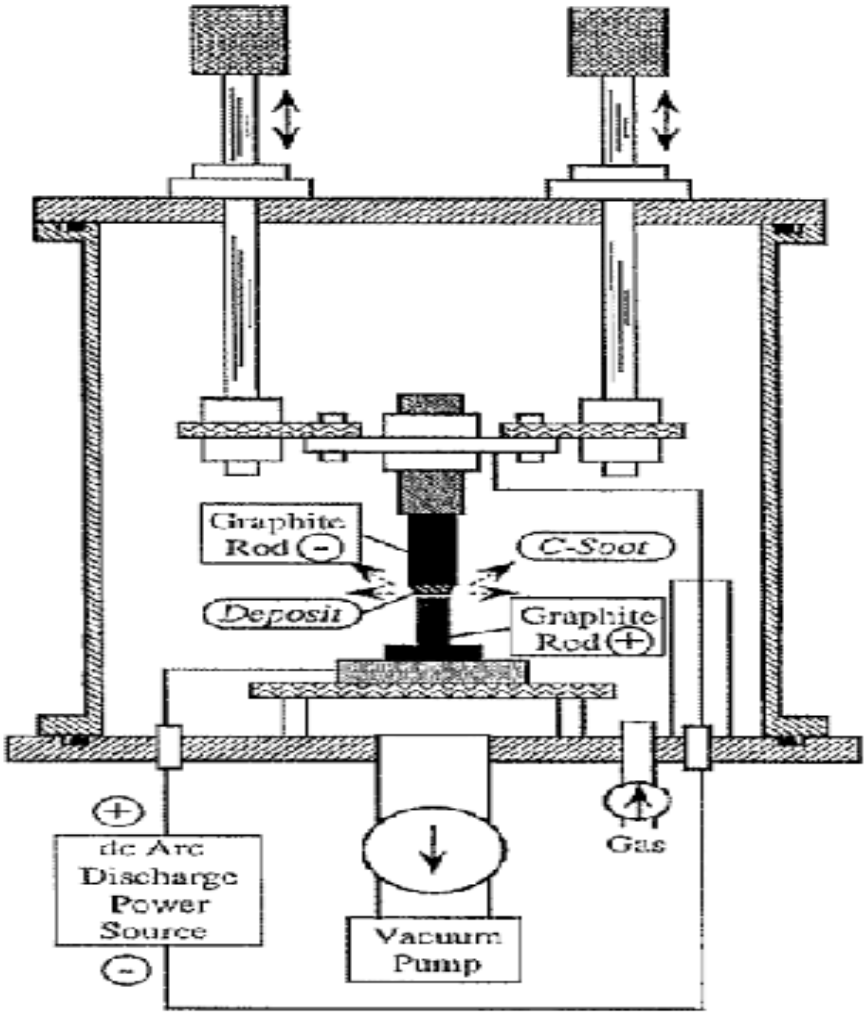

Figure 2.2: Schematic diagram of an arc discharge system (Anyo *et al.* 2006)

At the same time, advancements had been developed to replace the vacuum chamber with hydrogen gas chamber. By carefully controlling the synthesis process, high quality DWCNT could be obtained with production yield up to 55% (Li *et al.* 2005). As hydrogen gas required careful supervision and high cost, Helium chamber provides an alternative as the medium for arc discharge synthesis method. Previous study reported formation of SWCNT upon usage of constant power supply of 120 V dc and 78.50 A in helium gas chamber. Analysis of the relative purity of SWCNT samples suggested that highest SWCNT relative concentration could be obtained at background pressure of about 200 – 300 Torr, where the measured anode ablation rate increased linearly with background pressure (Warldoff *et al*. 2004). Besides, another discovery had been made where arc discharge synthesis method could be carried out in ambient dry air chamber, but only MWCNT was observed from this method (Kim *et al.* 2006).

2.2.2. Laser Ablation

The laser ablation process was developed by Dr. Richard Smalley and co-workers in Rice University. In the Rice design, nanotubes were synthesized in argon flowing in a 25-mm tube inside a 56-mm tube, all heated to 1473 K in a tube furnace. A composite ablation target was located in front of the 25-mm inner tube, and consisted of 1 at. % each of Ni and Co uniformly mixed with graphite. This configuration resulted in the best purity and yield of SWCNT. It was suspected that the effect of the 25-mm inner tube was somehow to confine spatially the laser-ablation plume and maintained conditions more conducive to nanotube formation and growth. A single flow tube without any inner tube had been used in some configurations (Scott *et al.* 2001). The laser ablation method is first used to blast various metals to produce metal molecules. The MWCNT was produced by

replacing metals with graphite in laser ablation blasting. After that, the team used graphite and cobalt/nickel mixture of metal catalyst particles composites to synthesis SWCNT (Guo *et al.* 1995). Schematic diagram of laser ablation method is shown in Figure 2.3 (Scott *et al.* 2001).

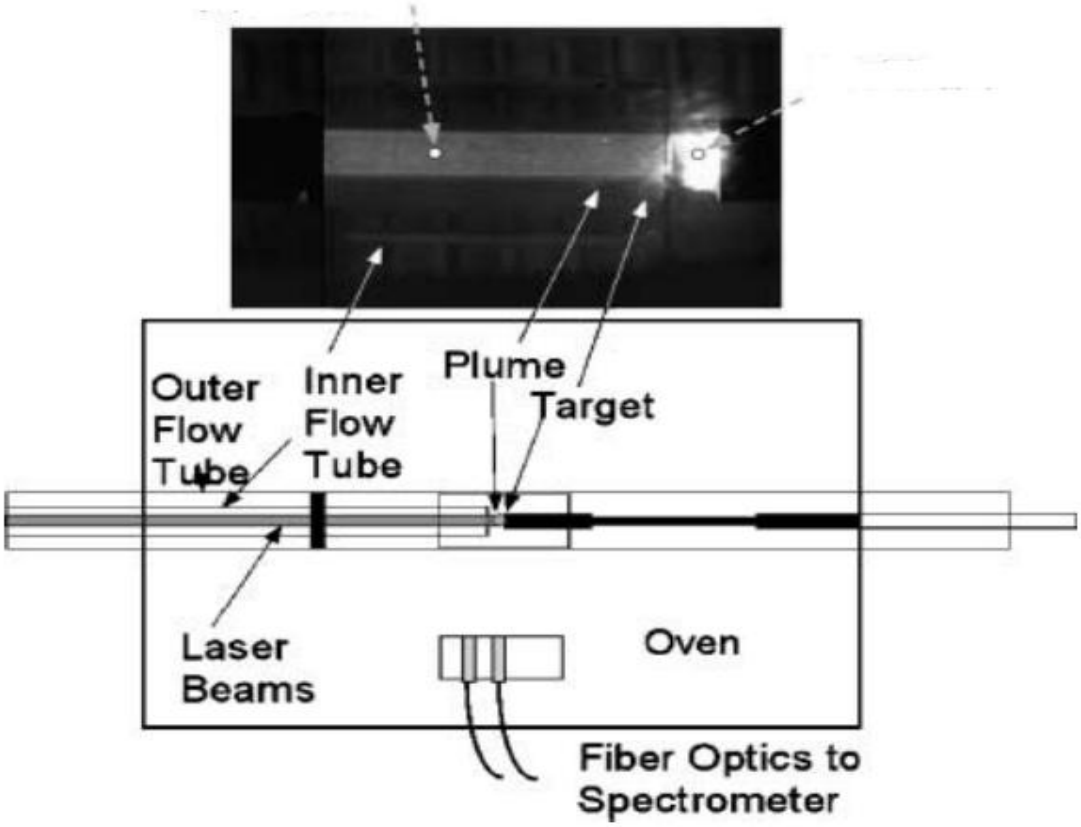

Figure 2.3: Schematic diagram of a laser ablation method (Scott *et al.* 2001)

Besides the mentioned methods, various studies have been carried out by investigating the variation of synthesis parameters on the CNT quality. Zhang *et al.* (1998) investigated the production of SWCNT in a nitrogen atmosphere, comparing the product with that produced in argon in similar conditions. Their findings indicated that the nanotubes were created in the high-temperature zone close to the target in a region where nitrogen was

essentially excluded by the ablation products. Later, after mixing of the plume with background nitrogen, amorphous carbons were formed that had nitrogen inclusions. Kokai *et al.* (1999) reported a yield greater than 60 percent for an oven temperature of 1473 K. Using high-speed video and emission spectroscopy, they found that carbonaceous materials with SWCNT were visible about 3 ms after the beginning of the laser pulse. Although this method has higher yield as compared to Arc-discharge method, however, laser ablation is still the most expensive method as compared to arc-discharge and Chemical Vapor Deposition (CVD) methods (Collins 2000).

2.2.3. Chemical Vapor Deposition

Chemical Vapor Deposition (CVD) is a simple and relatively cheap technique; it might be the most promising method for large-scale production of carbon nanotubes under reasonably mild conditions. Additionally, with the CVD method, the growth of CNT can be successfully controlled by adjusting the reaction conditions and preparing proper catalysts (Balogh *et al.* 2008). In CVD synthesis, a substrate is prepared with a layer of metal catalyst (Ni/Co/Fe) (Ishigami *et al.* 2008), which plays a major role in catalyzing the synthesis process. Depending on the growth procedure, the CVD method includes the seeded catalyst method, which uses the catalysts seeded on a substrate within a reactor, and floating catalysts method, which uses the catalysts floating in the reactor space (Ci *et al.* 2001). To initiate the growth of nanotubes, the substrate is heated to 700 ℃. After that, a process gas ($NH_4/N_2/H_2$) and a carbon-containing gas (acetylene/ethylene/ethanol/methane) are mixed and introduced into the reacting chamber. Nanotubes grow on the metal catalyst substrate. The mechanisms in formation of CNT can be explained in two simple steps. The carbon-containing gas is first dissociated by high temperature and catalyst particles. After

that, individual carbon atoms are diffused to the edges of the catalyst substrates and form nanotubes (Naha *et al.* 2008). This process is known as thermal catalytic decomposition where it involves decomposition of hydrocarbon with presences of elevated temperature and catalysts. The remaining catalyst particles would either found at the tips of CNT or at the CNT's base (Banerjee *et al.* 2008).

There have been studies in alignment of CNT in CVD synthesis process. The direction of CNT growth is strongly influenced by electrical field applied. CNT's growth would follow the direction of plasma presence, which could be applied via strong electrical field. Therefore, by carefully adjusting and monitoring the application of strong electric field, it is possible to synthesize vertically aligned CNT (Ren *et al.* 1998). The schematic diagram of CVD process is shown in Figure 2.4 (Kumar *et al.* 2010).

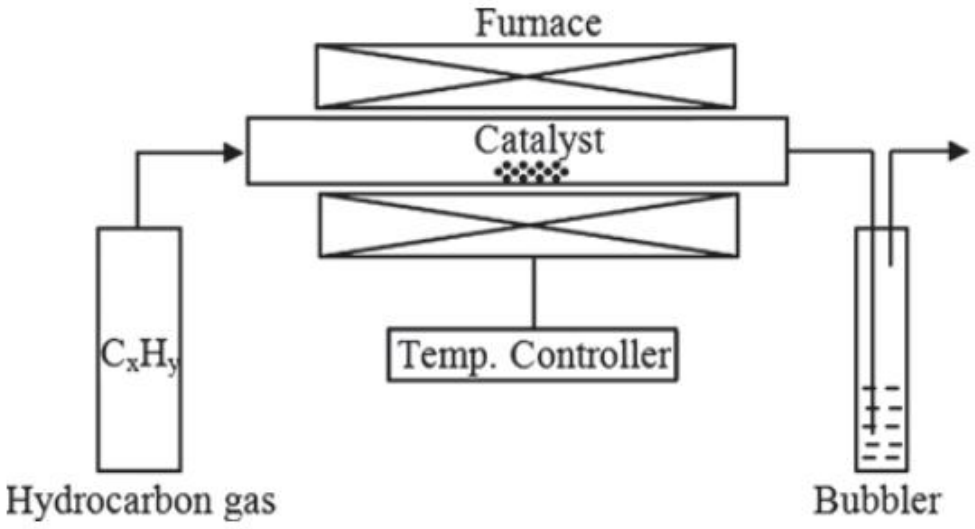

Figure 2.4: Schematic Diagram of CVD method (Kumar *et al.* 2010)

Besides the conventional methods, CVD injection method reports successful formation of SWCNT. One of the advantages of CVD injection method is allowing excellent control of the catalyst to carbon ratio, which the nanotube's diameter, length, and alignment can be controlled by varying the reaction parameter (Singh *et al.* 2002). Apart from the controllable parameters, sizes of catalytic nanoparticles use in CVD would have certain degree of influence on the diameter of the CNT. Previous study reported that iron nanoparticles with average diameters of 3, 9, and 13 nm were used to grow CNT with average diameters of 3, 7, and 12 nm, respectively, and the successful formation of MWCNT proves the significant impact of catalytic nanoparticles use on the CNT's diameter (Chin *et al.* 2002).

2.2.4. Hydrothermal Synthesis

It has been reported that high-temperature hydrothermal process is an alternative route for the synthesis of CNT. Synthesis of CNT was carried out using polyethylene (PE), ethylene glycol (EG) and other sources with and without catalysts Fe/Co/Ni under hydrothermal conditions at 700–800 ℃ and 60–100 MPa (Gogotsi *et al.* 2000; Calderon-Moreno *et al.* 2001). As this temperature range is still similar to CVD method, various studies have been carried out to obtain a method which required low synthesis temperature. Recently, a relatively low synthesis temperature for synthesis of MWCNT is 175 ℃, from decomposition of CCl_4 using iron-encapsulated polypropyleneimine dendrimers as a catalyst in supercritical carbon dioxide medium was reported (Jason *et al.* 2004). The synthesis temperature was then reduced to 160 ℃ after various studies. Synthesis of MWCNT by the decomposition of polyethylene glycol in a basic aqueous solution with high concentration of NaOH under hydrothermal conditions at a temperature

as low as 160 ℃ without the addition of catalyst Fe/Co/Ni was carried out. In a typical synthesis, 80 mL ethyl alcohol, 10 mL distilled water, 7 g NaOH and 2 g PEG were stirred for 30 min, and then sealed in a Parr reactor and then kept at 160 ℃ for 20 h in a furnace, and then cooled down to room temperature. The products were washed with alcohol and distilled water for several times, and then dried in a vacuum oven at 60 ℃ for 10 h. The obtained product was MWCNT with diameter of 18 nm (Wang *et al.* 2004). However, this method is yet to be practical in large scale production as it took much longer time as compared to CVD method. Another method was reported which use 160 ℃ as synthesis temperature, but in different reacting condition. MWCNT was prepared by a facile hydrothermal method, which was hydrothermally fabricated by using dichloromethane, cobalt chloride and metallic lithium as starting materials in 5 mol/lit NaOH aqueous solution. However, the obtained diameter of MWCNT was relatively larger with values ranging from 40-80nm as compared to the previous method (Manafi *et al.* 2008). Combining and comparing both methods, the final product of hydrothermal synthesis can varies with synthesis condition with the same temperature condition. As this hydrothermal is not established compared to CVD method, CVD method is still preferred in large scale production.

2.3 Synthesis methods for Amorphous CNT

A-CNT has attracted much attention due to their unique properties and simple production steps. It possesses high potential usage in different applications including field emitter, gaseous adsorbent, nanoelectronics and optical applications. As compared to crystalline CNT, a-CNT has added advantages due to their porous and defective walls. Developments in synthesizing methods for a-CNT have been popular among researchers

due to its high potential in mass production. Therefore, this section will discuss the synthesis techniques for a-CNT which have also been utilized for the production of crystalline CNT.

2.3.1. Chemical Vapor Deposition

As Chemical Vapor Deposition (CVD) is currently the most commercial method in synthesizing CNT, CVD method is also applicable in synthesizing a-CNT. In previous study, $Ni(OH)_2$/Al colloid was used as catalyst and calcined in air to form aluminum oxides. Methane (60 ml/min) was used as the carbon source and hydrogen (420 ml/min) as the carrier gas in forming CNT. The CVD was carried out at 480 ℃ for 30 min, after which the system was cooled to room temperature under a nitrogen atmosphere and a black powder product was obtained. Entangled a-CNT was formed with diameters ranging from 10 to 25 nm (Zhao *et al.* 2006). On the other hand, reducing the rate of hydrogen flow to 100ml/min and increasing the synthesis temperature to 1100-1200 ℃ creates nanotubes with larger range of diameter, 10 – 60 nm with amorphous structures (Ci *et al.* 2001).

Electron Cyclotron Resonance Chemical Vapor Deposition (ECR-CVD) is a modified method of conventional CVD to synthesize a-CNT. This method applied plasma during the synthesis process to enhance alignment of CNT. Previous research reported formation of a-CNT with even alignment and relatively large diameter of 240 nm with Argon gas flows and high plasma density at a temperature of 100 ℃, which is relatively low compared to above-mentioned conditions (Tsai *et al.* 2000).

Another modified method of CVD was introduced to synthesize a-CNT. Vapor Deposition Polymerization (VDP) has similar features with CVD as the substrates react in gaseous states. Acid-attapulgite in 2.0g was mixed with 3 ml of furfuryl alcohol and sealed in the high-pressure autoclave and heated at temperature of 180 ℃ for 6 h. Thereafter, the furfuryl alcohol–attapulgite mixture was carbonized in a pipe furnace under N_2 atmosphere at 600 ℃ for 2 h, and after that heated to 800 ℃ and held for 2 h to get the carbon–attapulgite composite. The process formed uniform diameter of tubes with amorphous morphological appearance (Sun *et al.* 2012). Combining the above, it is obvious that the morphology and diameters of a-CNT is highly dependent on the synthesis parameters such as temperature, pressure, and types of carrier gas used.

2.3.2. Arc Discharge

Typically, arc-discharge method can be carried out in an atmosphere of hydrogen gas at a pressure of 50kPa with arc current maintained at 100 A. Before the arc discharge, the temperature in the furnace can be varied and maintained at that temperature for 10 min before arcing. The temperature is controlled by a thermocouple during heating and arc discharge. Previous study reported that as temperature in the furnace set to be 500 ℃ or higher, CNT would form and its diameter ranged from 10 to 15 nm with high purity. However, weak fringes, broken end, and discontinuous order of the tubes indicated amorphous structure of the tubes (Liu *et al.* 2004). This represented the formation of a-CNT at temperature of 500 ℃.

As temperature and catalysts play a major role in arc-discharge synthesis of a-CNT, the cooperative function of temperature and catalyst plays an important role in the soot production rate and the relative a-CNT purity. Another study has been carried out where the soot production rate increases from around 1 g/h to 8 g/h as temperature increases from 25 to 700 ℃. The best relative a-CNT purity at 600 ℃ can reach up to 99% compared to the room temperature sample with diameter ranging from 7 – 20 nm. Without Co-Ni alloy powder as catalyst, only graphite plate is formed at 25 ℃ and very few CNT are found when temperature increases to 600 ℃ (Zhao *et al.* 2005). The importance of Co-Ni alloy powder catalyst was reflected, where the absence of catalysts would form very few CNT even at most optimum synthesis temperature. The cruciality in presence of catalysts in arc-discharge methods limits its applications in low-cost production. However, arc-discharge method is still relatively inefficient as compared to CVD synthesis method.

2.3.3. Other Methods

Another common method for synthesis of a-CNT would be template-confined growth, which well-aligned 1D nanomaterials with adjustable diameter, length, morphology can be obtained easily. Typically, porous anodic aluminum oxide (AAO) templates with different channel structures were used to grow CNT through the pyrolysis of ethylene at 700 ℃. The synthesis of CNT was performed in a fixed-bed reactor with a quartz tube, where the template was placed in a quartz tube laid in the middle of the reactor. The reactor was heated to 700 ℃ in nitrogen followed by the introduction of a mixture of 10% acetylene in nitrogen at a flow rate of 20 sccm for 1 h. After that, the reactor was cooled to room temperature in nitrogen ambient. A-CNT are formed with irregular bottom and quasi-hemispherical top ends with branched parts as observed in HRTEM images (Yang *et*

al. 2003). The AAO template-confined growth process had been improved where the synthesis temperature can be lowered by introducing an organic acid (citric acid) as a carbon precursor. Due to the hydrogen bonds between the citric acid and the –OH groups at the walls of the AAO templates, a-CNT at various diameters were obtained at a low temperature of 450 ℃. The hydrogen bonds were changed by the concentration of H^+ in the solution; consequently the graphitization degree and the orientation of graphene layers could also be adjusted by controlling the pH (Zhao *et al.* 2009).

Besides template-confined growth of a-CNT, alternative methods have been developed for synthesis process with inferior alignment of final product. Synthesis of a-CNT via chemical route often provides simple and cost-effective methods in small-scale production. Previous researches reported successful formation of a-CNT with Fe/C coaxial nanocables via solvothermal treatment of ferrocene and sulfur. In synthesis of a-CNT, 1 mmol ferrocene and 2 mmol sulfur powder were put into a Teflon-lined autoclave, which was filled with benzene to 90% of total volume. The autoclave was maintained at 200 °C for 70 hours and then cooled to room temperature naturally. Long a-CNT of 50 nm in diameter with 10 nm of wall thickness were observed from TEM images (Luo *et al.* 2006). As sulfur plays an important role in solvothermal synthesis process (Tibbetts *et al.* 1994), the solvothermal process is undesirable for large-scale synthesis of a-CNT as it would emits large amount of poisonous sulfur gas during the synthesis process.

A popular approach used in synthesis of a-CNT is the self-catalysis-decomposition of ferrocene. A reduction agent is often used to reduce Fe content in ferrocene into atomic iron, at which Fe atoms acted as a catalyst in formation of a-CNT. An example of self-catalsis decomposition of ferrocene is via pyrolysis of ferrocene and sodium in benzene

solution. Ferrocene and sodium were put into Teflon-lined autoclave, which was then filled with benzene. The autoclave was sealed and maintained at 210 ℃ for 24 h, then allowed to cool to room temperature. The obtained CNT exhibited amorphous structure with outer diameter of 60 nm and wall thickness of around 10 nm, with purity of above 95 % (Xiong *et al.* 2004). During the process, ferrocene was first reduced to atomic iron and cyclopentadienyl group by metallic sodium, where atomic iron produced from ferrocene would agglomerate into iron clusters and acted as a catalyst for the pyrolysis of hydrocarbon compounds to CNT by catalyzing the decomposition of cyclopentadienyl group to amorphous CNT (Ci *et al.* 2000).

Besides pyrolysis of ferrocene and sodium in benzene solution, another self-catalysis-decomposition of ferrocene method was developed by reacting ferrocene and ammonium chloride powder in elevated temperature. Ferrocene and ammonium chloride fine powders were first mixed and placed in a quartz boat. Then, the quartz boat was put into an air furnace and heated to 200 ℃ at a rate of 10 ℃/min. After being held for 0.5 h, the furnace was allowed to cool down naturally. The powder obtained was washed with HCl solution and de-ionized water in sequence for several times, and then dried in an oven at 50 ℃ for 24 hours. CNT with amorphous structures are observed in TEM images, with 100 nm in diameter and 6–10 mm in length, respectively. During the process, ferrocene vapor was first oxidized to ferricenium cation, which would act as an electron acceptor and reacted with NH_4Cl vapor near the surface of NH_4Cl particles to form $(C_5H_5)_2FeCl$. The product was further oxidized by dehydrogenation and reacted with NH_4Cl. The presence of oxygen is crucial in formation of end product, where oxidation of ferrocene powder into ferricenium cation is the initiation step of overall process (Liu *et al.* 2007). This process is relatively simple where flow of specific gases is not required as presence of air is crucial

for formation of a-CNT. As compared to pyrolysis of sodium and ferrocene in benzene solution, this method provides a more environmental friendly approach where usage of poisonous benzene solution is not required.

2.4 Properties of Amorphous CNT

A-CNT has unique properties due to its porous and defective structures which initiates high potential in usage of amorphous CNT in various applications. Although CNT has outstanding mechanical, thermal and electrical properties, the porous and defective structures of a-CNT exhibit inferior properties as compared to fully crystalline CNT. However, a-CNT has added advantages in further tube's surface modification and functionalizing with active functional groups, as those functional groups would tend to form on defective sites and tubes' ends. Therefore, this section will discuss the general properties of amorphous CNT including electrical properties, thermal stabilities, suspension stabilities, and optical properties.

2.4.1. Mechanical and Thermal Properties

The mechanical characteristic of a solid depends largely on the strength of its interatomic bonds and based on the known knowledge on the property of graphite. Besides, the nanotubes have also been discovered to be flexible as they can be twisted, elongated, flattened or bent into circles before fracturing, which allowed structure to relax elastically while under compression. This flexibility contributes to mechanical properties of CNT distinguished significantly with the mechanical properties of carbon fibers, which will be fractured easily upon application of stress (Paradise *et al.* 2007). As discussed in section 2.1.1, CNT exhibits outstanding mechanical tensile strength and Young's modulus

(Poncharal *et al.* 1999; Yu *et al.* 2000; Demczyk *et al.* 2002; Files *et al.* 2000), which agreed well with the statements developed by Paradise *et al.* relating the interatomic bonds with mechanical strength. However, as a-CNT has short-ranged order with porous and defective structure, and predicted to have inferior mechanical properties compared to fully crystalline CNT. As there are still limited exposure on the mechanical properties of a-CNT, information on the mechanical strength and Young's modulus of a-CNT are still unestablished.

The thermal conductivity of CNT is relatively high. For MWCNT, its thermal conductivity at room temperature can reach up to 2586 W/mK (Samani *et al.* 2012). Therefore, CNT is often used as fillers in composites to enhance thermal conductivity. Usage of CNT as fillers would improve both thermal conductivity and thermal stability of polymer electrolytes (Ibrahim *et al.* 2012). However, attachment of gold particles on CNT bodies would affect the thermal stability of CNT. In spite of the benefits and potential applications of gold nanoparticles decorated CNT; the attachment of gold nanoparticles affects thermal stabilities of gold nanoparticles decorated CNT. This influence will limits its usage at elevated temperature. Previous study shows that the decoration of gold nanoparticles on the CNT surface would shift the highest peak of a Thermogravimetric Analyses (TGA) derivative curve towards low temperature side (Zhang *et al.* 2000). This represents maximum of mass lost at lower temperature, which indicates poor thermal stability upon attachment of gold nanoparticles (Mizoguti *et al.* 2000).

2.4.2. Electrical Properties

Electrical conductivity of conducting nanoparticles/polymer matrix composite can be explained by the established percolation theory (Kirkpartick, 1973), where conductive pathways will be formed when a critical filler concentration, commonly named percolation threshold, is achieved. Percolation theory is originally developed for spherical particles. Due to the high dependence of aspect ratio (length/diameter ratio) of percolation theory, rod-like fillers such as CNT with higher aspect ratio are generally advantageous over spherical particles to achieve percolation (Florian *et al.* 2006). Therefore, a low filler content of CNT is expected to achieve conductive network. Two approaches can be used to improve the electrical conductivity of CNT/epoxy composite, minimize the contact resistance between nanotubes and improve the conductivity of individual CNT by post-synthesis treatments (Li *et al.* 2007). Post synthesis treatments of CNT include oxidization of CNT fiber in HNO_3 or attachment of gold particles. These surface modification steps remarkably improved conductivity and change CNT conduction behavior (Deepak *et al.* 2010). At the same time, minimizing contact resistance between nanotubes could be done by improving the alignment of CNT to maximize contact area between tubes (Li *et al.* 2007). According to the static model percolation theory, the low percolation threshold has commonly been attributed to the high aspect ratio and a good dispersion of CNT. However, the composite's matrix is often in molten state or wet solution, and flow or shearing will be applied on the composite for dispersion which give effects to the formation of conductive network (Bryning *et al.* 2005). Besides, re-agglomeration nature of CNT (Kansala *et al.* 2007) contributed to high contact area between CNT. Previous study suggested that CNT clustering could favors the formation of a percolating network (Aguilar *et al.* 2010), where agglomerated CNT/matrix composite

possessed a relatively higher electrical conductivity than finely dispersed CNT/matrix composite in general. CNT's agglomeration can be related to viscosity of liquid state polymer matrix and its curing temperature. This has been noticed that the very low percolation threshold is always achieved with a low viscosity system (Kovacs *et al.* 2007). According to Andrade equation:

$$\eta = A \bullet 10^{B/T} \qquad (2.1)$$

where A and B are constants characteristic of the polymer or other material and T is the absolute temperature. Viscosity will be reduced as temperature increases which will enable the composites to reach a low percolation threshold. Besides, a previous study proves that elevated temperature condition promotes re-agglomeration of particles in a liquid-based suspension (Moseley, 1993). Therefore, preliminarily it is proven high curing temperature will improve electrical conductivity.

The conduction mechanisms of pure a-CNT are dominated by hopping and tunneling of free ions (Yosida, 1999). However, the conduction mechanisms of gold particles in gold decorated a-CNT are yet to be discovered. To investigate the percentages of electron/ionic conductions, transference number acted as a useful parameter which explains the fractional contribution of cations in electrical conduction. Wagner's dc polarization method offers a simple approach to determine the transference number (Hema *et al.* 2002). When a steady potential difference is applied between two terminals of a composite, at t = 0 s, both ions and electrons move and contribute to the current flow. The level current flow drops gradually until a steady current is reached, where only ions can be depolarized and move. The equation can be described as follow:

$$t = \frac{I_0 - I_{ss}}{I_0} \quad (2.2)$$

t, I_{ss} and I_0 are transference number, current at steady state and current at initial state respectively. From the equation, changes in transference number represent changes in fractional contributions of ions in electrical conduction respectively.

2.4.3. Optical Properties

Optical properties of CNT can be explained via optical absorption, Raman, and FTIR approaches. These methods provide intensive and non-destructive studies on the properties, natures, structures and quality of CNT. Many researches and studies have been carried out to further justify the reliabilities and accuracy of these tests in characterizations. As non-tubular carbon content, structures, chirality and structural defects of the as-produced CNT dictates the resulting mechanical, electrical and electrochemical properties, optical tests have become increasingly important to identify these factors. However, optical applications of CNT are still unestablished. In this section, the use of different optical spectroscopy for characterizing CNT would be discussed.

Electrical properties of CNT could be predicted via optical absorption spectra. Previous study reported that electrical properties of CNT predicted from optical absorption spectra is similar to band gap calculations. Kataura and coworkers reported that SWCNT with different diameter distribution where optical absorption spectra have been measured, three large absorption bands were observed from infrared to visible region. These absorption bands are due to the optical transitions between spike-like density of states, characteristics of SWCNT. Absorption peaks sensitively shifted to higher energy side with decreasing tube

diameters as the band calculation predicted (Kataura *et al.* 1999). From this observation, we can conclude that optical absorption properties of CNT are highly related with its electrical properties. Kataura has further expands the study of relations between calculated gap energies with different diameters for different types of materials, which has plotted these relations into Kataura Plot as shown in Figure 2.5. Kautara plot shows peaks of theoretical gap energies between mirror-image spikes in an absorption spectrum for tubes with a given range of diameters. From this plot, we can observe the absorption features from nanotubes with different structures often overlap, which gives an obscure comprehension about nanotube structures, indicating the limitations of using gap energies obtained from optical absorption spectra to determine the tubes' structures and diameters.

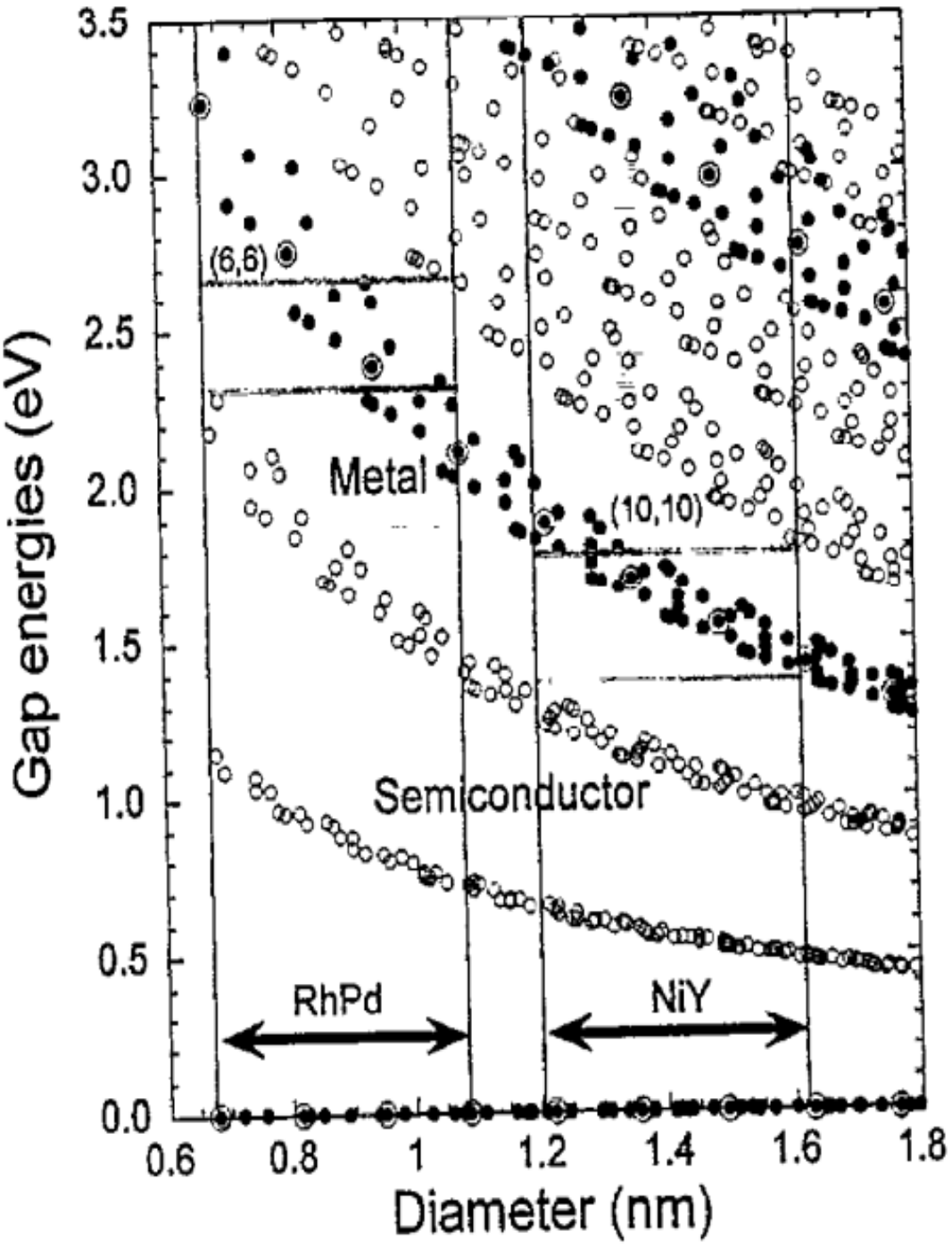

Figure 2.5: The kataura plot that shows calcualted gap energies with different diameters for different types of materials (Kataura *et al.* 1999)

An evidence of justifying the relations between optical absorption properties and electrical conduction properties of CNT is shown by Minami and coworkers (2001). During the study, Minami *et al.* demonstrated that optical absorption spectra of SWCNT changed drastically by the doping of halogens and alkali metals. Disappearance of absorption peaks upon doping was attributed to interband optical transitions as a semiconducting phase of SWCNT was doped. Emergence of new absorption peaks induced by heavy doping is explained by invoking the involvement of low-lying valence states (or high-lying conduction states) in the optical transition. The good correspondence of the these results to theoretical works justified the sensitivity of optical absorption properties with transition of metallic-semiconducting properties of CNT (Minami *et al.* 2001).

Besides optical absorption properties, CNT show Raman scattering phenomena when an electromagnetic wave is irradiated to them. Most photons are elastically scattered from atoms or molecules (Rayleigh scattering), where the kinetic energy of scattered and incident photons is conserved. However, a small portion of the scattered photons are due to excitations, having a kinetic energy lower than the incident photons. This phenomenon is known as inelastic scattering of photons (Harris *et al.* 1989). As electron is excited by an incident photon and transfer from the electronic ground state to the higher electronic excited state, the electron is then emits a photon and relaxes back to the ground state. In Stokes scattering, molecule obtains energy by absorbing a phonon, while in anti-Stokes process, the molecule loses energy since it emits a phonon (Jorio *et al.* 2008). The energy level diagram of stokes and anti-stokes Raman scattering is shown in Figure 2.6.

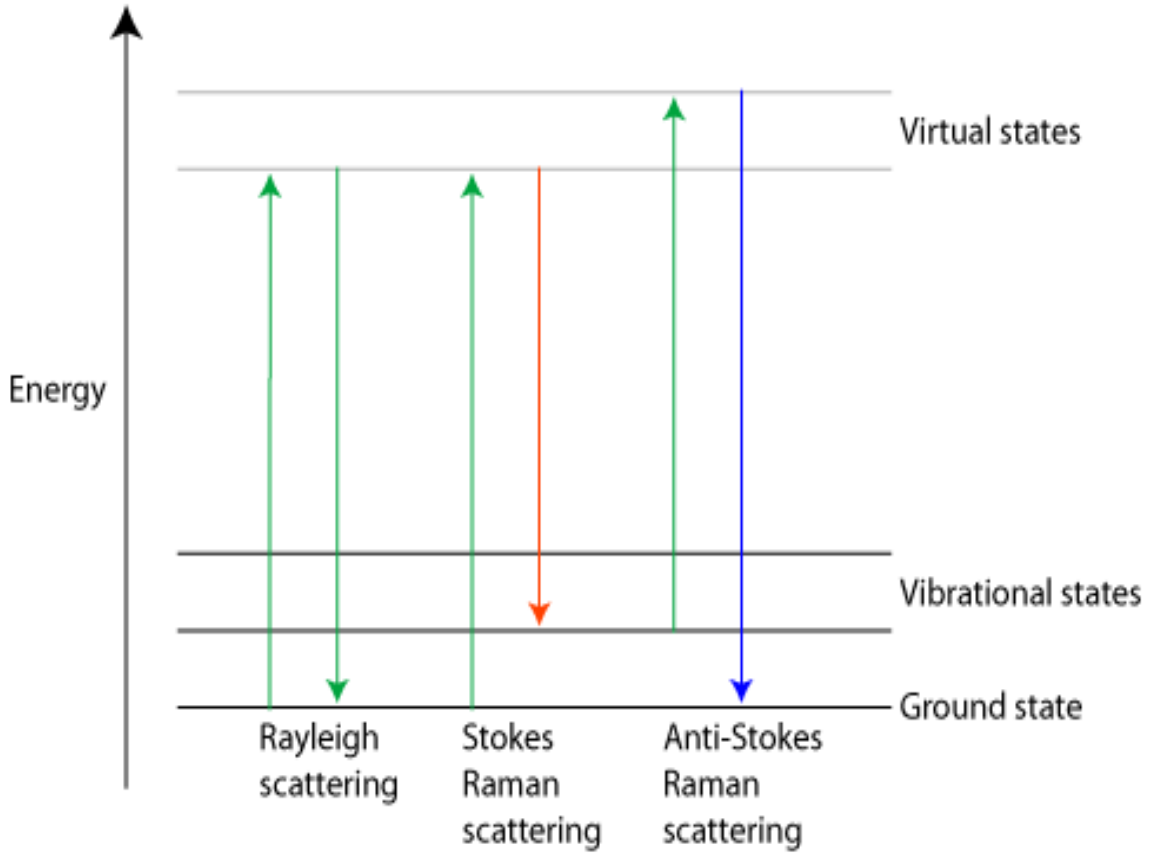

Figure 2.6: Energy level diagram of stokes and anti-stokes Raman scattering

Due to discreet characteristics of Stokes Raman scattering and Anti-Stokes Raman scattering, Raman spectroscopy has provide a sensitive and yet non-destructive method to determine the structural defects of CNT. As Raman measures phonon frequencies, the electronic structure of nanotubes could be predicted via this technique under resonance conditions. The electronic structure of a nanotube is determined by its (n,m) indices or chiral vector enabling determination for the geometrical structure of a SWCNT from resonance Raman spectrum (Dresselhaus *et al.* 2002). When incident or scattered photons are in resonance with the energy of strong optical absorption electronic transitions, the

Raman intensity becomes large due to the strong vector are thus depended on the various features, including G- and D- lines or G- and D- bands, and radial breathing mode (RBM). A typical raman spectrum of CNT is shown in Figure 2.7.

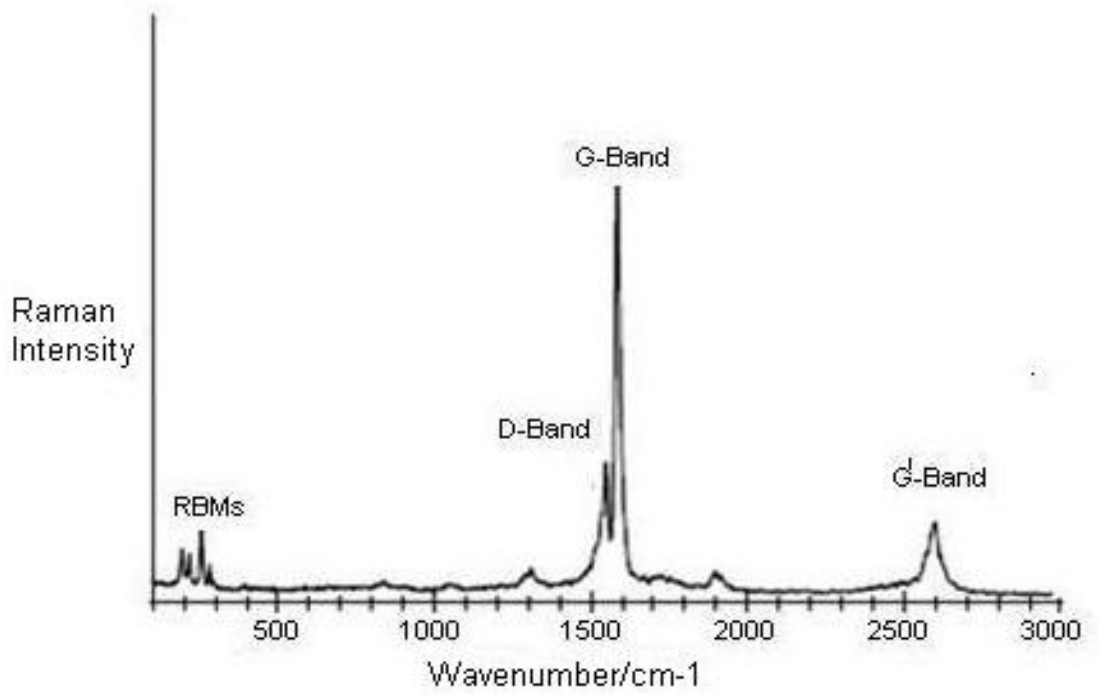

Figure 2.7: A typical raman spectrum from a SWCNT sample (Irurzun *et al.* 2010)

Raman spectroscopy is conventionally known to be used in determination of defect structures in CNT. However, by means of calculations and predictions, assessment to CNT samples' purity is possible via raman intensity measurements of CNT (Irurzun *et al.* 2010). The predictions consists of measuring the G-band intensity of liquid suspensions of SWCNT samples as a function of solid concentration where a simple equation is proposed in which one of the two adjustable parameters is the SWCNT purity. The measurement of G/D ratio in liquid suspensions as a function of solid concentration agrees well with the

electron microscopy, thermogravimetric analysis and optical absorption results on the same series of samples. General properties of defects-to-crystalline ratios can be determined via Raman spectroscopy, which could indicate the degree of imperfection in CNT, and therefore provided information about the degree of tube surface damage due to the presence of functional groups (Lafi *et al.* 2005). Besides, chirality and (n,m) indices can also be determined by elucidating the vibrational and electronic structure of CNT as reported in previous study (Dresselhaus *et al.* 2002). Other characteristics of CNT which could be assessed via Raman spectroscopy including the values of the in-plane coherence lengths, the planar projection of graphene sheets, and the line-width behavior related to the graphitization step (Delhaes *et al.* 2006). However, these values need to be further confirmed by other characterization techniques including electron microscopy, thermogravimetric, analysis and optical absorption results.

2.4.4. Suspension Stability

Dispersion of CNT in selected solvent has always been a limitation in utilizing the unique properties of CNT. Degree of separation or dispersion of CNT dictates the properties or qualities of final product, either in hybridization process of nanocomposites on CNT tubes' body, or addition of CNT in liquid form matrix. However, due to the hydrophobic and inert nature, as-prepared CNT are unfavorable for these applications (Xia *et al.* 2007). It was found that CNT would tend to agglomerate due to unique molecular morphologies (Kasaliwal *et al.* 2010) which cause difficulties in dispersion and further surfaces modifications. Addition of oxygen-containing functional group; -COOH group for instance, will favors the dispersion, reduce overall length of CNT bodies, and creates open ends tubes which favorable for both attachment of nanocomposites and dispersion in

solvent (Lim *et al.* 2004). Functional groups such as carboxyl, phenol, dodecylamine, 1-octadecanol or polyethylene glycol were successfully attached covalently on CNT body by thermal oxidation with acids, amidation or esterification (Abuilaiwi *et al.* 2007). Since most of the attachment of nanocomposites carried out in medium of distilled water (Ma *et al.* 2008), additions of oxygen-containing functional group are seems effective as they would improve dispersion of CNT in distilled water (Kyotani *et al.* 2001).

It was found that sonicating CNT samples with various types of acid create –COOH groups on its surface (Naseh *et al.* 2009). There are two types of mechanisms in functionalization of CNT via covalent attachment, functionalization via "end and defect-side chemistry" and via "sidewall functionalization" (Azamian *et al.* 2002). As explained by these two mechanisms, defects are potential sites for chemical modification. By treatment of nanotubes in strong oxidizing or acidic medium, the oxygen-containing groups will be introduced to the ends and sidewalls of the tubes. These groups, which are chemically attached to the tubes, are mostly represented by –COOH groups, less by –C=O, and –OH groups (Hamon *et al.* 1999). These groups can serve as starting points for further functionalization of the nanotubes (Klumpp *et al.* 2006). The schematic diagram of functionalization via "end and defect-side chemistry" is illustrated in Figure 2.8.

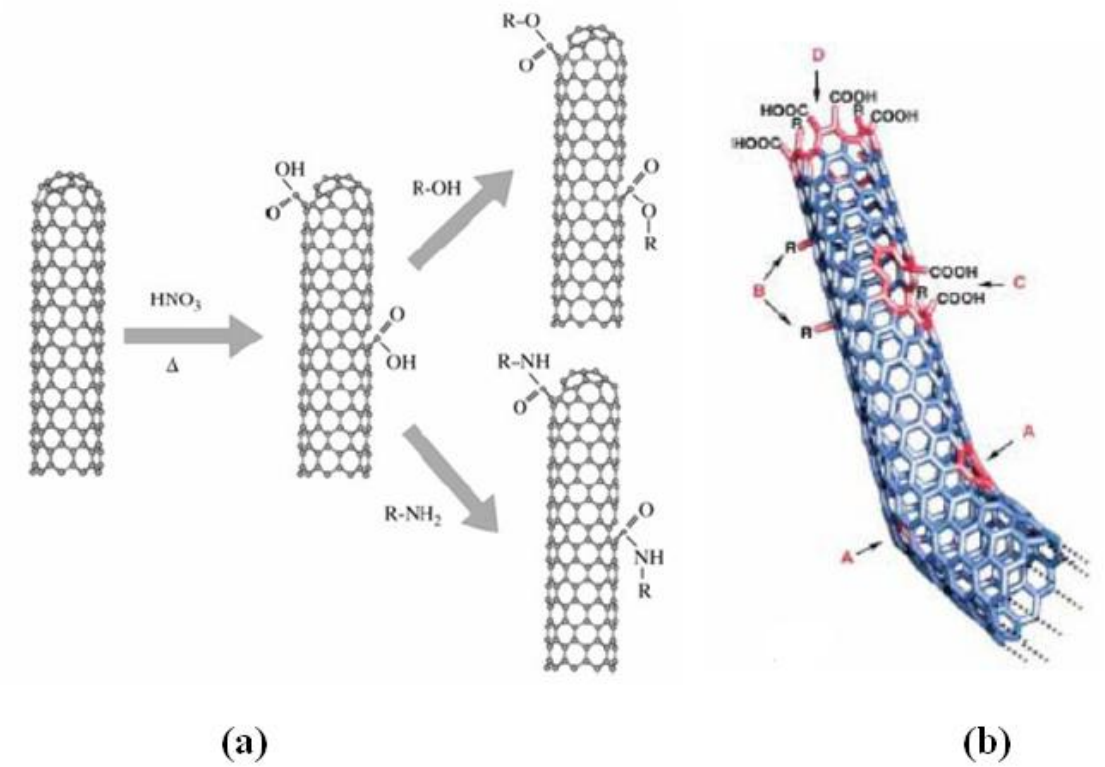

Figure 2.8: (a) Functionalization using –COOH site.(Balasubramanian, 2005). (b) Typical defects in CNT (Hirsch, 2002)

As compared to fully crystalline nanotubes, a-CNT are known to be highly porous (Dinesh *et al.* 2007) and highly defective (Collins 2009). Therefore, attachment of functional group on a-CNT expected to have more significant results.

2.4.5. Hybridization Properties

The development of a DNA hybridization biosensor by applying gold hybrid CNT has rising potential in biomedical applications A DNA sensor that selectively capture its complementary target nucleic acids has been reported. Therefore, the solid support, gold-hybrid carbon nanotubes should offer good surface chemistry for the systematic

attachment of DNA. In addition, there is a growing interest to apply nanomaterials such as CNT and gold nanoparticle as electrochemical transducers for biological processes. Hence, a hybrid of gold nanoparticles and CNT will be a compatible heterostructure with many biological systems (Lim *et al.* 2004). Pre-treatment of CNT is required where attachment of carboxyl groups is required before attaching gold particles. Since a-CNT possesses relatively thin wall and large diameter (Hu *et al.* 2006) with open ends (Liu *et al.* 2007), we expect a more significant and effective hybridization of gold particles into a-CNT.

One of the main mechanisms of attaching nanoparticles on CNT bodies based on wet chemistry. When the nanotubes are filled with some compounds, the active chemical groups on CNT body reacts under particular thermal or chemical conditions with nanoparticles. These nanoparticles then become trapped in the nanotubes (Hirsch *et al.* 2002). In year 1992, Broughton and Pederson predicted that CNT absorb some liquids by capillary action (Pederson *et al.* 1992). Capillary absorption is caused by extra pressure given by the Laplace equation of capillarity.

$$\Delta P = (2\gamma\cos\theta)/R \qquad (2.3)$$

$\Delta P = P_a - P_m$ represents pressure difference between atmospheric pressure, P_a, and pressure under the meniscus, P_m. γ, R represent the surface tension at the liquid/air interface and inner radius of the nanotube respectively and θ is the liquid-solid contact angle. The schematic diagram of Laplace equation illustrated in Figure 2.9.

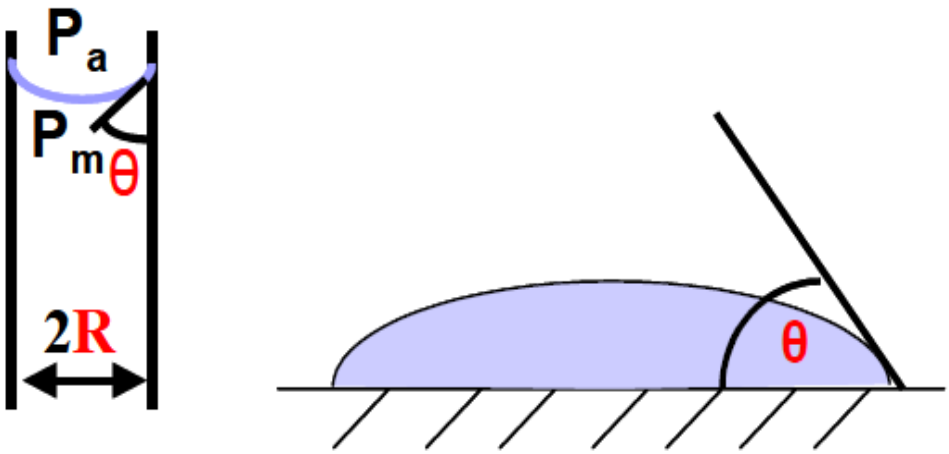

Figure 2.9: Illustration to the Laplace Equation

From the Laplace equation, we see that the difference $\Delta P = Pa - Pm$ will be positive whenever $\theta < 90°$, and negative when $\theta > 90°$. Since the meniscus forms spontaneously, this extra pressure will pull the liquid into the nanotube if $\Delta P > 0$, provided that the pressure in the reservoir is atmospheric. In other words, to fill the nanotubes with some liquid, the contact angle that the meniscus forms with the nanotube wall must be less than 90 ° (Durjadin *et al.* 1994). The angle θ represents degree of wetting of suspension with desired nanocomposites on CNT body itself. Addition of oxygen-containing functional group; -COOH group for instance, will improve dispersion and hence decreases surface tension of liquid-solid contact, or θ (Lim *et al.* 2004). In the case of gold nanoparticles, attachment on carboxyl functionalized carbon nanotubes is through electrostatic interactions between carboxyl groups on a-CNT bodies and cationic nanoclusters (Jiang *et al.* 2003). Figure 2.10 illustrated the mechanisms in formation of Au nanoclusters coated CNT:

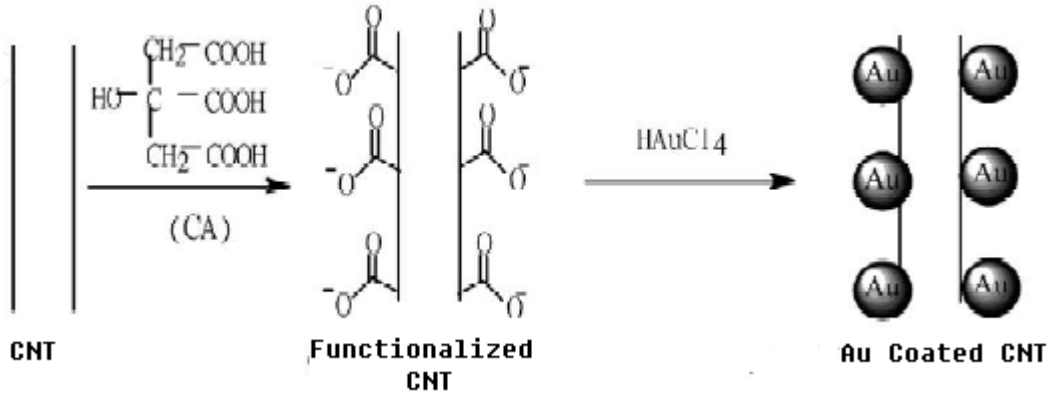

Figure 2.10: Simulative view of the process for attaching gold nanoparticles to carboxyl functionalized CNT (Jiang *et al.* 2003)

More carboxyl groups present on CNT bodies would results in higher effectiveness of attaching gold nanoparticles on a-CNT bodies. The indication on amount of carboxyl groups present on CNT bodies can be represented by surface charges, which can be done via zeta potential measurement.

2.5 Potential Applications of amorphous CNT

As CNT have been reported as functional materials with outstanding mechanical, electrical, electrochemical, optical, and thermal properties, enormous researches have been carried out to investigate the potential applications of CNT in nanotechnology, semiconductors, electrics and electronics, medical delivery systems and other potential contributions in materials science and engineering. These include electrochemical applications, drug delivery in cancer treatment, electrochemical capacitors, or even natural gas storage or hydrogen gas storage. On the other hand, a-CNT has attracted great attentions in these applications due to its highly porous and defective structures, and high

yield with low synthesis temperature.

Previous research has reported the outstanding electrochemical performance of a-CNT upon removal of outer amorphous carbon layers by nitric acid (He *et al.* 2007). A-CNT could be cut shorted and some active functional groups were found on the open end of CNT body, which would easily modify its electrochemical natures that enables it to be applied in various electrochemical applications. According to "ends and defect sites chemistry", these active functional groups would tend to form on ends and defected sites of CNT. As a-CNT possessed relatively defective structure, a more significant modification in properties upon functionalizing would be predicted (Azamian *et al.* 2002). This tunable characteristic of a-CNT contributes high potential applications in fabrication of electrochemical capacitors and electrochemical sensors (Zhao *et al.* 2009).

Besides outstanding electrochemical properties, CNT are considered to be an ideal candidate for the field emission (FE) display devices by virtue of their high aspect ratio (length to diameter), sharp tip curvature, chemical inertness and mechanical strength. Various enhancements in the FE property were achieved by modifying the surface of CNT (Xiao *et al.* 2008). By suitable functionalization, the work function of the material could be reduced significantly which in turn helped in the enhancement of FE characteristics. Similar to electrochemical applications, as a-CNT has highly defective and porous structure; it would exhibits more significant changes in various properties, which would be highly potential to create Field Emission Transistors (FET) by different means. Previous research reported a significant improvement of FE properties as a-CNT was functionalized with concentrated acid (Jha *et al.* 2011). The as prepared a-CNT sample showed good FE properties and the FE properties were significantly improved for the stearic acid

functionalized a-CNT.

An important application of a-CNT is hydrogen production and hydrogen storage. Application of CNT as the catalyst support in hydrogen production appears to be effective and attractive owing to their special structural morphology and characteristics. As surface of CNT is usually modified to create the functional groups for specific needs, a-CNT has added advantages than fully crystalline CNT as its porous and defective structures enable highly effective functionalizing. Catalysts for hydrogen production supported on CNT have been produced by impregnation, precipitation, chemical reduction and a hydrothermal method (Orinakova *et al.* 2011).

Hydrogen storage represents one of the essential challenges in developing clean-burning hydrogen. Efforts have been directed on optimizing the current state of production as well storage technologies. Nanostructured carbon materials exhibit commercial advantages over other storage methods. As well, they assign to flexibilities relating to their design and the option to employ physical and/or combined physicochemical storage strategies. Previous study has reported advancement on developing of a-CNT in hydrogen storage. It was reported that a-CNT have 1.29 wt% of hydrogen up-take capacity at room temperature under pressure of 10 Mpa (Ci *et al.* 2003). In combining physisorption and chemisorption modes, composite storage materials comprising metal dopants and carbonaceous supports have shown a propensity to display the advantages of both.

The outstanding mechanical properties of CNT play an important role in fabricating high mechanical strength composites. Fama and coworkers reported increments of almost 70% in stiffness and 35% in ultimate tensile strength, keeping deformations higher than

80% without break for Starch/MWCNT composites with filler weight percentage as low as 0.027-0.055 wt%. Besides, enhancements of up to 100% in biaxial impact parameters were also observed (Fama *et al.* 2011). Apart from mechanical strength, CNT also improves tribological properties of composites. Previous study reported that CNT-reinforced composites exhibits higher wear resistance and lower friction coefficient that graphite-reinforced composites. At the same time, CNT composites revealed a lower wear rate and friction coefficient compared with pure matrix, and their wear rates and friction coefficients showed a decreasing trend with increasing volume fraction of CNT (Chen *et al.* 2003). Generally, CNT composites show highly significant improvements in mechanical, electrical and thermal properties (Gao *et al.* 2005) that contributes high potential in applications of various extreme environment -operating composites (elevated temperature, high wearing rate, high cyclic stress loading, etc.). Due to porous and defective structure of a-CNT, these applications are seem inferior in performance as compared to fully crystalline CNT. However, the low synthesis temperature and high production yield of amorphous CNT add credits to applications that required low production costs.

Due to outstanding and unique electrical properties of CNT, it has high potential microwave applications as nano-antennas and nano-switches. These applications can be enable elements for communication networks and other applications requiring ultraminiaturized, lightweight components that operate at low voltage, low power, and high speed. A study reported that switching of CNT has been demonstrated with pull voltages of a few volts, and speed measurements have revealed switching times of a few nanoseconds. As for the antenna prospects, an excess inductance of the order 10 time of the inductance of a thin-wire antenna has been observed. This provides to CNT antennas' unique property to require a wavelength of current excitation 100 times smaller than the wavelength of the

far-field radiation (Demoustier *et al.* 2008). Due to unique conduction properties of a-CNT, the application of a-CNT in nano-antennas and nano-switches are highly possible.

Besides industrial applications, various researches have explored the possibilities of using CNT in biomedical applications. As Bioglass has been developed for bone-filling material in orthopedic and dental applications, CNT/bioglass composites exhibits high mechanical strength compared to pure bioglass matrix. Jia and coworkers reported MWCNT/45S5Bioglass composite had appreciable lower hardness, while flexural strength and fracture toughness increased 159% and 105%, respectively as compared to pure 45S5Bioglass matrix (Jia et. al. 2011). The improved structural and physical properties of the MWCNT/45S5Bioglass composites suggested their potential to be used as artificial teeth or scaffold matrix materials in bone tissue engineering.

As gold particles decorated CNT exhibits outstanding improvements in electrical properties, numerous studies have exposed its potential usage in biomedical applications, specifically on bio-sensors. Wu and coworkers reported a detection of cytochrome c with modified gold electrode. Gold electrode was modified with gold nanoparticles decorated MWCNT was used to detect cytochrome c and a pair of well-defined redox waves was obtained. It was found that the composite film promoted the redox of horse heart cytochrome c and its effect was developed for the determination of cytochrome c (Wu *et al.* 2005). Besides, gold nanoparticles decorated CNT has good biosensing ability in detection of glucose. Previous research reported investigation on gold nanoparticles/functionalized MWCNT nanocomposites and its glucose biosensing application (Li *et al.* 2009). Gold nanoparticles/functionalized MWCNT composite exhibits good electrocatalysis toward oxygen and hydrogen peroxide reduction with good biocompatibility with glucose oxidase

due to its good biocatalysis toward glucose substrate, which offered a friendly environment for the immobilization of biomolecules and provides potential applications in fabrication of biosensors. As a-CNT with highly defective and porous structure exhibits unique and novel electrical properties, the applications of a-CNT in bio-sensing applications have high potential towards unique and outstanding performances. However, the actual applications are still yet to be discovered and optimized.

Besides detection of glucose and cytochrome c, gold nanoparticles decorated CNT could also be applied in antigen immunosensor. Gao and coworkers reported outstanding detection ability of carcinoembryonic antigen by chitosan–carbon nanotubes–gold nanoparticles nanocomposite film, which reflected the good sensitivity of immunosensor based on chitosan–carbon nanotubes–gold nanoparticles nanocomposite film as the antibody immobilization matrix (Gao *et al.* 2011). Due to good biosensing ability, gold nanoparticles-decorated MWCNT was used in determination of choline. Previous study reported choline sensing ability of gold nanoparticles-decorated MWCNT-poly(diallyldimethylammonium chloride) biocomposite, which the biocomposites reacted sensitively with presence of choline with fast response time, good reproducibility, anti-interferant ability and long-term stability (Qin *et al.* 2010). Due to unique electrical properties and high production efficiency of a-CNT, it has high potential in applications in biosensors fabricated based on gold nanoparticles decorated CNT.

CHAPTER THREE

MATERIALS AND METHODS

This chapter describes the materials and synthesis steps used in the study, including synthesis of a-CNT, functionalization of a-CNT with concentrated acid, hybridization of gold particles on a-CNT and fabrication of CNT/Epoxy composites. The raw materials have been selected carefully to suit the productions and the synthesis steps are designed and carried out based on literature studies. All relevant characterization methods with required conditions and parameters were explained and illustrated.

3.1 Raw Materials

The main precursor materials used in synthesis of a-CNT are ferrocene ($Fe(C_5H_5)_2$) and ammonium chloride (NH_4Cl) powders. $Fe(C_5H_5)_2$ has purity of 98% and was supplied by ACROS Organics. As ferrocene is an organometallic chemical compound, it contains both irons and organic compounds with two cyclopentadienyl rings bound on opposite sides of a central metal atom. On the other hand, NH_4Cl compound with analytical grade was used as catalyst during the reaction.

Hydrochloric acid (HCl), in concentration of 20 % and deionised water which had been purified (>15 MΩ.cm) were used for purification treatment. Hydrochloric acid (HCl), sulfuric acid (H_2SO_4), nitric acid (HNO_3) and citric acid ($C_6H_8O_7$) with concentrations of 20 % were also prepared to serve the purpose of performing oxidation. The oxidized a-CNT was then hybridized by the as-prepared gold (III) chloride ($AuCl_3$). The epoxy resin and

hardener used in fabricating CNT/Epoxy composites are from Epofix^{TM} Kit with amine based hardener. All mentioned analytical chemicals were used as received without any further purification.

3.2 Preparation of Samples

In this work, as-synthesized a-CNT were synthesized via modified reduction process. 4 g of NH_4Cl and 2 g of $Fe(C_5H_5)_2$ were mixed homogeneously. The mixture was then transferred to a beaker with capacity of 500 mL. The beaker was then covered and heated to 220 ℃ inside a convection oven. The mixture was hold at this temperature for 30 minutes and cooled down naturally to room temperature. After cooling, the mixture was taken out and mixed homogeneously.

In removing of other impurities and residuals, the obtained black powder was soaked and washed with concentrated HCl and heated at 90 ℃. The black powder was allowed to sediment completely. This process was carried out for several times for better purification. The black powder was then washed with deionised water for several times. Dehydration was performed using a convection oven at 80 ℃ for 10 h to obtain a sample which denote as “as-synthesized a-CNT” as shown in Figure 3.1.

Figure 3.1: As-synthesized a-CNT in powder form

A-CNT were oxidized and functionalized via ultra-sonication treatment in concentrated acids. 0.5g of as-synthesized a-CNT were immersed in 30 ml of nitric acids (HNO_3) (20%) and sonicated for 30 minutes. The obtained mixture is then diluted and excessive acids were dried at temperature of 150 ℃. The functionalization process is then repeated by replacing nitric acids with citric acids ($C_6H_8O_7$), sulphuric acids (H_2SO_4), and hydrochloric acids (HCl). A-CNT treated with different acids were subjected to zeta potential tests, where most dispersible sample was named as "functionalized a-CNT".

Loading of gold (Au) particles on the surfaces of a-CNT was carried out by using a modified wet method (Lim *et al.* 2004). The "functionalized a-CNT" were stirred with 100 ml of auric chloride ($AuCl_3$) solution at 1200 rpm for 1 hour at 70 ℃. The concentration of $AuCl_3$ was 2.5 g/dm^3. In other set of experiments the functionalized samples were stirred with $AuCl_3$ solution having concentration of 5.0, 7.5, and 10 g/dm^3. Then, 50 ml of citric acid was added drop-wise to the solution as a reducing agent for Au cations (Ebbesen *et al.*

1996). Again stirring was continued for another 4 hours followed by filtering and drying.

The as-synthesized a-CNT and modified a-CNT were dispersed in epoxy resin for the purpose of measuring the electrical resistance (Zhu *et al.* 2010). Epoxy resin suspensions were prepared by incorporating 5 wt% of as-synthesized a-CNT and gold particles decorated a-CNT treated with 2.5, 5.0, 7.5, and 10 g/dm^3 $AuCl_3$ solution. A high-speed (1200 rpm) mechanical stirring was employed to the suspension for 4 hours at the room temperature. 2 ml of amine-based hardener was added to the mixture and each mixture was allowed to cure at room temperature and 15 ℃ respectively for 24 hours. The cured samples in the shape of solid coins as shown in Figure 3.2 were collected to perform the electrical properties test. The preparation works for all samples are summarized in Figure 3.3.

Figure 3.2: a-CNT/Epoxy composite in coin shape

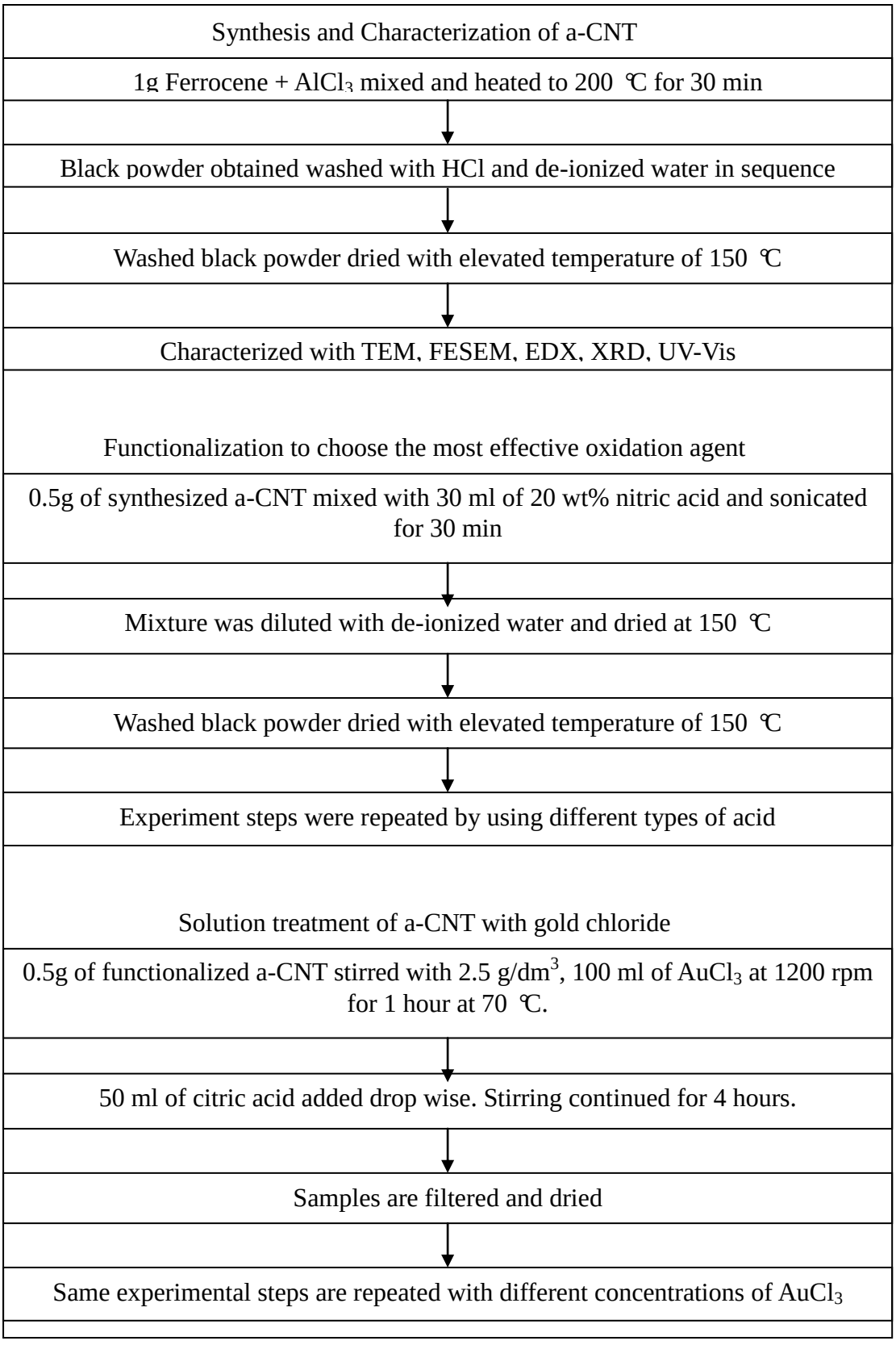

Figure 3.3: Flow chart of sample preparation

Curing of modified a-CNT/Epoxy composite
0.2g of synthesized a-CNT mixed with 3.8g of epoxy resin and stirred at 1200 rpm for 4 hours.
↓
50 ml of citric acid added dropwise. Stirring continued for 4 hours.
↓
2 ml of amine based hardener added to the mixture. Each mixture is cured and room temperature and 15 ℃ for 24 hours to form solid coin
↓
The same experimental steps are repeated for modified a-CNT

(Continued)

3.3 Characterization Method

As-synthesized, functionalized and hybridized a-CNT/Au samples were subjected to characterization methods, including morphological, microstructural, elemental, optical, thermal and electrical characterizations.

3.3.1. Morphological Studies

All samples were observed under TEM (LIBRA 120, Germany), HRTEM (Philips TECNAI 20, Netherlands) and FE-SEM (AURIGA, ZEISS, Germany) in performing qualitative analysis on the nanotubes surface morphology and microstructure. The used TEM was operated using accelerating voltage of 120 kV. As for the HRTEM images in high resolution were obtained using an accelerating voltage of 200kV that could produce magnification up to 1,000,000 times. The FE-SEM was equipped with detectors of secondary electrons and EDX spectrometer. The micrographs were generated to backscattered electron detector in FE-SEM. All of these characterization methods could

observe the surface morphologies of the tubes. Besides, by means of measurements, geometry of the tubes, including tubes' diameters and tubes' lengths, can be determined.

3.3.2. Microstructural Studies

Microstructural analysis was studied by using X-Ray Diffraction (XRD, SIEMENS D5000, German) with Cu-K α X-radiation of wavelength 1.54056Å at 60 kV and 60 mA. The diffraction was conducted in the Bragg angles between 5 °to 100 °in order to examine the crystallinity of as-synthesized and gold particles modified nanotubes. From these microstructural studies, the presence of elements could also be performed and identified.

3.3.3. Elemental Analysis

Energy Dispersive X-ray (EDX) spectrometer embedded in FE-SEM equipment was employed to perform elemental analysis on the nanotubes at room temperature. The EDX test was carried out by the FE-SEM, where elemental analysis would be performed after FE-SEM images being captured. The voltage used for this test should be more than 10 kV and located at 8 mm working distance in order to obtain better quantitative elemental analysis.

3.3.4. Suspension Stability

Zeta Potential measurement used to indicate suspension stability was performed using Zetaseizer. Each sample was suspended in distilled water with 0.03 wt% and sonicated for 30 minutes. The pH level of each sample suspension was tested with blue and red litmus papers.

3.3.5. Optical Studies

The Ultra-Violet Visible (UV-Vis) absorption spectra were recorded using a spectrophotometry (Cary Win UV 50, Australia). A 1 cm quartz cuvette was used to measure the optical absorption and transmittance via scanning of all samples at a slow rate over the range 190 – 800 nm, which includes ultraviolet, infrared, visible and adjacent regions of optical waves. The samples preparations prior to UV-Vis measurement were performed by ultrasonicating a sample containing 0.03 wt% of nanotubes in methanol as solvent for 1 hour to obtain better dispersion of the sample.

Raman characteristics of the as-synthesized and surface-modified amorphous CNT were conducted by inVia Raman microscope (RENISHAW, United Kingdom). The He-Ne laser with wavelength at 633 nm was irradiated to a well-dispersed nanotubes/methanol suspension. At the same time, FTIR spectroscopy was carried out in the range of 400-4000cm^{-1} via a FTIR spectrometer (PerkinElmer, Spectrum 400, USA) to investigate the attachment of organic bonding groups on the nanotubes. The samples for FTIR measurements were made into pellets with average diameter of 10 mm, with thickness of 2.8 mm at room temperature.

3.3.6. Thermal Studies

Thermal stability of the a-CNT was investigated using a TGA instrument (TGA/SDTA 851^{c} – Mettler Toledo) at heating rate of 10 ℃ per minute in temperature range of 40 – 1000 ℃. The measurement was conducted in argon atmosphere, where all samples with weight of about 10 mg were used for this thermal analysis. Results presented in TGA

spectra were then analyzed with the V8.10 STAR e software package. The rate of weight losses and temperature characteristic of weight losses experienced by the samples would determine their thermal strengths and stabilities.

3.3.7. Electrical Studies

The electrical impedances analyses of all samples were obtained using Impedance Spectroscopy (IS, Hioki Hitester 3532). The frequency range was set from 50-5, 00,000 Hz, taking 500 measurements per sample, where each measurement was taken every 1 second. The obtained data were plot as Nyquist plots and resistances of all samples were taken when the frequency of alternating current is zero ($\omega=0$). The resistivity values of all samples were then calculated by using the thickness and diameter of all samples. The electrical transference number study carried out using Gamry Potentiostat 600 where 5 mV was applied on all samples to investigate the variation of current with time.

CHAPTER FOUR

RESULTS AND DISCUSSION

In this chapter, samples of as-synthesized a-CNT, functionalized a-CNT, and hybridized a-CNT/Au are examined via several analytical techniques. The elemental, optical, thermal and electrical properties of all six samples are discussed. However, microstructural analysis were only performed on as-synthesized a-CNT and hybridized a-CNT/Au samples as functionalization process would not expect changes in crystal structures. Besides, only three samples (as-syntheiszed, functionalized and hybridized a-CNT/Au) are used to investigate their morphological properties as the qualitative investigation on morphological properties of a-CNT treated with different concentrations of gold chloride solutions do not exhibit significant differences.

4.1 Morphological Studies of as-synthesized a-CNT

Figure 4.1 presents both low and high magnifications of FE-SEM images for the as-synthesized a-CNT. The tubular structures are clearly seen in low magnification FE-SEM images (Figure 4.1(a)). The surfaces of tubular structures are observed to be relatively rough and uneven compared to fully crystalline CNT (Banerjee *et al.* 2010) due to amorphous carbon layers formed on the tube's surface. The nanotubes may have agglomerated to each other during the purification of as-synthesized a-CNT. Figure 4.1(b) shows a higher magnification of as-synthesized a-CNT. The open-ended structures are clearly observed in the image. A relatively significant effect upon treated with concentrated acid according to “ends and defect sites” chemistry were observed (Azamian *et al.* 2002).

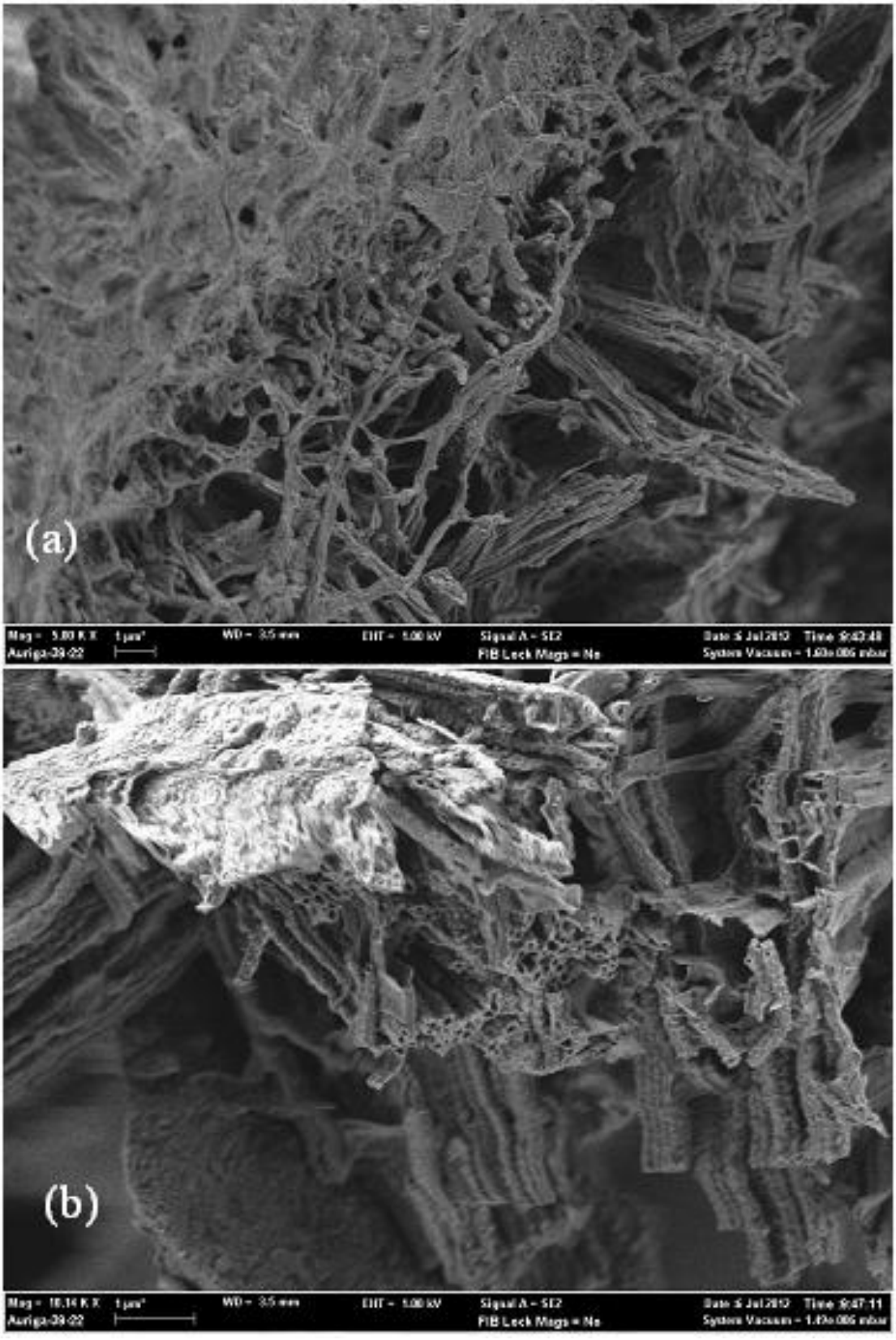

Figure 4.1: FE-SEM images of the as-synthesized a-CNT at different magnification: (a) 5000 X; (b) 10000 X

Figure 4.2 shows the TEM images of as-synthesized a-CNT in low and high magnification. A-CNT is randomly agglomerated among themselves as shown in Figure 4.4(a). This is in a good agreement with FESEM image in Figure 4.1 where as-synthesized a-CNT tends to form bundles and agglomerates. Besides, the open-ended tubes observed in Figure 4.2(b) also well accorded with FE-SEM images in Figure 4.1(b). The a-CNT diameter is relatively large (51.4 nm) which is similar with Liu *et al.* (2007) who produce 50 nm of a-CNT diameter.

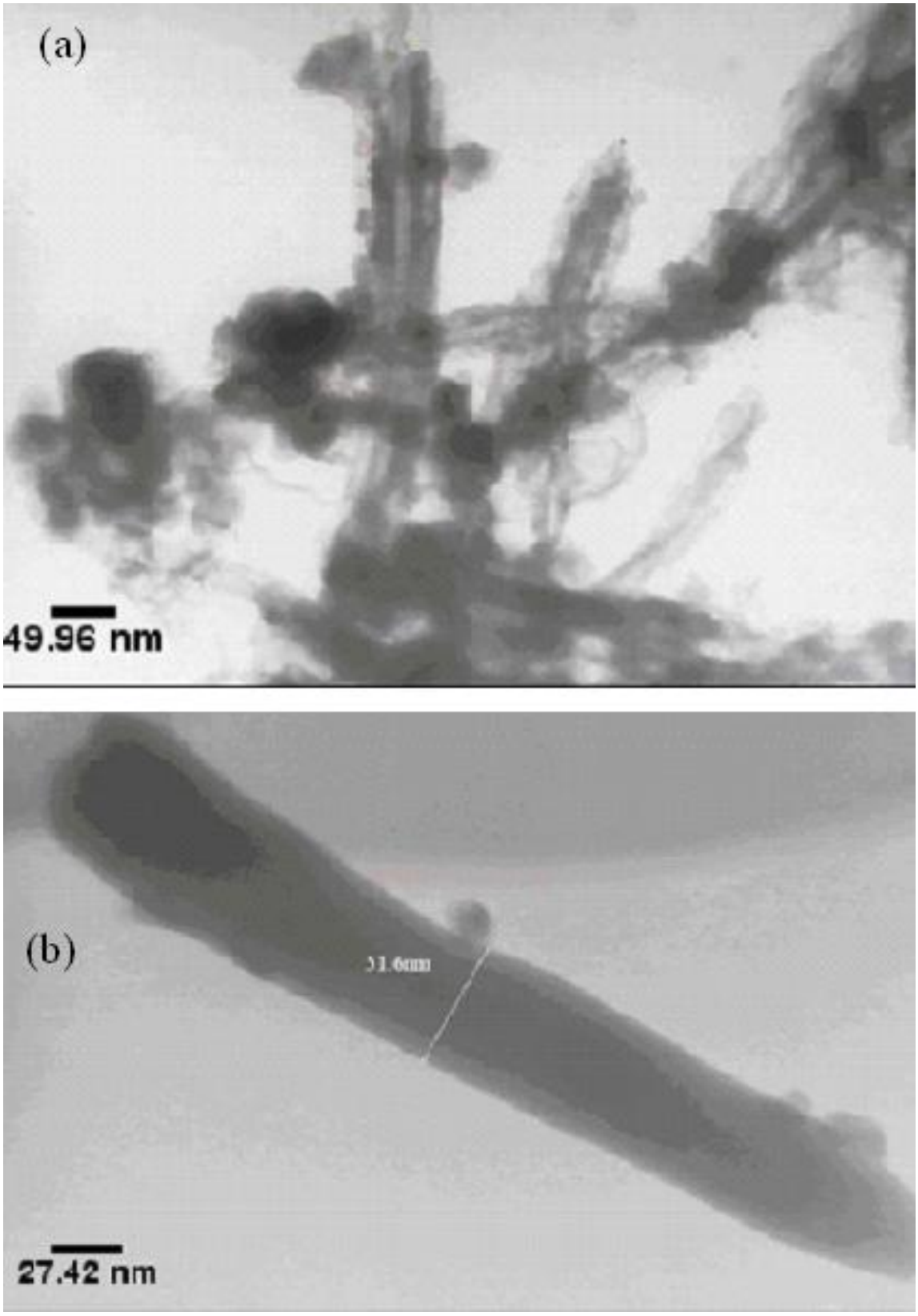

Figure 4.2: TEM images of as-synthesized a-CNT at different magnification: (a) 28000 X; (b) 75000 X.

Figure 4.3 shows the HRTEM image of as-synthesized a-CNT. The dark area in the image corresponds to the amorphous wall of the nanotube as no crystalline pattern being observed. The feature of amorphous is well accord with FE-SEM images in Figure 4.1.

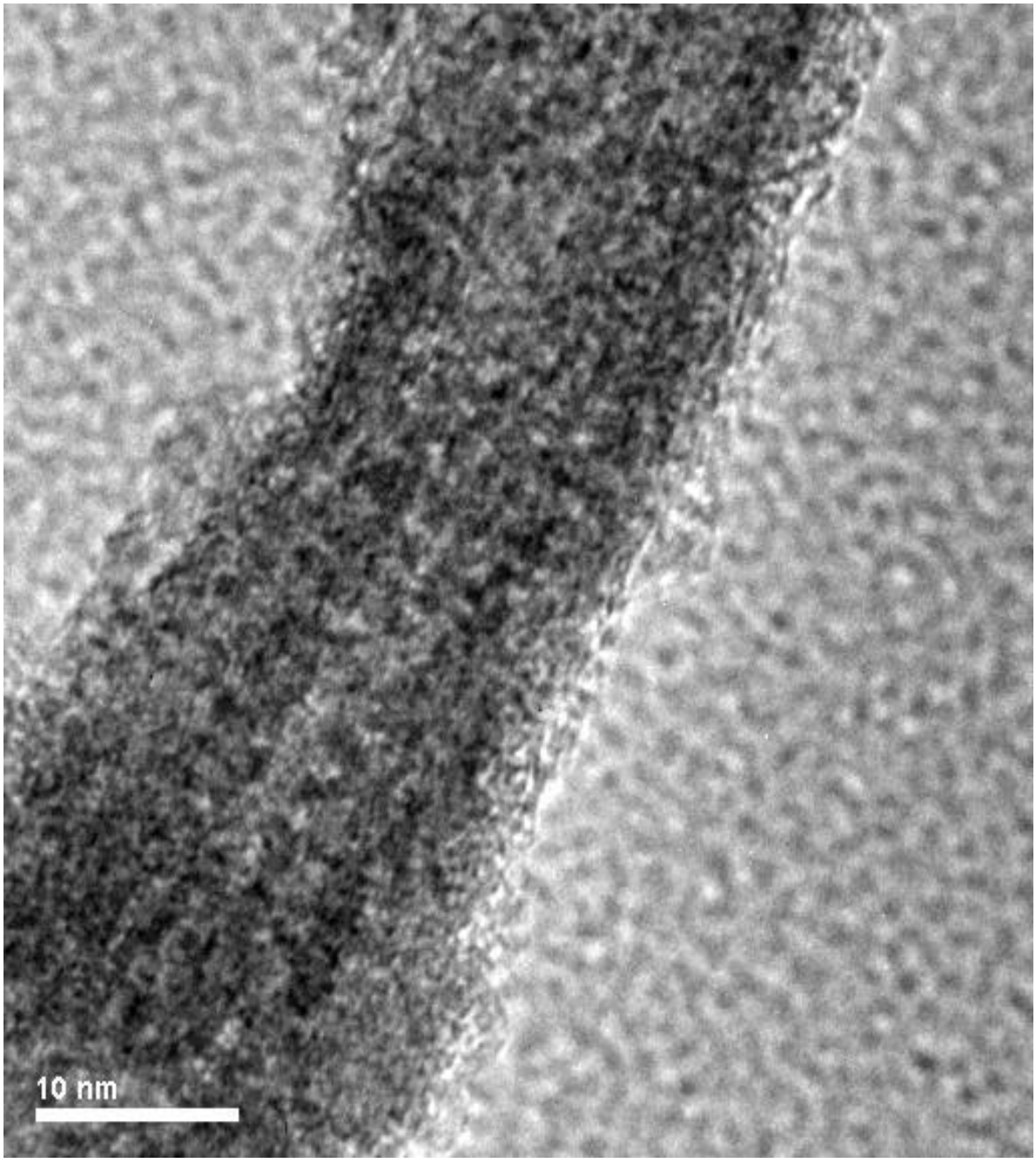

Figure 4.3: HRTEM image of as-synthesized a-CNT

4.2 Functionalization of a-CNT

Zeta potential of as-synthesized and functionalized a-CNT with HNO_3, HCl, $C_6H_8O_7$ and H_2SO_4 is shown in Figure 4.4. HNO_3 functionalized samples has highest zeta potential, followed with H_2SO_4, citric acids, and HCl treated samples of -142.9, -60.3, -15.9 and -3.2 mV respectively. Here HCl functionalized samples have close zeta potential value with as-synthesis a-CNT. The suspensions are tested with both blue and red litmus papers. No change of colours is observed for both litmus papers, indicates the neutrality of the suspensions. As the weight percentages of a-CNT in respective suspensions are relatively low, the negative ends of carboxyl groups do not give significant effect on the acidity of the suspensions. Since zeta potential represent charge amount or number of carboxyl group present (Reed *et al.* 1994), it is preliminary proven that HNO_3 has highest functionalization ability for modification of a-CNT bodies in purpose of dispersion and nanocluster hybridization. The negative values of zeta potential for all samples indicate presence of negative charges on tube's surface due to the negative ends of carboxyl active functional groups (-COOH). The presence of carboxyl functional groups would be further confirmed in FTIR studies.

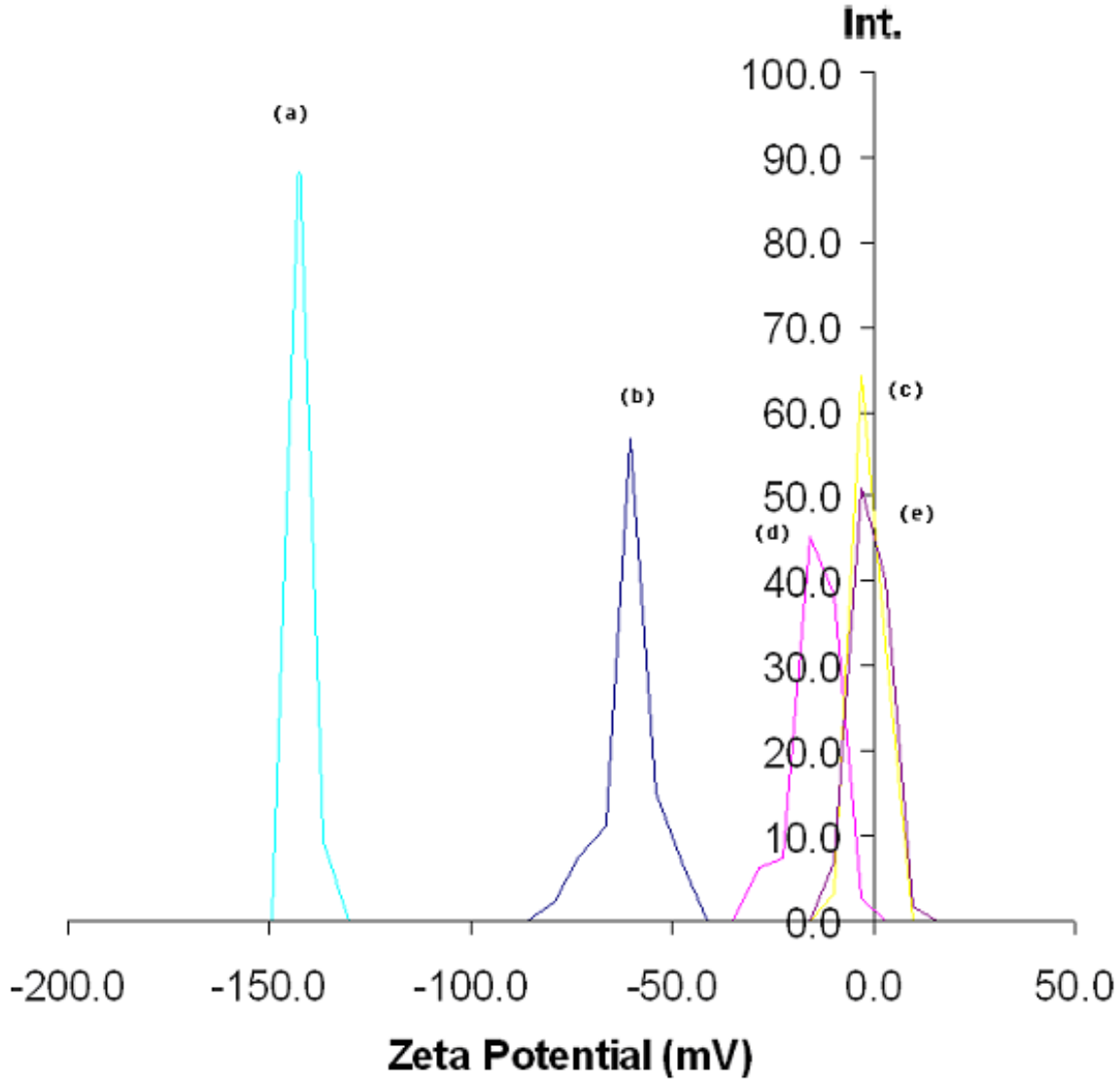

Figure 4.4: Zeta Potential for a-CNT functionalized with (a) HNO_3, (b) H_2SO_4, (c) HCl, (d) Citric Acids and (e) as-synthesis a-CNT

4.3 Morphological studies of modified a-CNT

Figure 4.5 shows the FE-SEM images for the functionalized a-CNT at low and high magnification. The tubular structures can be observed clearly upon functionalizing, and the tubes are separated from each other as compared to as-synthesized a-CNT. The separation of tubes indicates improved dispersion properties in solution due to the electrostatic repulsion of carboxyl groups among CNT. Besides, tubes' surfaces are much smoother and even due to removal of outer-surface's amorphous carbon layers. This agrees well with He *et al.* (2007) where the treatment of a-CNT with nitric acid would remove the amorphous layers (He *et al.* 2007).

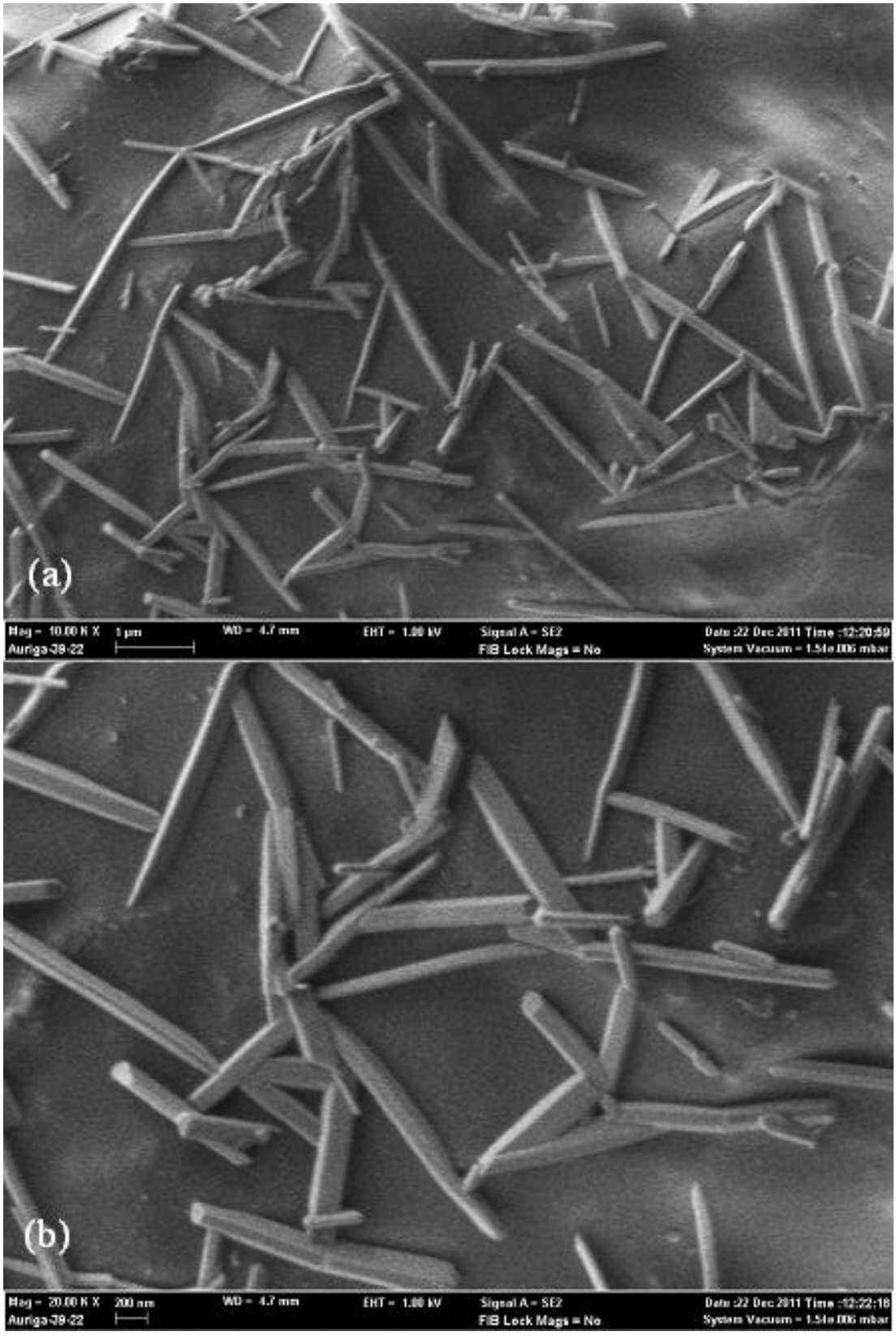

Figure 4.5: FE-SEM images of the functionalized a-CNT at different magnifications: (a) 10000 X; (b) 20000 X

Figure 4.6 shows the TEM image of functionalized a-CNT. The image shows no agglomeration as the nanotubes are hardly attached to each other due to repulsion forces between carboxyl active functional groups. It is observed that the walls of nanotubes are irregular in shape and rough indicates the amorphous structure of tubes sustains even after functionalizing with concentrated acid. These observations are confirmed by the HRTEM image in Figure 4.7. Oxidation treatment conducted on the treated sample by using concentrated acid introduced large amount of defects for the nanotubes (Wiltshire *et al.* 2004). This agrees well with the observations in Figure 4.7. The tube's structure of functionalized a-CNT is observed to be more defective as compared to HRTEM image in Figure 4.3.

Figure 4.6: TEM image of nitric acid functionalized a-CNT

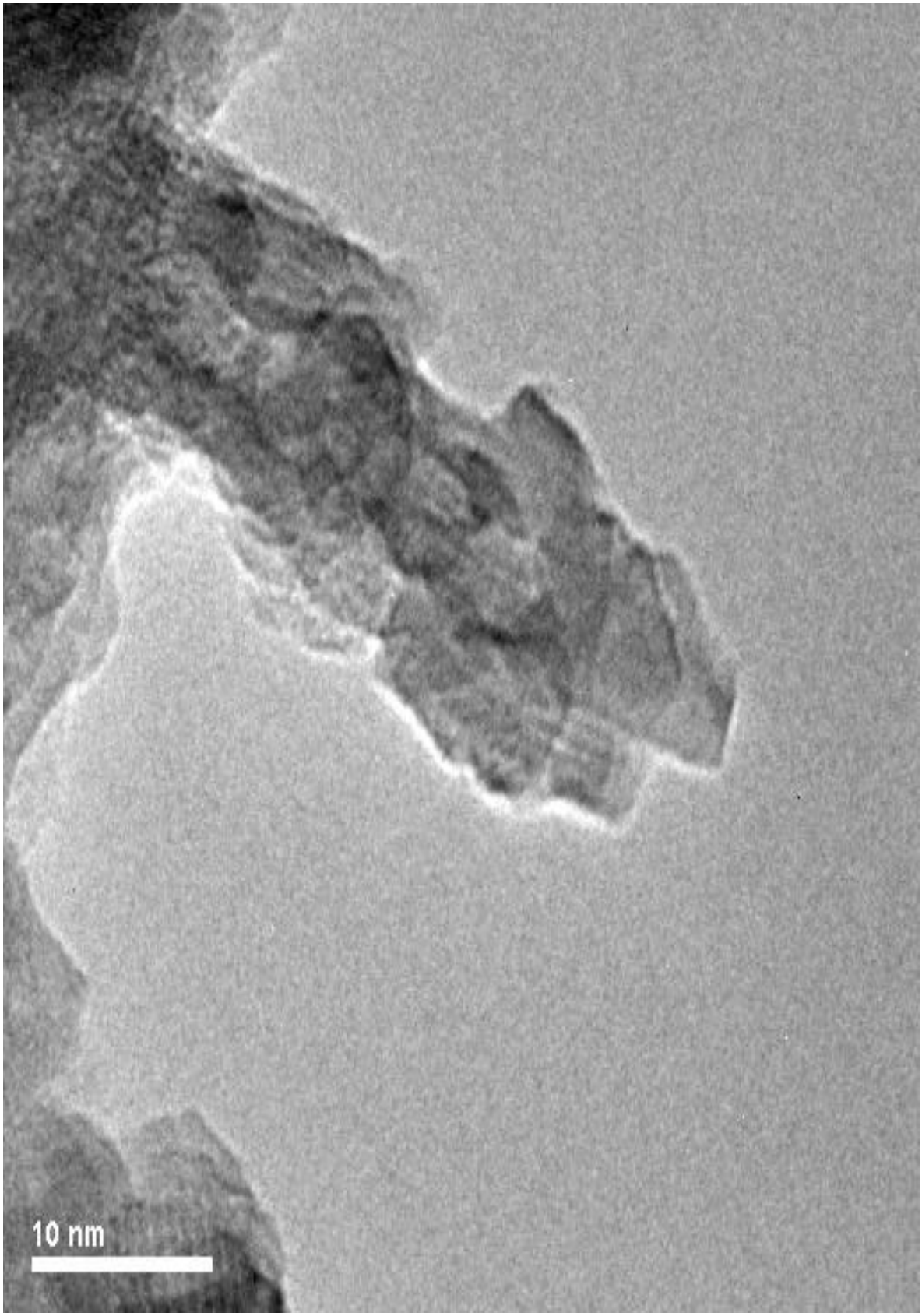

Figure 4.7: HRTEM image of nitric acid functionalized a-CNT

It is important to highlight that the diameter for acid functionalized a-CNT has been reduced to 40 nm as compared to diameter of as-synthesized a-CNT which is measured to be 51.6 nm. The reduction in diameter indicates removal of amorphous carbon layers by nitric acid ultra-sonication, which agrees well with He *et al.* (2007).

Figure 4.8 shows the FE-SEM images of hybridized a-CNT/Au for 10 g/dm^3 $AuCl_3$. From the perspective of geometrical appearances, the images do not show significant differences compared to functionalized a-CNT. However, the powdery texture of tubes' surfaces is preliminary to be predicted as the consequence of gold particles decoration. The powdery texture can be clearly seen in Figure 4.8(b) where the surfaces are slightly rough as compared to functionalized a-CNT.

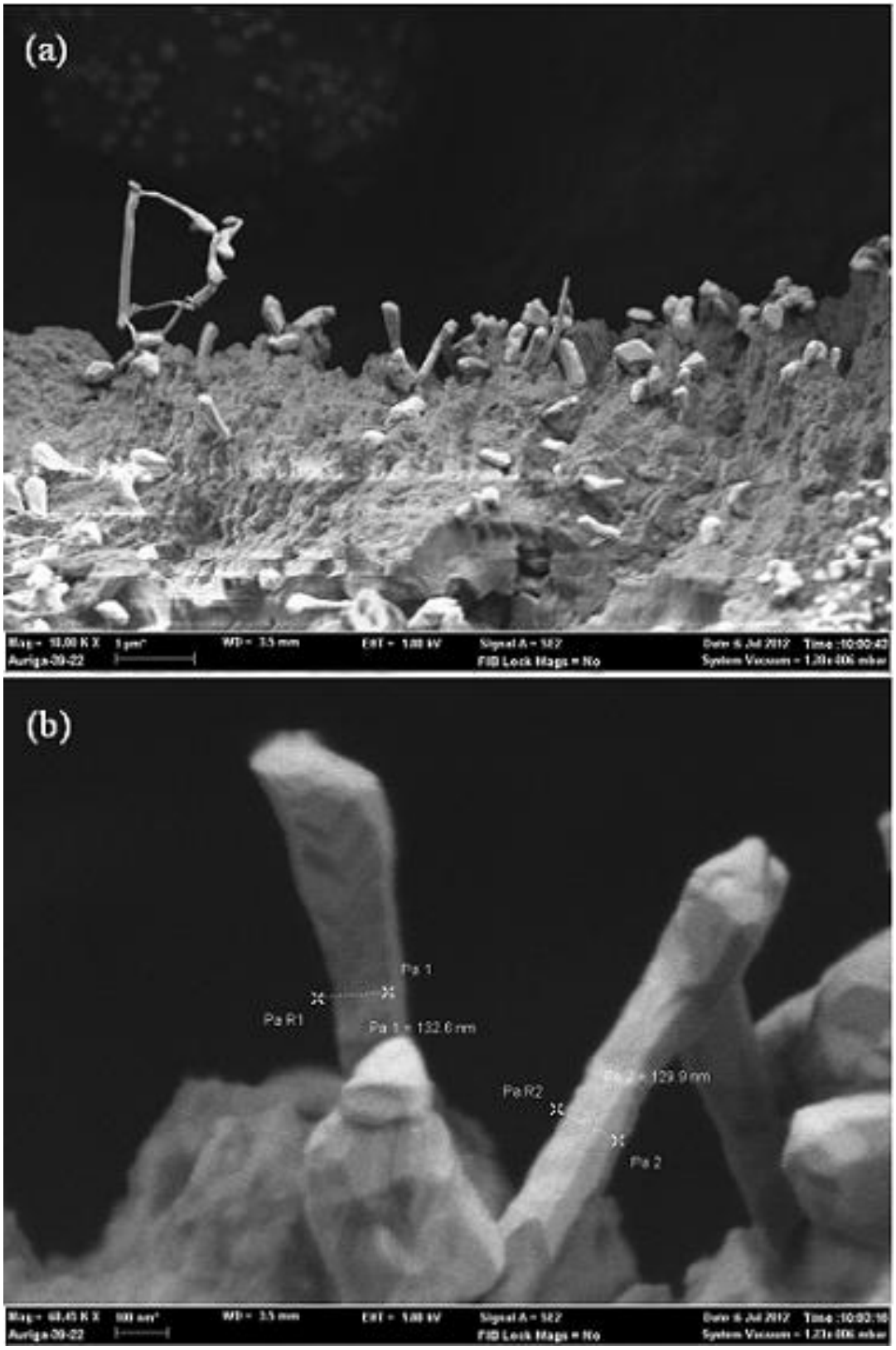

Figure 4.8: FE-SEM images of hybridized a-CNT/Au at different magnifications: (a) 10000 x magnifications; (b) 70000 x magnification

Figure 4.9 shows the HRTEM images of hybridized a-CNT/Au of low and high magnification. The diameter of nanotube is further reduced upon treated with gold chloride solution. In Figure 4.9(a), the inner and outer diameter is 6.1 and 10.2 nm, respectively with the wall thickness of about 2.1 nm. The reduction of diameter is due to high defective structures formed upon attachment of gold particles. It is important to note that even and well-ordered fringes are formed as shown in Figure 4.9(a), indicating the successful attachment of crystalline gold particles on tube's body (Tello *et al.* 2008). However, the actual crystalline structure of gold on the tube's body needs to be determined via X-Ray diffraction study. Figure 4.9(b) shows agglomeration features of gold particles decorated a-CNT, where tubes tend to re-agglomerate due to attractive force. According to Section 2.4.5, attachment of gold particles on CNT bodies are initiated by the electrostatic force between gold cations and negative ends of carboxyl groups on CNT. Therefore, successful attachment of gold particles on tubes' bodies would hinder the negative ends of carboxyl groups on tubes' body, and therefore reduced the repulsive force between nanotubes.

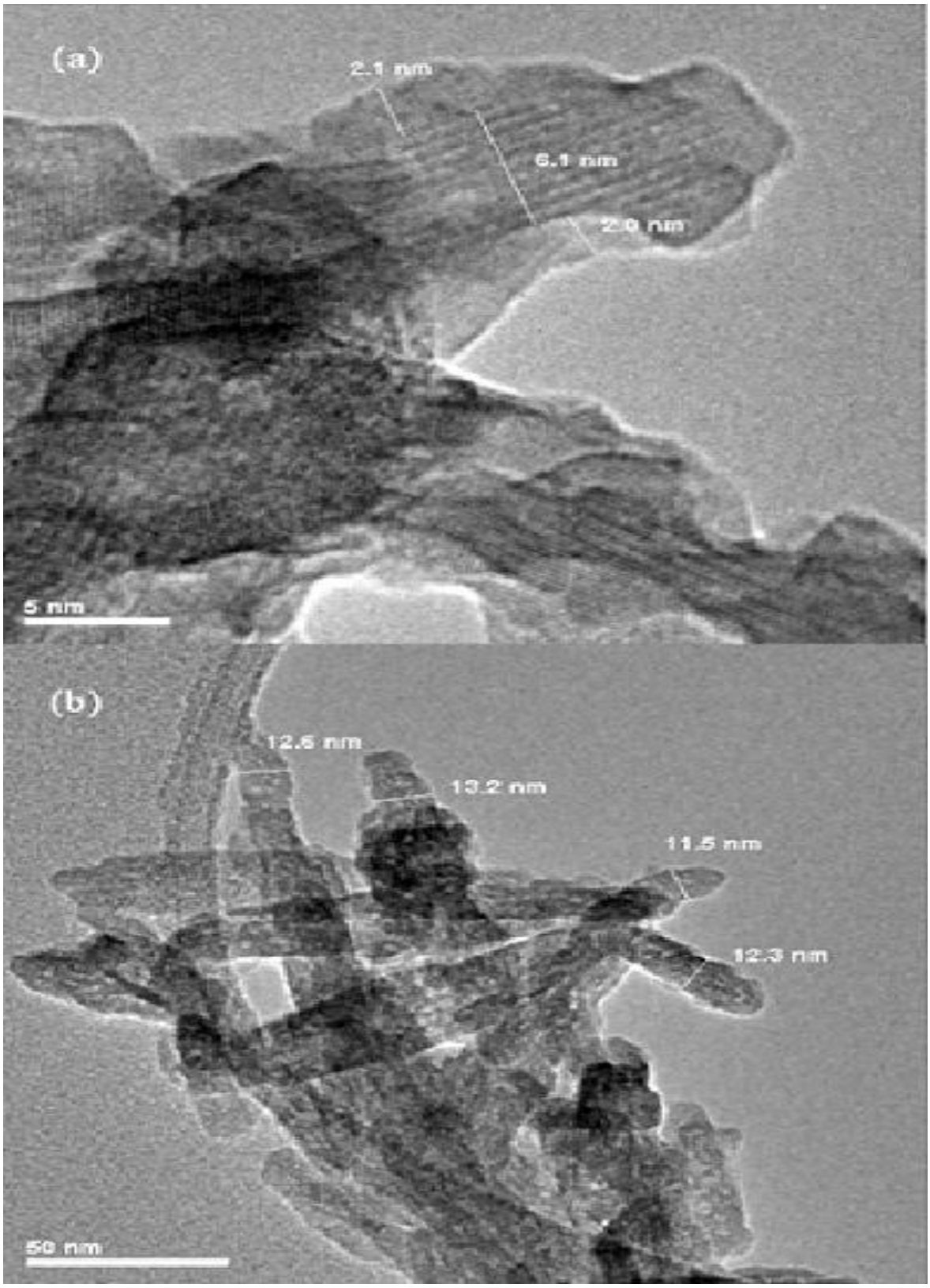

Figure 4.9: HRTEM images of hybridized a-CNT/Au at different magnification: (a) 4,000,000 X; (b) 400,000 X.

4.4 Microstructural Studies

Figure 4.10 displays the XRD patterns for as-synthesized a-CNT and hybridized a-CNT/Au. There is no diffraction peak being detected in the XRD pattern of the as-synthesized a-CNT indicates complete removal of iron residuals resulted from ferrocene. Besides, broad peaks with relatively low intensity indicate amorphous phase of as-synthesized a-CNT. This is well agrees with the previous FE-SEM images.

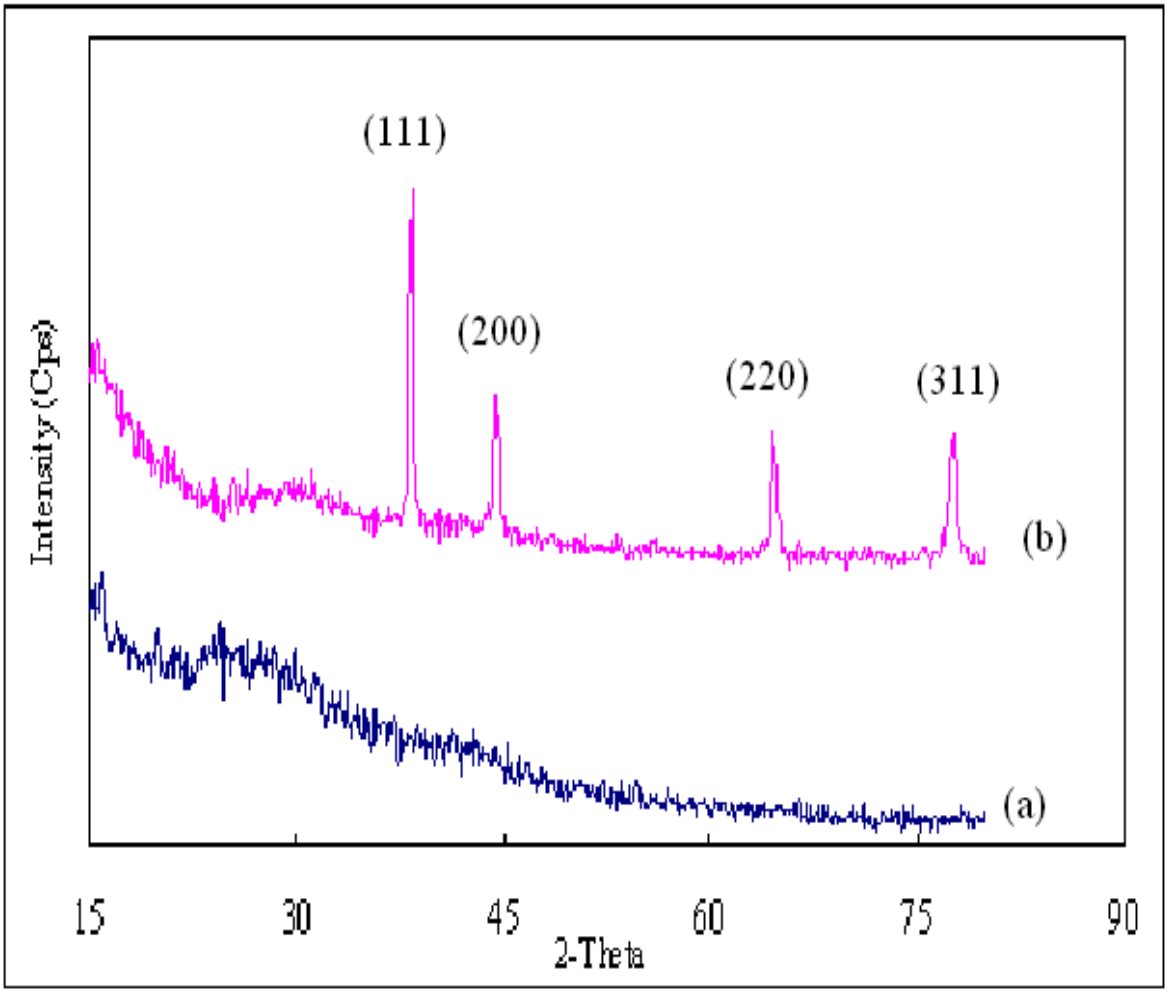

Figure 4.10: XRD patterns for (a) as-synthesized a-CNT; and (b) hybridized a-CNT/Au

XRD pattern for hybridized a-CNT/Au shows relatively sharp peaks at 2θ angle of 37.5 °, 45 °, 65 ° and 77 ° corresponding to diffraction from (111), (200), (220) and (311) planes, respectively. The interplanar spacing (d_{hkl}) as calculated from HRTEM, XRD, and their respective lattice constant (a) are summarized in Table 1. The peaks correspond from (111), (200) and (220) indicates formation of gold nanocubes with lattice constant of 4.11 Å (Huang *et al.* 2006). However, a peak due to diffraction from (311) plane appears with calculated lattice constant of 6.83 Å indicates the detection of a relatively long lattice constant atomic plane apart from gold nanocubes. The resulting shape of gold particles formed on a-CNT is predicted to be in nanoboots form with crystal structure of fcc (JCPDS 4-0783; Hu *et al.* 2007). The formation of crystalline gold particles on a-CNT bodies agrees well with the observations on HRTEM images of hybridized a-CNT/Au, where even and ordered fringes found on the tube's body.

Table 4.1: Interplanar spacing (d_{hkl}) from HRTEM, XRD and lattice constant (a) with corresponding (*hkl*) values of gold particles

d_{HRTEM} (Å)	d_{XRD} (Å)	(hkl)	a (Å)
2.25	2.37	(111)	4.11
1.96	2.06	(200)	4.12
1.38	1.43	(220)	4.05
2.05	2.06	(311)	6.83

4.5 Elemental Studies

Figure 4.11 shows the EDX spectra for all samples. The respective weight percentages for the elements are presented in Table 4.1. The dominant element for all samples is carbon, due to the formation of a-CNT via the synthesis method. The presence of oxygen indicates that as-synthesized a-CNT and functionalized a-CNT have been oxidized to some extent. The oxidation of as-synthesized a-CNT occurred during the washing and purifying process with HCl, where the sample was slightly oxidized. As compared to as-synthesized a-CNT, functionalized a-CNT reflects higher oxygen content. During the functionalization process, the nanotubes are chemically modified and attached with active carboxyl functional groups. This explains the higher oxygen content of functionalized a-CNT.

The presence of gold elements in the $AuCl_3$ solution treated a-CNT provides a good evidence for the successful hybridization between a-CNT and gold particles (Figure 4.11(c-f)). It is seen that the gold content in the sample increases with increasing concentration of $AuCl_3$. The presence of iron (Fe) in the samples was due to the residual of Fe particles from ferrocene and the presence of Nitrogen (N) was due to the residual ammonium chloride while synthesizing a-CNT. However, the presence of Fe is not reflected in XRD as the relative weight percent are low and insignificant as compared to gold content. Presence of chloride (Cl) caused by two factors, which are residual hydrochloric acid (HCl) during washing and purification of a-CNT, and residual Cl particles from $AuCl_3$ solution. The presence of carbon peak in the EDX spectra for all samples may also originate from carbon-based contaminations from the FE-SEM chamber.

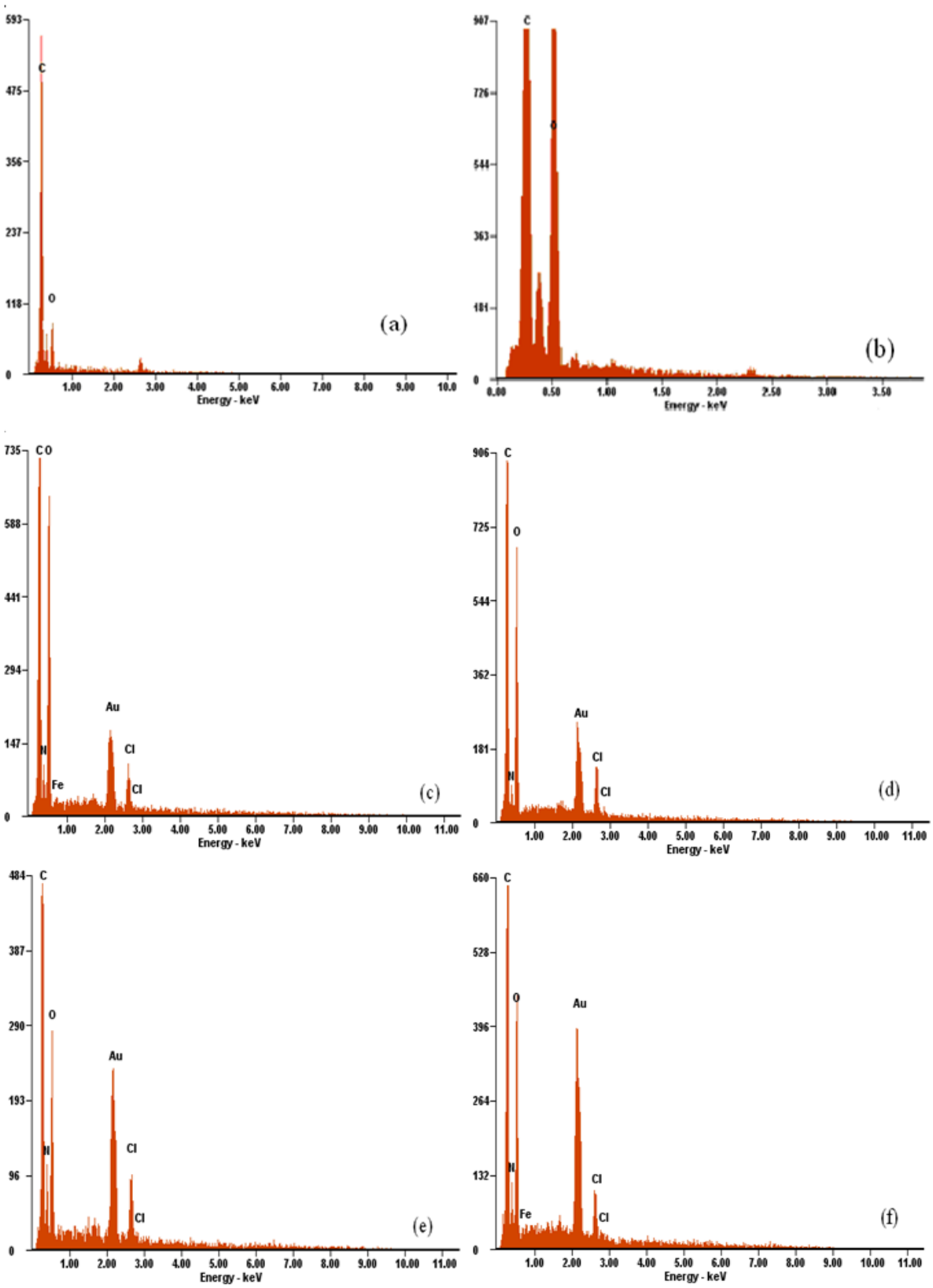

Figure 4.11: EDX spectra of a-CNT for (a) as-synthesized; (b) functionalized; (c) 2.5g/dm^3; (d) 5g/dm^3; (e) 7.5g/dm^3; (f) 10g/dm^3 $AuCl_3$ solution treated

Table 4.2: EDX Elemental analysis for all samples

a-CNT	C(wt%)	O(wt%)	Fe(wt%)	Au(wt%)	Cl(wt%)	N(wt%)
As-synthesized	61.36	9.1	0	0	16	13.55
Functionalized	50.29	33.76	0	0	2.77	13.19
2.5 g/dm^3 $AuCl_3$ Solution Treated	43.36	24.52	2.95	17.7	3.79	7.67
5 g/dm^3 $AuCl_3$ Solution Treated	47.2	22.51	0	19.38	5.01	5.9
7.5 g/dm^3 $AuCl_3$ Solution Treated	39.98	14.64	0	28.96	5.23	11.18
10 g/dm^3 $AuCl_3$ Solution Treated	38.09	14.49	1.62	33.47	3.33	9

4.6 FTIR Studies

Figure 4.12 shows the FTIR spectra for as-synthesized and functionalized a-CNT with HNO_3, HCl, $C_6H_8O_7$ and H_2SO_4. The peak at about 1678cm^{-1} shows the presence of C=O stretch. This proves the presence of carboxyl groups. A tiny peak is observed at about 1168cm^{-1} corresponding to C-O stretch. However, the O-H stretch broad peaks of citric acid and HCl functionalized a-CNT are relatively small indicates lower abundance of –OH group presents. C-O, O-H and C=O stretches presences prove the successful formation of carboxyl groups, -COOH, on the tubes' bodies. The overall absorption of citric acids and HCl treated a-CNT are significantly lower than HNO_3 and H_2SO_4 functionalized a-CNT. At the same time, the absorption of as-synthesized a-CNT is much lower compared to functionalized a-CNT. The peaks of –COOH group are not found at as-synthesized a-CNT spectrum. However, amide (-NH) and nitrile (-C≡N) functional groups formed in 3500-3700 and 2220-2260 cm^{-1}, respectively indicate the presences of nitrogen. The

presences of nitrogen are due to residuals from NH_4Cl. This supports the finding in EDX elemental analysis for as-synthesized a-CNT.

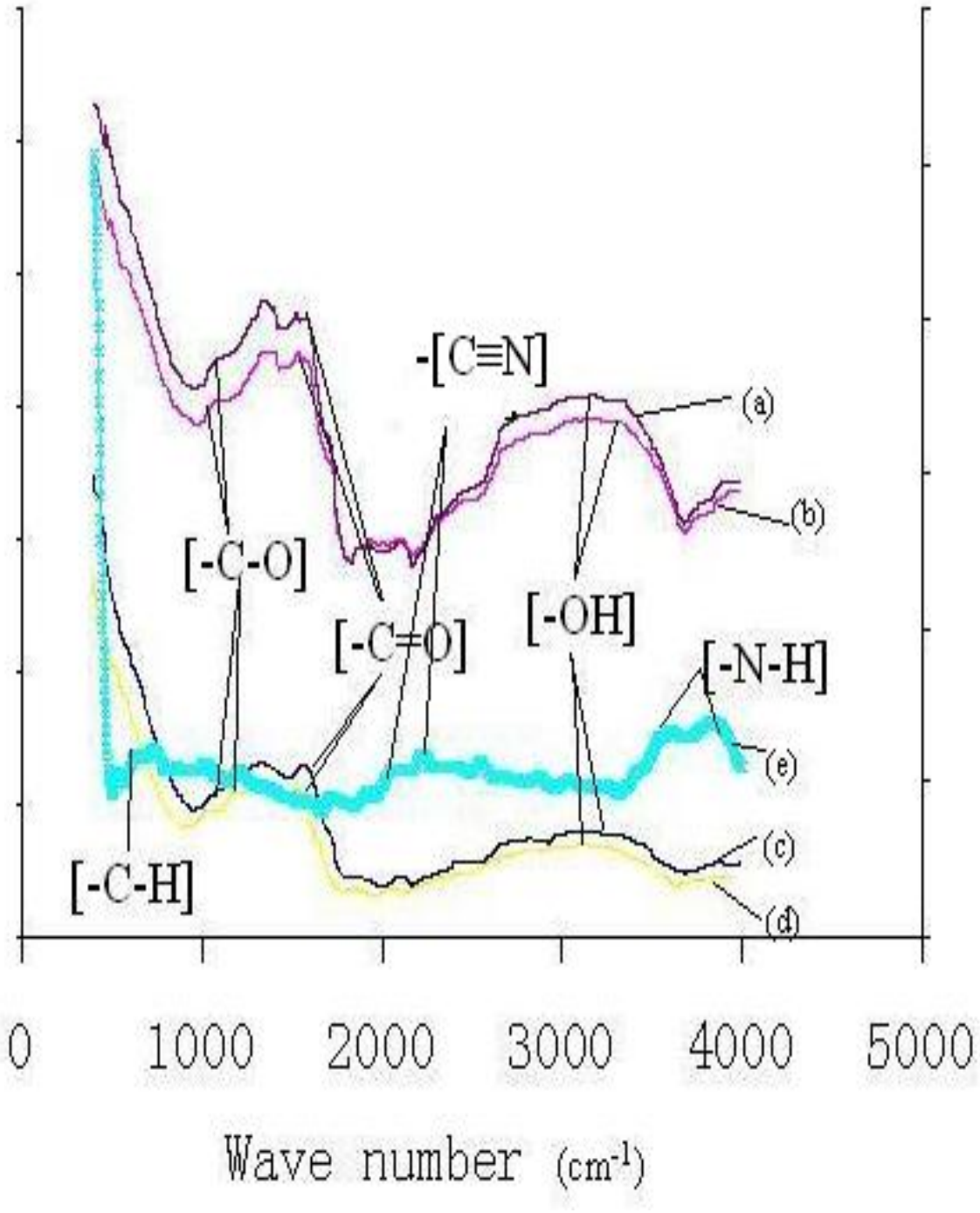

Figure 4.12: FTIR spectra for a-CNT functionalized with (a) HNO_3, (b) H_2SO_4, (c) Citric Acid, (d) HCl and (e) as-synthesis a-CNT

The broad peak observed in the 2746-3472 cm^{-1} region corresponds to the hydroxyl group (-OH) for functionalized a-CNT. This band is attributable to the deformation vibration of water molecules. Exposure of samples to air initiates the absorption of moisture where attachment of –OH groups occurred towards the amorphous walls of nanotubes. This phenomenon is obvious for the functionalized sample that possessed higher amount of defects during oxidation (Wiltshire *et al.* 2004; Azamian *et al.* 2002). However, no peak corresponds to –OH groups appear for the as-synthesized a-CNT. This implies that the moisture absorption is relatively insignificant in as-synthesized a-CNT. It is suggested that the structure is less defective as compared to functionalized a-CNT, where less moistness are trapped within the tubes as compared to functionalized a-CNT.

Combining the results of FTIR and zeta potential, it reflects that HNO_3 exhibits the most effective functionalization characteristic where it creates most –COOH groups on a-CNT. Therefore, nitric acid is selected as the main oxidation agent in functionalization of a-CNT throughout the whole study.

4.7 Optical Studies

Figure 4.13 shows the UV-Vis absorption spectra of all samples in the range of 200-400 nm, all samples exhibit similar absorption characteristics. Functionalized a-CNT shows higher absorption wavelength and an extra peak at 300 nm as compared to as-synthesized a-CNT. This indicates relatively high absorbance upon functionalizing. Spectra for hybridized a-CNT/Au shows a peak shoulder at wavelength ranging from 306-312 (Zhang *et al.* 2008). However, the concentrations of the $AuCl_3$ solution used in treating a-CNT have not shown significant effects on its optical absorption properties. This

is probably due to the low concentration of gold particles modified a-CNT in methanol suspension while preparing samples for UV-Vis scanning. Relatively low weight percentage of Au-decorated a-CNT hinders the effects of gold content in the samples towards the optical absorption properties. In spite of that, the absorption wavelength of hybridized a-CNT/Au increases significantly compared to functionalized and as-synthesized a-CNT, representing a significant change of optical absorption properties upon decoration of gold particles.

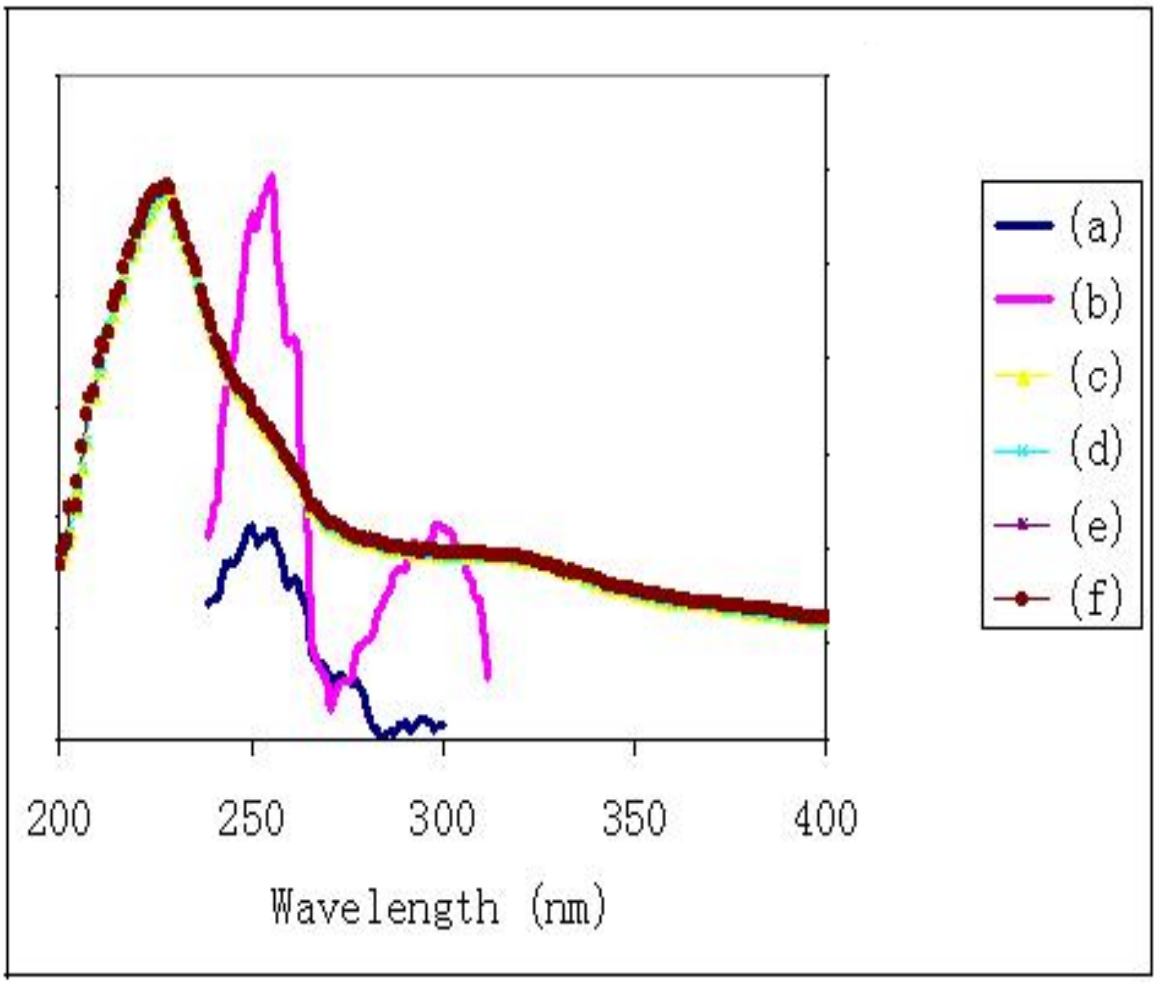

Figure 4.13: UV-Vis absorbance spectra for (a) as-synthesized; (b) functionalized; (c) 2.5 g/dm^3 (d) 5 g/dm^3 (e) 7.5 g/dm^3 (f) 10 g/dm^3 $AuCl_3$ solution treated; a-CNT.

The optical band gap (E_g) for the a-CNT is calculated by using Tauc/Davis-Mott model (Li *et al.* 2009). The relation between E_g and optical absorption is expressed by Equation (4.1)

$$(\alpha h\nu)^n = B(h\nu - E_g) \quad (4.1)$$

where B is a constant, $h\nu$ is the photon energy of the incident light and n is the characterization index for the type of optical transition. The absorption coefficient (α) is defined by the Lambert-Beer law:

$$\alpha = -\ln A / t \quad (4.2)$$

where A is the absorbance and t is the sample thickness. E_g can be obtained from the extrapolation of the linear parts of the curves for $(\alpha h\nu)^n$ against $h\nu$ where absorbance is zero near the band edge region.

The value of n = 2 is selected to obtain the suitable Tauc/Davis-Mott plots as the samples are mainly consist of amorphous structures (Li *et al.* 2009). The Tauc/Davis-Mott plots for all samples are plotted in Figure 4.14. The observed phenomenon as previously discussed agrees well with the optical band gaps obtained from the Tauc and Davis-Mott model.

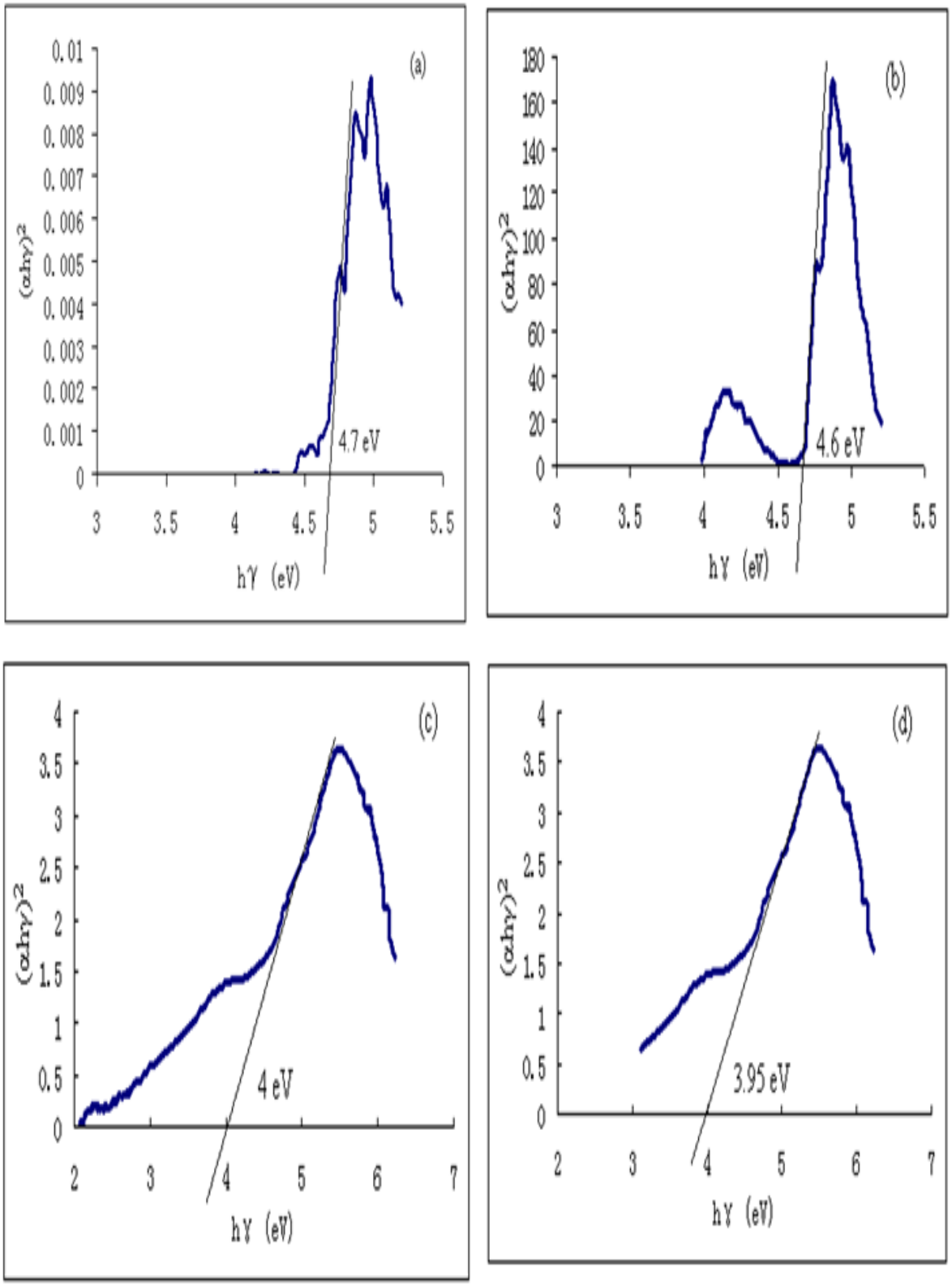

Figure 4.14: Tauc/Davis-Mott plots for (a) as-synthesized; (b) functionalized; hybridized with (c) 2.5 g/dm^3 (d) 5 g/dm^3; (e) 7.5 g/dm^3; (f) 10 g/dm^3 $AuCl_3$ solution.

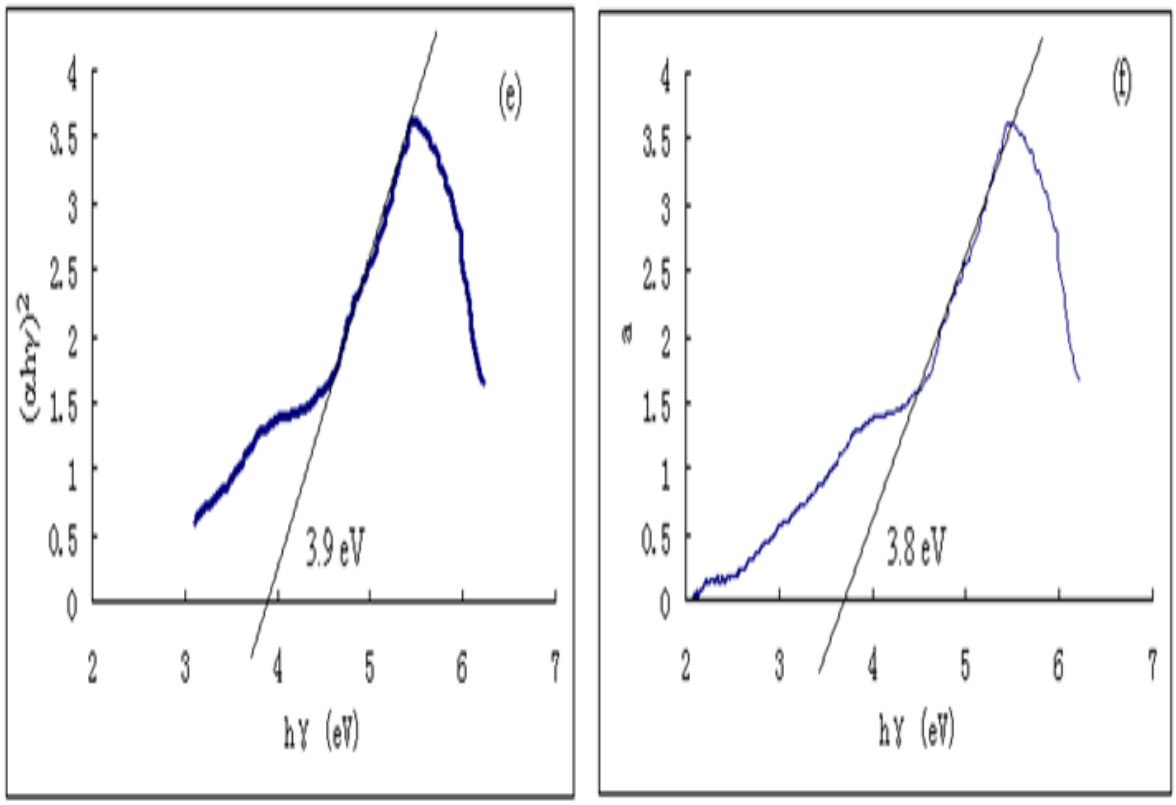

(Continued)

Table 4.3 summarizes the data obtained from both experimental UV-Vis spectra and the computed Davis-Mott model. It is observed that a-CNT have similar absorption behavior with crystalline CNT since their absorption peaks fall in the same range (Kataura *et al.* 1999). E_g values of a-CNT decreases slightly upon functionalizing with concentrated HNO_3, and further decreases upon hybridized with gold particles. Note that E_g values of hybridized samples do not shows a significant changes with gold content presents. In spite of insignificant changes in E_g, it shows a slight decreasing trend of E_g values as gold content in the samples increases. As band gap energy has a direct impact on the electrical conductivity of the samples, decreasing in band gap energies indicates increases in electrical conductivity. However, as the sample concentration prepared for UV-Vis scanning is low (0.03 wt %), the effects of gold content is insignificant. The respective electrical

conductivity of all samples would be discussed in further section.

Table 4.3: Absorption wavelength and E_g values

Sample Name (a-CNT)	Absorption Wavelength (nm)	*Eg* (eV)
As-synthesized	250	4.7
Functionalized	255	4.6
2.5 g/dm^3 $AuCl_3$ solution treated	306	4
5 g/dm^3 $AuCl_3$ solution treated	307	3.95
7.5 g/dm^3 $AuCl_3$ solution treated	309	3.9
10 g/dm^3 $AuCl_3$ solution treated	312	3.8

4.8 Raman Studies

Figure 4.15 displays the Raman characteristics (D- and G-bands) for all samples at room temperature. It is apparent that all a-CNT samples possess the similar raman features of crystalline CNT (Lou *et al.* 2003). However, D-bands of a-CNT are relatively broader compared to crystalline CNT (Lou *et al.* 2003) due to structural defects. The presence of the D-band for all samples infers the amorphous structure of nanotubes. Meanwhile, presence of G-band indicates the existence of crystallinity in the structure of a-CNT due to the sp^2 bonded carbon atoms.

Functionalized a-CNT shows a broader D-band as compared to that of the as-synthesized a-CNT. This indicates that a higher concentration of defects occurred in the functionalized a-CNT. Poor structural ordering and a higher concentration of defects are

attained as the oxidation treatment leads to amorphization of the nanotubes' structure. After the oxidation treatment, the structure of nanotubes were destroyed by introducing a large amount of defects (Wiltshire *et al.* 2004). However, the defects are not uniformly distributed along the nanotube walls. As for gold hybridized samples, the D-band becomes broader as compared to pure a-CNT. The relatively broad D- and weak G-band indicate that the hybridized samples are composed of almost amorphous carbon atoms. In other words, the hybridized sample is rich with unsaturated carbon atoms at degree of high disorder with dangling bonds (Yu *et al.* 2006).

The D- and G-bands, and their ratios for all samples are shown in Table 4.4. The D/G ratio of hybridized samples increase with increasing concentration of gold chloride ($AuCl_3$), revealing the disordered carbon in tubes' walls and. Many structural defects are introduced along the nanotube walls during the solution treatment and it contributes to more formation of amorphous nanotubes. The effect of introducing structural defects on tube's wall is more significant as concentrations $AuCl_3$ of in solution treatment increases. The increase of D/G ratio implies that the number of the sp^2 bonded carbon atoms without dangling bonds have decreased. Thus both of oxidation and solution treatment processes substantially reduce the crystallinity of nanotubes. The increases of defective structures supports the HRTEM observations in Figure 4.8, where reduction of diameter upon attachment of gold particles on a-CNT is due to further introduction of defective sites.

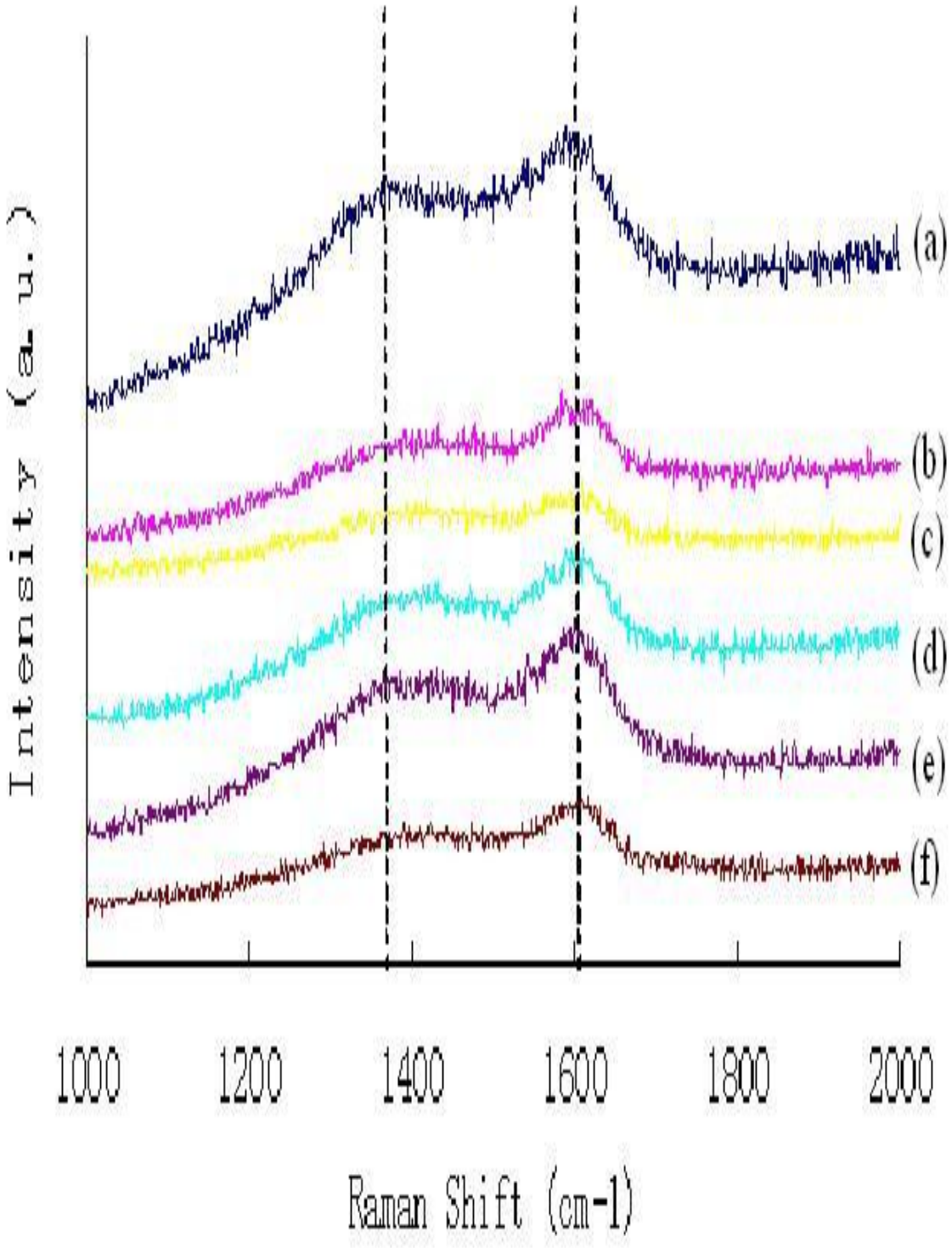

Figure 4.15: Raman Spectra of (a) as-synthesized; (b) functionalized; (c) 2.5 g/dm^3; (d) 5 g/dm^3; (e) 7.5 g/dm^3; (f) 10 g/dm^3 $AuCl_3$ solution treated; a-CNT

Table 4.4: The corresponding peaks' frequency (Raman shift) for all samples in Raman Spectra

Sample Name (a-CNT)	D-band (cm^{-1})	G-band (cm^{-1})	D/G ratios
As-synthesized	1363.83	1588.98	0.964
Functionalized	1389.33	1602.75	1.36
2.5g/dm^3 solution treated	1393.57	1608.26	1.53
5g/dm^3 solution treated	1387.91	1596.56	1.58
7.5g/dm^3 solution treated	1385.08	1586.22	1.62
10g/dm^3 solution treated	1389.33	1604.13	1.7

4.9 Thermal Studies

Figure 4.16 shows the TGA results of all samples while Table 4.5 summarizes the results. All samples undergoes weight loss as temperature rises. The first weight loss occurred during Stage 1 due to the evaporation of adsorptive moisture in the samples. Then, samples would undergo Stage 2 where decomposition of oxygen-containing groups, such as, hydroxyl, and carbonyl, etc occured. At Stage 3, the weight loss involves the decomposition of CNT (Hu *et al.* 2011). Functionalized a-CNT possesses a larger weight loss during Stage 3 compared to the as-synthesized a-CNT. This indicates higher purity of a-CNT, where excessive impurities and amorphous carbon layers were removed. However, hybridized samples show the smallest weight loss.

As the gold content in a-CNT increases, the relative weight percentage of a-CNT in the sample was reduced in Stage 3. The stabilized masses of samples after Stage 3 can be use to determine the residuals after decomposition of a-CNT. For hybridized samples, the

residuals' weight after CNT decomposition can be used to estimate gold content in the samples (Vermisoglou *et al.* 2009). Residuals of functionalized sample show a 3%, lower than as-synthesized a-CNT with 6% of residuals. The reduction is due to removal of amorphous carbon layers of as-synthesized a-CNT. In other words, there are still 3% of amorphous carbon residuals in functionalized sample after ultrasonicating with nitric acid. As solution treatment was performed on functionalized a-CNT, the weight percentages after Stage 3 of hybridized samples are predicted to be mixture of amorphous carbon residuals from functionalized sample and gold particles. Therefore, the weight percent of gold content can be calculated by subtracting 3% (residuals' weight percentage of functionalized sample after T_s) from weight percentages after T_s for gold modified a-CNT respectively. The obtained values are slightly higher than gold content indicated by EDX results. The additional weight percentage can be due to gold particles that are unattached to the tubes' bodies and remains after washing with distilled water.

Overall, all samples undergo Stage 1 in the temperature range of 40-120 ℃. The variation of weight loss in Stage 1 by different samples indicates a difference in moisture content. The same applied to Stage 2 where decomposition of oxygen-containing groups varies with moistness and abundance of oxygen-containing groups in the samples. As compared to as-synthesized a-CNT, functionalized a-CNT shows higher decomposition temperature and stability temperature of 373 and 826 ℃, respectively. These results are in accordance with Hsieh *et al.* (2010) where addition of carboxyl groups on CNT bodies would increase the decomposition temperature and hence indicates enhancement of thermal stability of CNT. However, hybridized samples possessed lower decomposition and stability temperature as compared to functionalized a-CNT, which indicates an inferior thermal stability. As for oxidation temperatures, as-synthesized a-CNT shows the highest

oxidation temperature at 497 ℃, which reduces to 395 ℃ upon functionalizing. The oxidation temperatures curves of derivatives shifted to a direction of lower temperature when gold particles attached to tubes' bodies, which supports the earlier findings (Zhang *et al.* 2000; Mizoguti *et al.* 2000). As high values of T_o, T_s, and T_c indicates better thermal stability (Zhang *et al.* 2000), 7.5 g/dm^3 $AuCl_3$ solution treated a-CNT has best thermal stability compared to a-CNT treated with $AuCl_3$ solution at other concentrations. Although stability temperature, T_s, of 7.5 g/dm^3 $AuCl_3$ solution treated a-CNT is slightly lower than 5 g/dm^3 $AuCl_3$ solution treated a-CNT, however; it shows highest oxidation temperature and decomposition temperature among a-CNT treated with other concentrations of $AuCl_3$ solutions, which indicates outstanding thermal stability. Therefore, it is proven that 7.5 g/dm^3 is ther most optimum concentration of $AuCl_3$ in solution treatment of a-CNT in order to achieve high thermal stability.

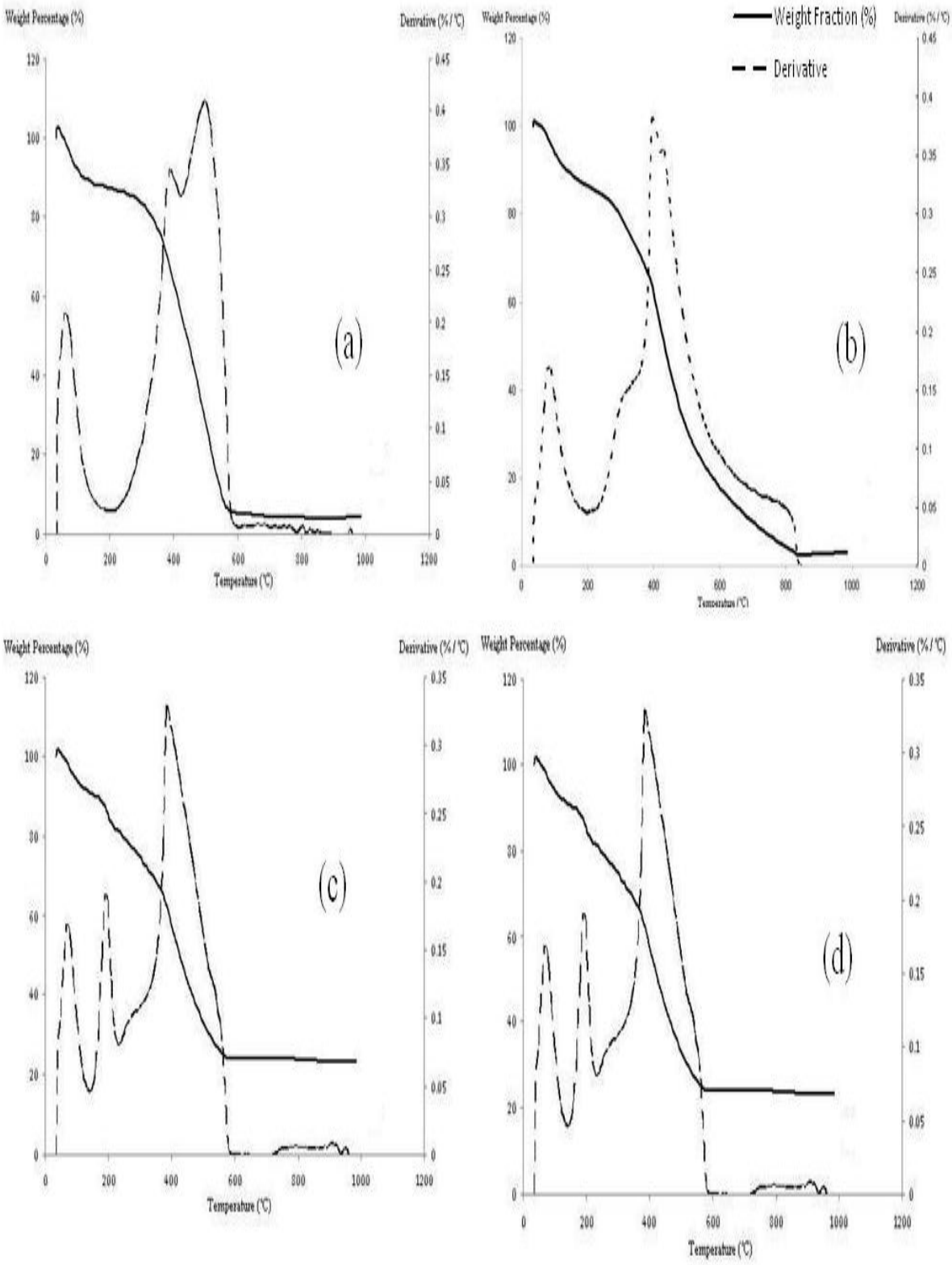

Figure 4.16: TGA curves and its derivative of (a) as-synthesized; (b) functionalized; hybridized with (c) 2.5 g/dm^3; (d) 5 g/dm^3;(e) 7.5 g/dm^3; (f) 10 g/dm^3 $AuCl_3$ solution a-CNT

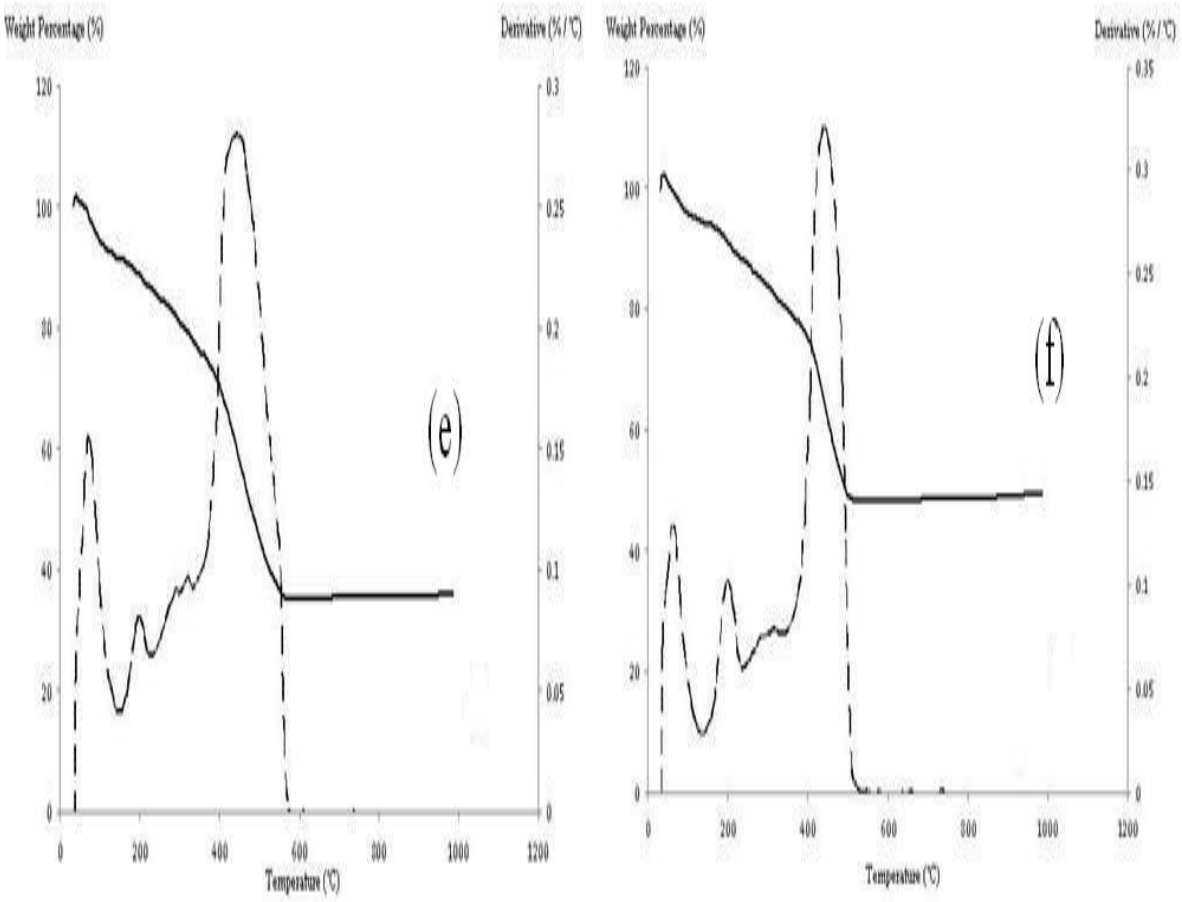

(Continued)

Table 4.5: Temperatures and percentage weight lost.

Samples (a-CNT)	Temperature (℃)			Weight Lost (%)				Weight %	Weight %
	T_c	T_s	T_o	Stage 1	Stage 2	Stage 3	Total	after T_s	of Au
As-synthesized	302	572	497	9	9	77	95	5	
Functionalized	373	826	395	7	11	79	97	3	
2.5g/dm^3 solution treated	352	562	385	8	24	44	76	24	21
5g/dm^3 solution treated	385	573	408	10	21	41	72	28	25
7.5g/dm^3 solution treated	394	571	448	7	22	36	65	35	32
10g/dm^3 solution treated	393	503	437	5	21	26	52	48	45

4.10 Electrical Studies

The respective electrical conductivity of as-synthesized and surface modified a-CNT can be preliminary investigated by impedance spectrum. Figure 4.16 shows the Nyquist plot for as-prepared and modified a-CNT/Epoxy composites cured in room temperature. Overall, the electrical resistance reduces as Au content in the respective a-CNT samples increases. Besides, functionalized a-CNT exhibits better electrical conductivity as compared to as-synthesized a-CNT, where increase in electrical conductivity are due to addition of active carboxyl functional groups on a-CNT's body. This supports the outcomes from previous study (Deepak *et al.* 2010). However, re-agglomeration properties of a-CNT fibers in epoxy matrix can be further investigated by comparing the resistivity values of samples cured in room temperature and samples cured in 15 ℃.

Figure 4.17 and 4.18 shows the Nyquist plot for as-prepared and modified a-CNT/Epoxy composites cured in 15 ℃. Note that a-CNT/Epoxy composites exhibit a higher resistance when cured in lower temperature. As the re-agglomerations of a-CNT are slower in low temperature suspension as compared to room temperature suspension, the contact resistance between a-CNT increases, which results in a relatively higher electrical resistance. This result is supporting the previous reported findings, where re-agglomeration properties would significantly affects the contact resistance of a-CNT, and hence affects the overall electrical conductivity of the composites (Aguilar *et al.* 2010).

The electrical resistivity of functionalized a-CNT is similar both cured in room temperature and 15 ℃. It is predicted that a stable suspension formed in a-CNT/liquid epoxy composite in the case of functionalized a-CNT, where the effect of re-agglomeration is insignificant. Therefore, the resistivity of functionalized a-CNT/liquid expoy composite is similar curing at both 27 ℃ and 15 ℃. In general, with increasing concentration of $AuCl_3$ it results in the decrement of electrical resistivity of the composites for both cured at room and 15 ℃ temperature. As gold content decreases the electrical resistivity of a-CNT, excessive amount of gold particles on a-CNT helps the charge to transfer which in turn reduce the resistivity of the composites.

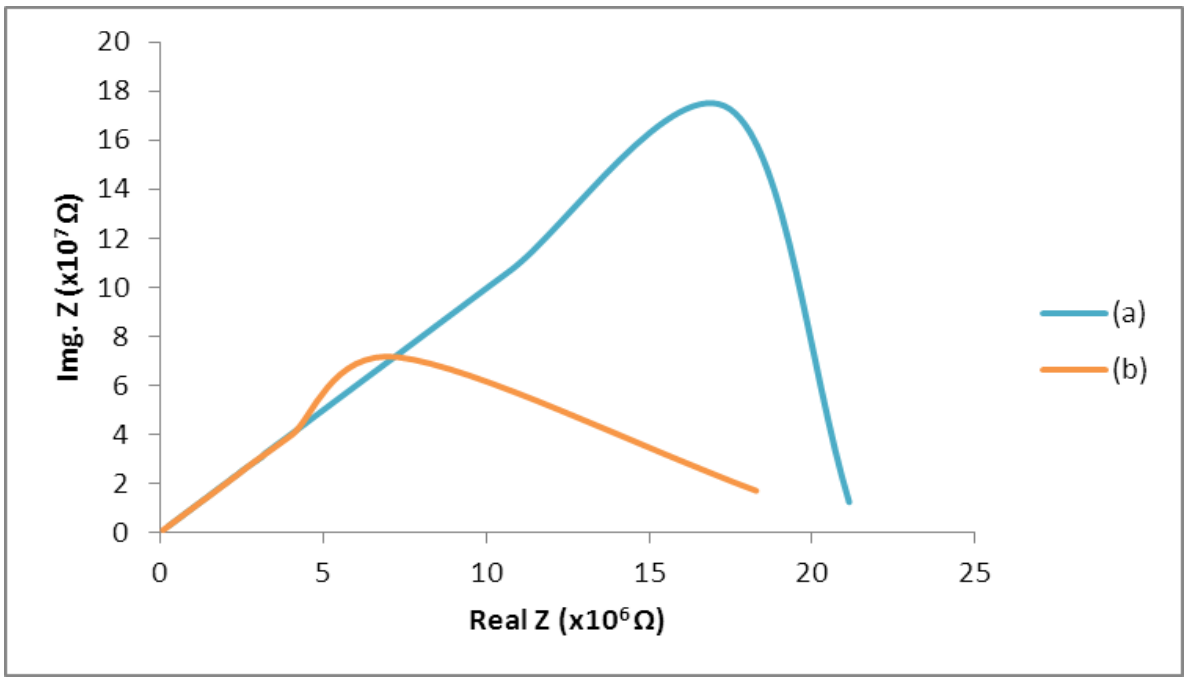

Figure 4.17: Nyquist plots of (a) as-synthesized; (b) functionalized; Hybridized (c) 2.5 g/dm^3; (d) 5 g/dm^3; (e) 7.5 g/dm^3; (f) 10 g/dm^3 $AuCl_3$ solution; a-CNT/Epoxy composites cured in room temperature

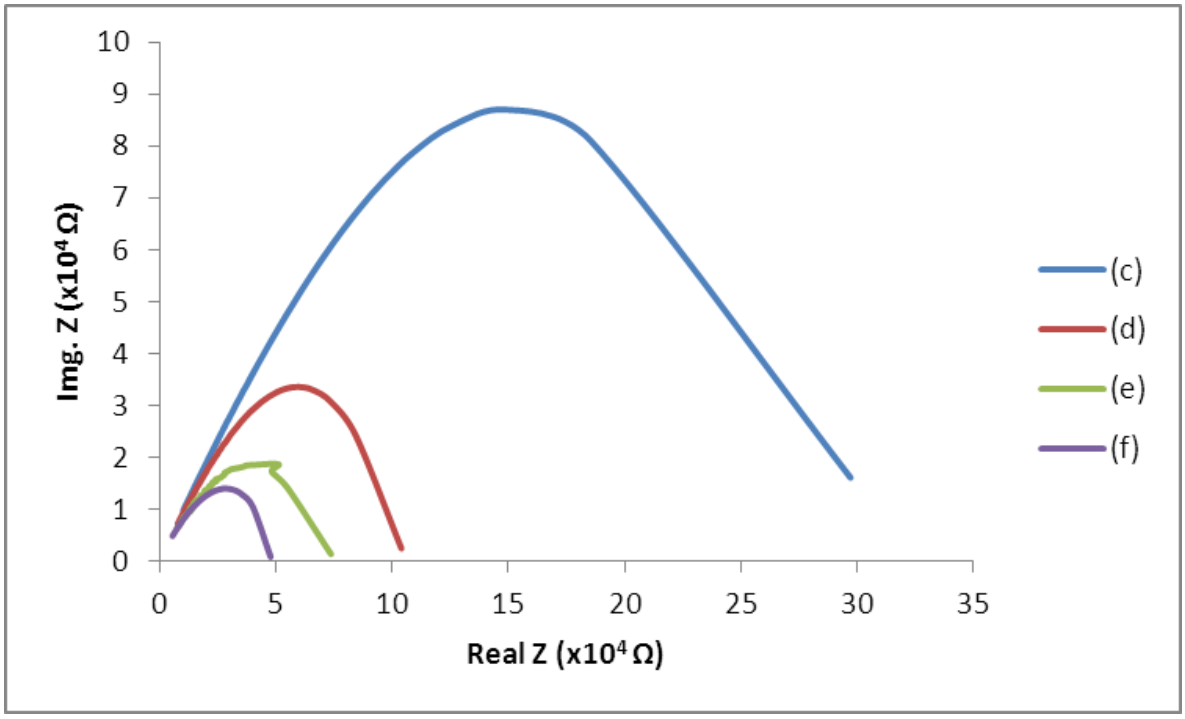

(Continued)

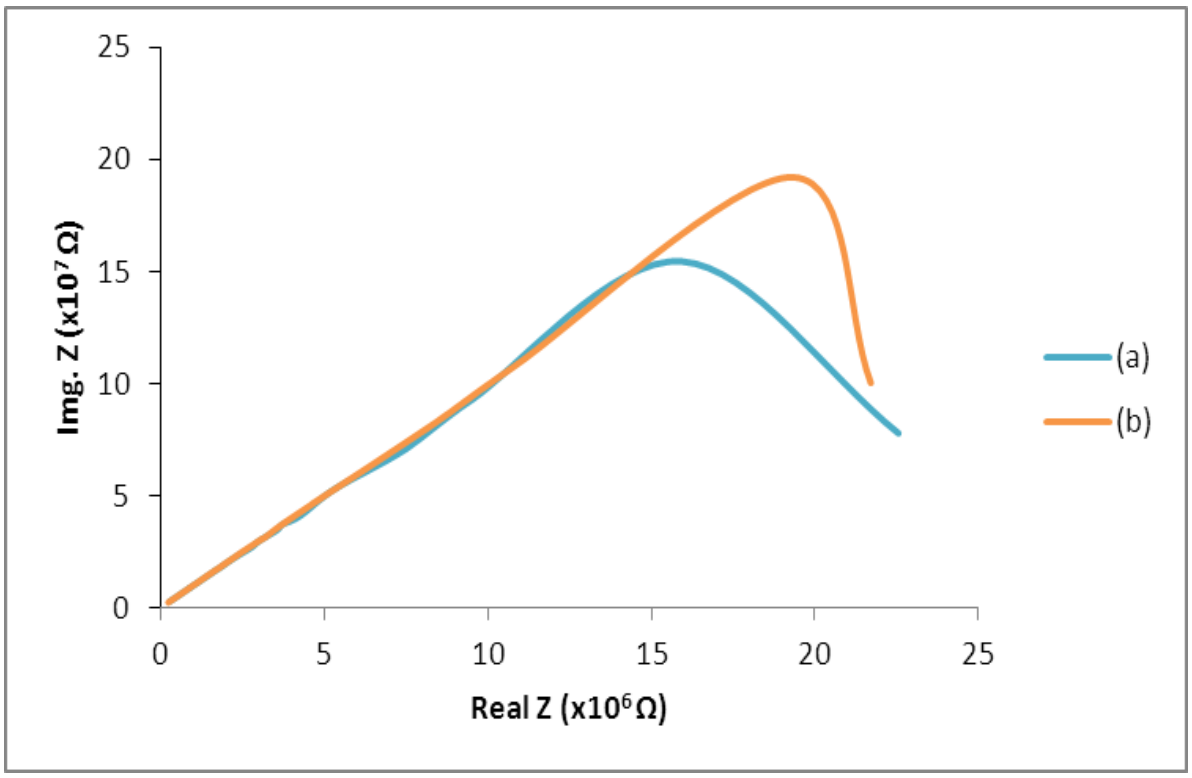

Figure 4.18: Nyquist plots of (a) as-synthesized; (b) functionalized; Hybridized (c) 2.5 g/dm^3; (d) 5 g/dm^3; (e) 7.5 g/dm^3; (f) 10 g/dm^3 $AuCl_3$ solution treated; a-CNT/Epoxy composites cured in 15 ℃

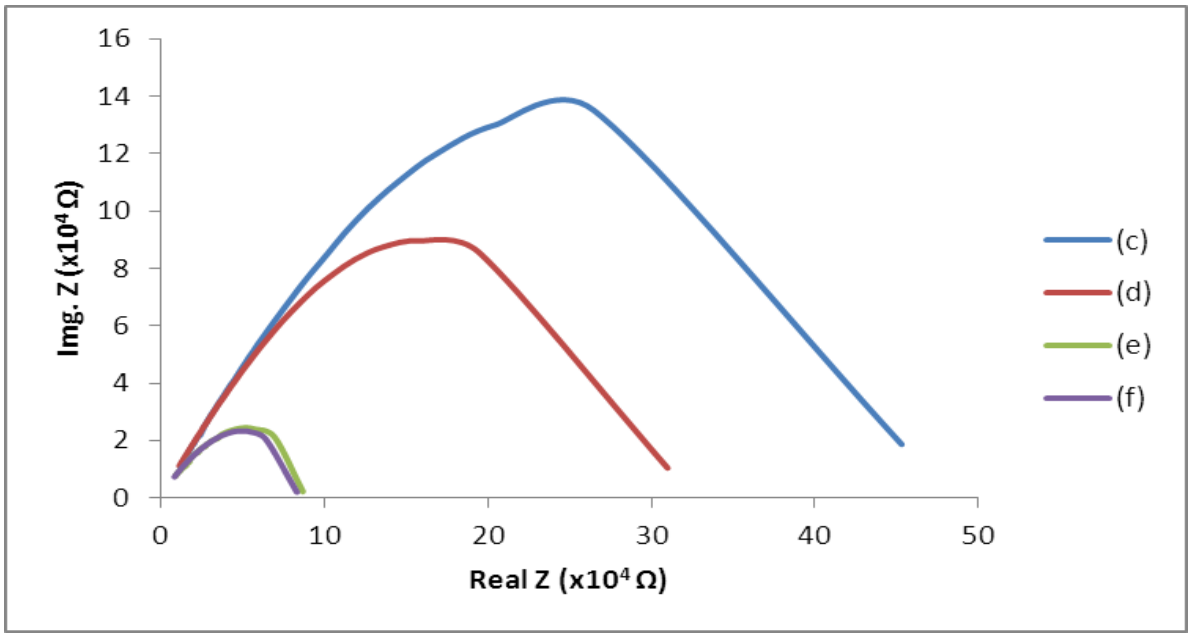

(Continued)

From elemental analysis, a-CNT treated with 7.5 g/dm^3 and 10 g/dm^3 $AuCl_3$ solutions have high possession of gold particles. It's predicted that gold particles have dictated the overall electrical conduction behavior where the re-agglomerations of a-CNT does not have significant effects on the overall conductivity. Therefore, 7.5 g/dm^3 and 10 g/dm^3 $AuCl_3$ solution treated a-CNT/Epoxy composites possess similar electrical resistivity both cured in room temperature and 15 ℃. The conduction nature of gold particles in a-CNT/Epoxy composites can be indicated by transference number measurements from respective samples.

To determine the electrical transference number, a fixed voltage applied on each samples. Variations of electrical current with time are shown in Figure 4.19, and the results are calculated and summarized in Table 4.6. Transference number of as-synthesized and functionalized a-CNT are relatively high indicate that the overall conduction of a-CNT dominated by ions, which explains the hopping and tunneling conduction mechanisms suggested by previous study (Yosida *et al.* 1999). However, transference number increases with increasing gold content on a-CNT. Electron conduction starts as a-CNT are treated with 2.5 g/dm^3 $AuCl_3$ solution and dominate more than half of the total conductivity when the concentration reaches to 7.5 g/dm^3. Combining results and analysis above, it is proven that gold particles on a-CNT' bodies contribute electron conduction to a-CNT's overall electrical conductivity. As electron conduction dominates, the re-agglomeration of tubes does not significantly affects the overall conductivity, which supports the results and analysis obtained from the electrical resistivity studies as mentioned earlier.

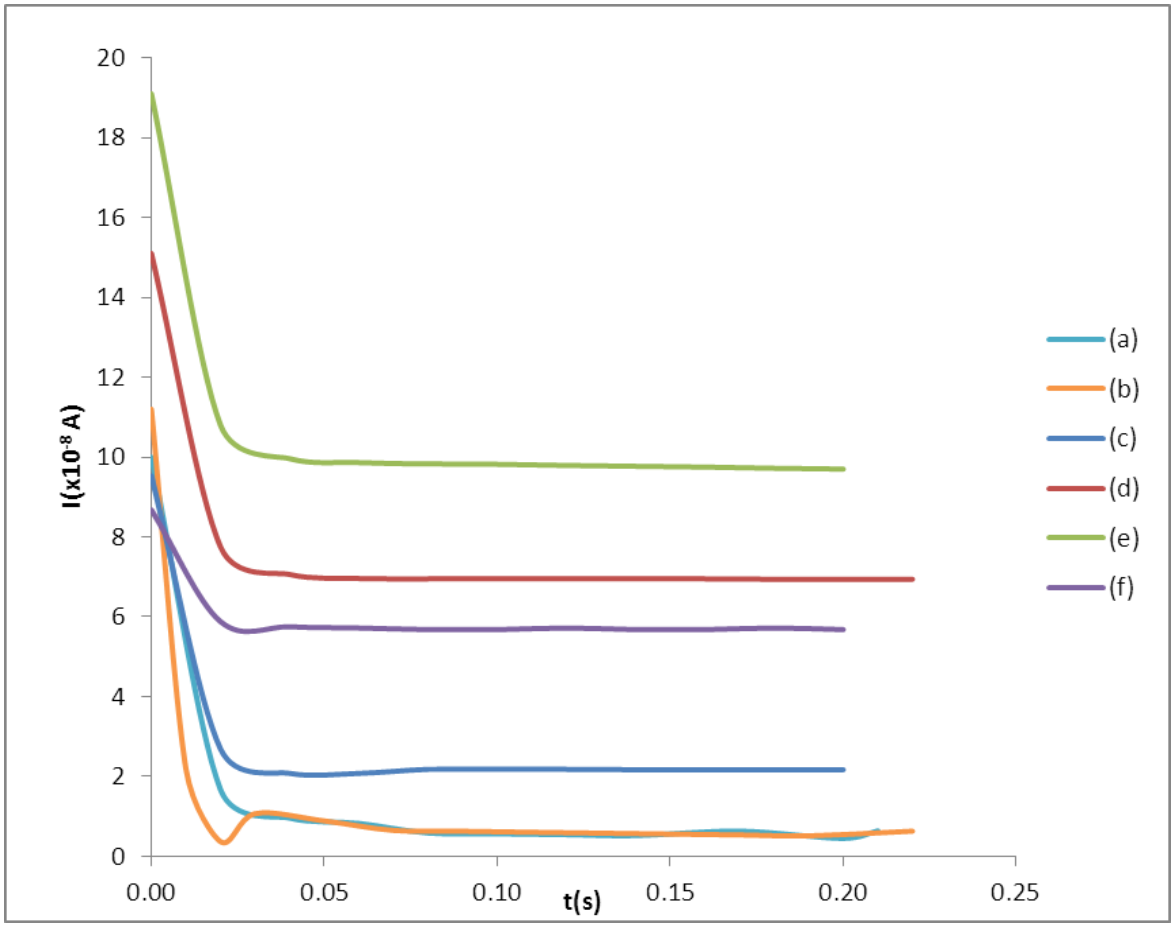

Figure 4.19: Current variations of (a) as-synthesized; (b) functionalized; (c) 2.5 g/dm^3; (d) 5 g/dm^3; (e) 7.5 g/dm^3; (f) 10 g/dm^3 $AuCl_3$ solution treated; a-CNT/Epoxy composites with time.

Table 4.6: Resistivity and t_i at 15 ℃ and 27 ℃

Samples	Resistivity (Ω.cm)		
	15 ℃	27 ℃	
(a)	8.42E+08	7.50E+08	0.95
(b)	5.50E+08	5.69E+08	0.94
(c)	1.19E+07	9.92E+06	0.77
(d)	7.47E+06	3.39E+06	0.54
(e)	2.52E+06	1.67E+06	0.49
(f)	1.87E+06	1.50E+06	0.34

CHAPTER FIVE

CONCLUSION AND RECOMMENDATIONS

The a-CNT has been successfully synthesized using both ferrocene and ammonium chloride powders via a simple synthesis method at relatively low temperature of 220 ℃. The a-CNT powders are purified by washing with HCl and de-ionized water in sequence. Morphological studies measured the diameter of a-CNT to be 51.6 nm with rough surfaces and high tendency to re-agglomerates due to amorphous structure. Combining zeta potential measurement and FTIR results, it was found that nitric acid acted as the most effective oxidation agent in functionalizing a-CNT, above citric acid, hydrochloric acid and sulfuric acid. Nitric acid treated a-CNT shows smaller diameter of 40 nm and much smoother surfaces as compared to as-synthesized a-CNT in morphological studies indicates removal of amorphous carbon layers by nitric acid. Gold particles decorated a-CNT shows a much lower diameter ranging from 10.2 to 13.8 nm indicates defective structures introduced by gold particles, where this defective structures were further justified by Raman Spectrum of all samples. Even and well-ordered fringes formed on gold particles decorated a-CNT indicates formation of crystalline gold particles, which could be further confirmed by XRD results. EDX scanning shows higher oxygen content in functionalized samples as compared to as-synthesized sample indicates successful formation of oxygen containing functional groups on a-CNT, which was further confirmed by FTIR results. Besides, EDX scanning also shows higher gold content as a-CNT were treated with higher concentration of gold chloride solution.

The thermal stability of a-CNT decreases with decorations of gold particles on its surface.

The most optimum concentration of gold chloride solution in treatment of a-CNT to obtain a thermally stable sample is 7.5 g/dm^3. UV-Vis spectrum found that functionalized a-CNT has higher absorption wavelength and lower band gap energy as compared to as-synthesized a-CNT. At the same time, gold particles decorated a-CNT has higher absorption wavelength and lower band gap energy as compared to functionalized a-CNT. However, the variation of band gap energy and absorption wavelength with varied gold content in a-CNT is not significant. Electrical conduction are proven to be improved by surface modification where functionalized a-CNT has lower electrical resistivity than as-synthesized a-CNT, and the electrical resistivity decreases significantly with increasing gold content. As-synthesized and modified a-CNT/Epoxy composites exhibits lower electrical resistivity when cured in room temperature compared to 15 ℃, where exception was found on functionalized a-CNT. The carboxyl groups on the tube's body established a stable suspension and the re-agglomeration properties exhibits less significant changes with temperature. Through transference number measurement, gold particles are found to contribute to the overall electrical conduction via electron conduction.

According to the "ends and defect sites chemistry", it could be predicted that a-CNT exhibits better efficiency in attachment of foreign particles. However, the actual comparisons of a-CNT and crystalline CNT on their effects due to solution treatments are still yet to be discovered. Morphological studies, Raman spectrometer, EDX, and XRD could be used to investigate the relative effects of using both a-CNT and crystalline CNT in solution treatments. Besides, the variation of electrical conductivity for all samples with temperature could be an important indication to access to their respective conduction behavior, either metallic or semiconducting to explore further on the electrical conduction. These could be used a approaches to further investigate the properties of a-CNT.

REFERENCES

Abuilaiwi, F.A., Laoui, T., Al-Harthi, M. & Atieh, A.M. (2010). Modification and Functionalization of Multiwalled Carbon Nanotubes (MWCNT) via Fischer Esterification, *The Arabian Journal for Science and Engineering*, 35(1C), 37-48.

Aguilar, J. O., Bautista-Quijano, J.R. & Aviles, F. (2010). Influence of Carbon Nanotube Clustering on the Electrical Conductivity of Polymer Composite Films. *eXPRESS Polymer Letters*, 4(5), 292-299

Ahmed, S.F., Mitra, M.K. & Chattopadhya, K.K. (2007). Low-macroscopic field emission from silicon-incorporated diamod-like caron film synthesized by dc PECV, *Applied Surface Science*, 253(12), 5480-5484

Ajayan, P.M. & Ebbesen, T.W. (1997). Nanometre-size tubes of carbon. *Reports on Progress in Physics*. 60, 1034-1040,

Ando, Y. & Zhao, X. (2006). Synthesis of Carbon Nanotubes by Arc-discharge method. *New Diamond and Frontier Carbon Technology*, 16(3), 123-137

Azamian, B. R., Coleman, K. S., Davis, J. J., Hanson, N., & Green, M. L. H. (2002). Directly observed covalent coupling of quantum dots to single-wall carbon nanotubes, *Chemical Communications*, 4, 366-367

Balogh, Z., Halasi, G., Korbely, B. & Hernadi, K. (2008). CVD-synthesis of multiwall carbon nanotubes over potassium-doped supported catalysts. *Applied Catalysis A: General*, 344, 191-197

Banerjee, D., Jha, A., Chattopadhyay, K.K. (2010). FESEM and HRTEM studies of some novel carbon nanostructures. *Microscopy: Science, Technology, Applications and Education*, 1674-1680

Banerjee, Soumik, Naha, Sayangdev, & Ishwar, K.P. (2008). Molecular simulation of the carbon nanotube growth mode during catalytic synthesis. *Applied Physics Letters*, 92, 233121

Baughman, R.H., Zakhidov, A.A. & Heer, W.A. (2002). Carbon nanotubes – the route toward applications. *Science*, 297, 787-792

Bernhole, J., Brennerm D., Nardeli, M.B., Meunier, V. & Roland, C. (2002). Mechanical and electrical properties of nanotubes, *Annual Review of Materials Research*, 32, 347-375

Bethune, D.S., Kiang, C.H., Devries, M.S., *et al.* (1993). Cobalt-catalysed growth of carbon nanotubes with single-atomic-layer walls. *Nature*. 363(6430), 605-607

Bockrath, M. (2006). Carbon nanotubes: The weakest link. *Nature Physics*, 2(3), 155

Bruce, P.G., Vincent, C.A. 2002. Steady state current flow in solid binary electrolyte cells. *Journal of Electroanalysis and Interfacial Electrochemisty*. 225(1-2), 1-17

Calderon-Moreno J.M. & Yoshimura M (2001). Hydrothermal processing of high-quality multiwall nanotubes from amorphous carbon. *Journal of American Chemical Society,* 123(4), 741–742

Charlier, J.C., Blase, X. & Roche, S. (2007). Electronic and transport properties of nanotubes. *Reviews on Modern Physics*, 79, 677-732

Chen, W.X., Tu, J.P., Wang, L.Y., Gan, H.Y., Xu, Z.D. & Zhang, X.B. (2003). Tribological application of carbon nanotubes in a metal-based composite coating and composites. *Carbon,* 41, 215-222.

Chin, L.C., Kurtz, A., Park, H. & Lieber, C.M. (2002). Diameter-Controlled Synthesis of Carbon Nanotubes. *Journal of Physical Chemistry B*. 106, 2429-2433.

Ci, L., Wei, B., Xu, C., Liang, J. & *et al.* (2001). Crystallization behavior of the amorphous carbon nanotubes prepared by the CVD method. *Journal of Crystal Growth*, 233, 823-828

Ci, L., Zhu, H., Wei, B., Xu, C. & Wu, D. (2003). Annealing amorphous carbon nanotubes for their application in hydrogen storage, *Applied Surface Science*, 205, 39-43.

Collins, P. G. (2009). DEFECTS AND DISORDER IN CARBON NANOTUBES. *Oxford Handbook of Nanoscience and Technology: Frontiers and Advances*. Irvine, University of California.

Collins, P.G. (2000). Nanotubes for Electronics. *Scientific American*, 67-69

Collins, P.G., Arnold, M.S. & Avouris, P. (2001). Engineering Carbon Nanotubes and Nanotube Circuits Using Electrical Breakdown. *Science*, 292, 706-709.

Deepak, J., Pradeep, T. & Waghmare, U.V. (2010). Interaction of small gold clusters with carbon nanotube bundles: Formation of gold atomic chains. Journal of Physics: *Condensed Matter*, 22, 125301 (6pp).

Delhaes, P., Couzi, M., Trinquecoste, M., Dentzer, J., Hamidou, H. & Vix-Guterl, C. (2006). A comparison between Raman spectroscopy and surface characterizations of multiwall carbon nanotubes, *Carbon,* 44, 3005-3013

Demczyk, B.G., Wang, Y.M., Cumings, J., Hetman, M., Han, W., Zettl, A. & Ritchie, R.O. (2002). Direct mechanical measurement of the tensile strength and elastic modulus of multiwalled carbon nanotubes. *Materials Science and Engineering A,* 334(1–2), 173–178.

Demoustier, S., Minoux, E., Baillif, M.L., Charles, M. & Ziaei, A. (2008). Review of two microwave applications of carbon nanotubes: nano-antennas and nano-switches, *C. R. Physique*, 9, 53-66.

Dinesh, J., Eswaramoorthy, M., Rao, C.N.R. (2007). Use of Amorphous Carbon Nanotube Brushes as Templates to Fabricate GaN Nanotube Brushes and Related Materials. *Journal of Physical Chemistry C,* 111(2), 510–513

Dresselhaus, M.S., Dresselhaus, G., Jorio, A., Souza Filho, A.G. & Saito, R. (2002).

Raman spectroscopy on isolated single wall carbon nanotubes, *Carbon*, 40(12), 2043-2061.

Dujardin, E., Ebbesen, T. W., Hiura, H., & Tanigaki, K. (1994). Capillarity and Wetting of Carbon Nanotubes, *Science*, 265(5180), 1850-1852.

Ebbesen, T.W., Lezec, H.J., Bennett, J.W., Ghaemi, H.F. & Thio, T. 1996. Electrical conductivity of individual carbon nanotubes. *Natural*, 382: 54-56.

Endo, M., Hayashi, T., Kim, Y.A., Terrones, M. & Dresselhaus, M.S. (2004). Applications of carbon nanotubes in the twenty-first century, *Philosophical Transaction of the Royal Society A*, 362, 2223-2238

Fama, L.M., Pettarin, V., Goyanes, S.N. & Bernal, C.R. (2011). Starch/multi-walled carbon nanotubes composites with improved mechanical properties, *Carbohydrate Polymers*, 83, 1226-1231.

Files, B.S., Yu, M.F., Arepalli, S. & Ruoff, R.S. (2000). Tensile loading of ropes of single wall carbon nanotubes and their mechanical properties. *Physical Review Letters*, 84(24), 5552–5555

Florian, H.G., Wichmann, M.H.G., Fiedler, B., Kinloch, I.A., Windle, A.H. & Schulte, K. (2006). Evaluation and Identification of Electrical and Thermal Conduction mechanism in Carbon nanotubes/Epoxy composites. *Polymer*, 47, 2036-2045.

Forro, L. & Schonenberger, C. (2001). Physical properties of multi-wall nanotubes, *Top Applied Physics*, 80, 329-391

Freitag, M., Martin, Y., Misewich, J.A., *et al.* Photoconductivity of Single Carbon Nanotubes. *Nano Letters*, 3(8), 1067-1071

Gao, X., Liu, L., Guo, Q., Shi, J. & Zhai, G. (2005). Fabrication and mechanical/conductive properties of multi-walled carbon nanotube (MWNT) reinforced carbon matrix composites, *Materials Letters*, 59, 3062-3065.

Gao, X., Zhang, Y., Wu, Q., Chen, H., Chen, Z. & Lin, X. (2011). One step electrochemically deposited nanocomposite film of chitosan–carbon nanotubes–gold nanoparticles for carcinoembryonic antigen immunosensor application, *Talanta*, 85, 1980-1985.

Gogotsi, Y., Libera, J.A., Yoshimura, M. (2000). Hydrothermal synthesis of multiwall carbon nanotubes. *Journal of Materials Research*, 15(12), 2591–2594.

Guo, T., Nikolaev, P., Rinzler, A.G., Tomanek, D., Colbert, D.T., Smalley, R.E. (1995). Catalytic growth of single-walled carbon nanotubes by laser vaporization. *Chemical Physics Letters*, 243, 49-54.

Hamon, M. A., Chen, J., Hu, H., Chen, Y. S., Itkis, M. E., Rao, A. M., Eklund, P. C., & Haddon, R. C. (1999). Dissolution of single-walled carbon nanotubes, *Advanced Materials* 11(10), 834-+.

Harns, P.J.F. (2009). *Carbon Nanotubes Science: Synthesis, Properties and*

Applications. New York: Cambridge University Press.

Harris, D.C. & Bertolucci, M.D. (1989). *Symmetry and Spectroscopy: An Introduction to Vibrational and Electronic Spectroscopy*, Dovers Publications

He, X., Jiang, L., Fan, C., Lei, J. & Zheng, M. (2007). Chemical elimination of amorphous carbon on amorphous carbon nanotubes and its electrochemical performance. *Chemical Physics*, 334, 253-258.

Hirsch, A. (2002). Functionalization of single-walled carbon nanotubes, *Angewandte Chemie-International Edition* 41(11), 1853-1859.

Ho, Y.H., Chang, C.P., Shyu, F.L., Chen, R.B., Chen, S.C. & Lin, M.F. (2004). Electronic and optical properties of double-walled armchair carbon nanotubes. *Carbon*, 42, 3159-3167

Hone, J., Llaguno, M.C., Nemes, N.M., Johnson, A.T., Fischer, J.E., Walters, D.A., Casavant, M.J., Schmidt, J. *et al.* (2000). Electrical and thermal transport properties of magnetically aligned single wall carbon nanotube films. *Applied Physics Letters*, 77(5), 666–668

Hong, S. & Myung, S. (2007). Nanotube Electronics: A flexible approach to mobility. *Nature Nanotechnology*, 2(4), 207–208

Hsieh, Y.C., Chou, Y.C., Lin, C.P., Hsieh, T.F. & Shu, C.M. 2010. Thermal Analysis of Multi-walled Carbon Nanotubes by Kissinger's Corrected Kinetic Equation. *Aerosol and Air Quality Research* 10: 212-218.

Hu, J., Wang, Z. & Li, J. (2007). Gold Nanoparticles With Special Shapes: Controlled Synthesis, Surface-enhanced Raman Scattering, and The Application in Biodetection, *Sensors*, 7, 3299-3311

Hu, Q., Gan, Z., Zheng, X., Lin, Q. & Xu, B. 2011. Rapid microwave-assisted synthesis and electrochemical characterization of gold/carbon nanotube composition. *Superlattices and Microstructures* 49: 537-542.

Hu, Z. D., & Hu, Y. F. (2006). Synthesis and Characterization of Amorphous Carbon Nanotubes by Pyrolysis of Ferrocene Confined with AAM Templates, *Journal of Physical Chemistry B*, 110, 8263 – 8267

Huang, C.J., Wang, Y.H., Chiu, P.H., Shih, M.C. & Meen, T.H. (2006). Electrochemical synthesis of gold nanocubes, *Materials Letters*, 60, 1896-1990

Iakoubovskii, K. *et al.* (2006). IR-Extended Photoluminescence Mapping of Single-Wall and Double-Wall Carbon Nanotubes. *Journal of Physical Chemistry B*, 110(35), 17420-17424

Ibrahim, S., Yasin, S.M.M., Ng, M.N., Ahmad, R. & Johan, M.R. (2012). Conductivity, thermal and infrared studies on plasticized polymer electrolytes with carbon nanotubes as filler, *Journal of Non-Crystalline Solids*, 358, 210-216.

Hema, M., Selvasekerapandian, S., Hirankumar, G., Sakunthala, A. 2002. Structural and thermal studies of PVA:NH_4I, *Journal of Physics and Chemistry of Solids*. 70(7): 1098-1103

Iijima, S. (1991). Helical microtubules of graphitic carbon. *Nature*. 354(6348), 56-58

Irurzun, V.M., Ruiz, M.P. & Resasco, D.E. (2010). Raman intensity measurements of single-walled carbon nanotube suspensions as a quantitative technique to assess purity, *Carbon*, 48, 2873-2881.

Ishigami, N., Ago, H., Imamoto, K., Tsuji, M., Iakoubovskii, K. & Minami, N. (2008). Crystal Plane Dependent Growth of Aligned Single-Walled Carbon Nanotubes on Sapphire. *Journal of American Chemical Society.* 130(30), 9918–9924

Itkis, M.E. *et al.*(2005). Comparison of Analytical Techniques for Purity Evaluation of Single-Walled Carbon Nanotubes. *Journal of the American Chemical Society*, 127(10), 3439–3448

Jason, K.V., Jonathan, J.B., Jeffrey, E.R., Allan E.B., Geoffrey, L.W. & Bradly, D.F. (2004). Low-temperature growth of carbon nanotubes from the catalytic decomposition of carbon tetrachloride. *Journal of American Chemical Society*, 126(32), 9936-9937

Jha, A., Banerjee, D. & Chattopadhyay, K.K. (2011). Improved field emission from amorphous carbon nanotubes by surface functionalization with stearic acid. *Carbon*, 49, 1272-1278.

Jia, Z., Zhang, J., Jia, C., Nie, J. & Chu, K. (2011). Preparation and characterization of mechanical properties of carbon nanotube/45S5Bioglass composites for biologic applications, *Materials Science and Engineering A*, 528, 1553-1557.

Jiang, L., & Gao, L. (2003). Modified carbon nanotubes: an effective way to selective attachment of gold nanoparticles, *Carbon*, 41, 2923–2929.

Jorio, A., Dresselhaus, G. & Dresselhaus, M.S. (2008). *Carbon nanotubes – advanced topics in the synthesis, structure, properties and applications*. New York: Springer-Verlag Berlin Heidelberg.

Kansala M. & Zhang, L.C. (2007). Fabrication and Application of Polymer Composites Comprising Carbon Nanotubes. *Recent Patents on Nanotechnology,* 1, 59-65.

Kasaliwal, G.R., Pegel, S., Göldel, A., Pötschke, P. & Heinrich, G. "Analysis of Agglomerate Dispersion Mechanisms of Multiwalled Carbon Nanotubes During Melt Mixing in Polycarbonate", *Polymer*, **51**(2010), pp. 2708–2720.

Kataura, H., Kumazawa, Y., Maniwa, Y., Umezu, I., Suzuki, S., Ohtsuka, Y. & Achiba, Y. (1999). Optical properties of single-wall carbon nanotubes, *Synthetic Metals*, 103, 2555-2558.

Kiang, C.H., Goddard, W., Beyers, R. & Bethune, D.S. (1995). Carbon Nanotubes with Single-Layer Walls. *Carbon*, 33(7), 903-914.

Kim, H.H. & Kim, H.J. (2006). Preparation of carbon nanotubes by DC arc discharge

process
Kirkpartick, S. (1973). Percolation and Conduction. *Rev. Modern Physics*, 45, 574-588

Klabunde, K.J. & Mulukutla, R.S. (2001) *Nanoscale Materials in Chemistry*. New York: WILEY

Klumpp, C., Kostarelos, K., Prato, M., & Bianco, A. (2006). Functionalized carbon nanotubes as emerging nanovectors for the delivery of therapeutics, *Biochimica Et Biophysica Acta-Biomembranes* 1758(3), 404-412.

Kokai, F., Takahashi, K., Yudasaka, M., Yamada, R., Ichihashi, T. & Iijima, S. (1999). Growth dynamics of carbon-metal particles and nanotubes synthesized by CO2 laser vaporization, *Journal of Physical Chemistry B*, 103, 4346

Kovacs, J. Z., Velagala, B.S., Schulte, K. & Bauhofer, W. (2007). Two percolation thresholds in carbon nanotube epoxy composites. *Composites science and technology*, 67(5), 922-928

Kroto, H.W., Heath, J.R., O'brien, S.C., Curl, R.F. & Smalley, R.E. (1985). C60: Buckminsterfullerene. *Nature*. 318(6042), 162-163

Kumar, M & Ando, Y. (2010). Chemical Vapor Deposition of Carbon Nanotubes: A Review on Growth Mechanism and Mass Production. *Journal of Nanoscience and Nanotechnology*, 10, 3739-3758

Kyotani, T., Nakazaki, S., Xu, W. & Tomita, A. (2001). Chemical modification of the inner walls of carbon nanotubes by HNO oxidation, *Carbon*, 39, 771 –785.

Lafi, L., Cossement, D. & Chahine, R. (2005). Raman spectroscopy and nitrogen vapour adsorption for the study of structural changes during purification of single-wall carbon nanotubes, *Carbon*, 43, 1347-1357

Li, C., Erick, Thostenson, E.T. & Chou, T.W. (2007). Effect of nanotube waviness on the electrical conductivity of carbon nanotube-based composites. *Composites Science and Technology*, 68, 1445-1452

Li, F., Wang, Z., Shan, C., Song, J., Han, D. & Niu, L. (2009). Preparation of gold nanoparticles/functionalized multiwalled carbon nanotube nanocomposites and its glucose biosensing application, *Biosensors and Bioelectronics*, 24, 1765-1770.

Li, L., Li, F., Liu, C. & Cheng, H.M. (2005). Synthesis and characterization of double-walled carbon composed of single-walled carbon nanotubes. Journal of Applied Physics. 86(2), 71-73

Li, Q., Li. Y., Zhang, X.F., Chikkannanavar, S.B. *et al.* (2007). Structure-Dependent Electrical Properties of Carbon Nanotube Fibers. *Advanced Materials*, 19, 3358-3363

Li, X., Zhu, H., Wei, J., Wang, K., Xu, E. *et al.* (2009). Determination of band gaps of self-assembled carbon nanotube films using Tauc/Davis–Mott model. *Applied Physics A: Materials Science & Processing*. 97: 341-344

Lim, S.H., & Wei, J. (2004). Electrochemical Genosensing properties of gold

nanoparticles-carbon nanotubes hybrid, *Chemical Physics Letter*, 400, 578-582

Little, R.B. (2003). Mechanistic aspects of carbon nanotube nucleation and growth. *Journal of Cluster Science*, 14, 135-185

Liu, B., & Jia, D. (2007). Low Temperature Synthesis of Amorphous Carbon Nanotubes in Air, *Carbon*, 45, 1696-1716

Liu, Y., Song, X., Zhao, T., Zhu, J. Hirshcer, M. & Philipp, F. (2004). Amorphous carbon nanotubes produced by a temperature controlled DC arc discharge, *Carbon*, 42, 1852-1855

Lou, Z., Chen, Q., Wang, W. & Zhang, Y. (2003). Synthesis of carbon nanotubes by reduction of carbon dioxide with metallic lithium, *Carbon*, 41(15), 3063-3067

Lu, X. & Chen, Z. (2005). Curved Pi-Conjugation, Aromaticity, and the Related Chemistry of Small Fullerenes (C60) and Single-Walled Carbon Nanotubes. *Chemical* Reviews, 105(10), 3643–3696

Ma, P. C., Tang, B.Z. & Kim, J.K. (2008). Effect of CNT decoration with silver nanoparticles on electrical conductivity of CNT-polymer composites, *Carbon*, 46, 1497-1505

Maganas, T.C. & Harrington, A.L. (1 September 1992). *Intermittent film deposition method and system*. U.S. Patent 5,143,745

Makarova, T. & Palacio, F. (2006). *Carbon-Based Magnetism: An Overview of the Magnetism of Metal Free Carbon-based Compounds and Materials.* Elsevier

Manafi, S., Nadali, H. & Irani, H.R. (2008). Low temperature synthesis of multi-walled carbon nanotubes via a sonochemical/hydrothermal method. *Materials Letters*, 62, 4175-4176.

Martel, R., Schmidt, T., Shea, H.R., *et al.* (1998). Single- and multi-walled carbon nanotubes field-effect transistors. *Applied Physics Letters*, 73(17), 2447-2449

Mashreghi, A. & Moshksar, M.M. (2011). Investigating the effect of chirality on structural parameters of chiral single-walled carbon nanotubes by molecular dynamics simulation. *Computational Materials Science*, 50, 934-938.

Mayuyama, R., Nam, Y.W., Han, J.H. & Strano, M.S. (2011). Well-defined single-walled carbon nanotube fibers as quantum wires: Ballistic conduction over micrometer-length scales. *Current Applied Physics*, 11, 1414-1418

Minami, N., Kazaoui, S., Jacquemin, R., Yamawaki, H., Aoki, K., Kautara, H. & Achiba, Y. (2001). Optical properties of semiconducting and metallic single wall carbon nanotubes: effects of doping and high pressure, *Synthetic Metals*, 116, 405-409.

Mingo, N., Stewart, D.A., Broido, D.A. & Srivastava, D. (2008). Phonon transmission through defects in carbon nanotubes from first principles. *Physical Review B*, 77(3), 033418

Minkel, J.R. (2002). Nanotubes in the fast lane. *Physical Review Letters*, 88.

Mizoguti, E., Nihey, F., Yudasaka, M., Iijima, S. & Nakamura, K. 2000. Purification of single-wall carbon nanotubes by using ultrafine gold particles. *Chemical Physics Letters* 321: 297-301.

Mizoguti, E., Nihey, F., Yudasaka, M., Iijima, S. & Nakamura, K. 2000. Purification of single-wall carbon nanotubes by using ultrafine gold particles. *Chemical Physics Letters* 321: 297-301.

Monthioux, M. & Kuznetsov, V. (2006). Who should be given the credit for the discovery of carbon nanotubes? *Carbon*. 44, 1621-1624

Monthioux, Marc; Spreadborough, J. (1960). Action of Graphite as Lubricant. *Nature*. 186(4718), 29-30

Moseley, J. L. (1993). A model for agglomeration in a fluidized bed. *Chemical Engineering Science*, 48(17), 3043-3050.

Naha, Sayangdev, & Ishwar, K. Puri. (2008). A model for catalytic growth of carbon nanotubes. *Journal of Physics D: Applied Physics,* 41, 065304

Naseh, M.V., Khodadadi, A.A., Mortazavi, Y., Sahraei, O.A., Pourfayaz, F. & Sedghi, S.M. (2009). Functionalization of Carbon Nanotubes Using Nitric Acid Oxidation and DBD Plasma. *World Academy of Science, Engineering and Technology,* 49, 177-179.

Oberlin, A., Endo, M. & Koyama, T. (1976). Filamentous growth of carbon through benzene decompositon. *Journal of Crystal Growth*. 32(3), 335-349

Orinakova, R. & Orinak, A. (2011). Recent applications of carbon nanotubes in hydrogen production and storage, *Fuel*, 90, 3123-3140

Paradise, M. & Goswami, T. (2007). Carbon Nanotubes – Production and industrial applications, *Materials & Design*, 28(5), 1477-1489.

Pederson, M. R. & Broughton, J. Q. (1992). Nanocapillarity in Fullerene Tubules, *Physical Review Letters,* 69(18), 2689-2692

Poncharal, P., Wang, Z.L., Ugarte, D. & de Heer, W.A. (1999). Electrostatic deflections and electromechanical resonances of carbon nanotubes. *Science*, 283(5407), 1513–1516.

Pop, E., Mann, D., Wang, Q., Goodson, K., Dai, H,. (2005). Thermal conductance of an individual single-wall carbon nanotube above room temperature. *Nano Letters*, 6(1), 96–100.

Popov, M., Kyotani, M., Nemanich, R. & Koga, Y. (2002). Superhard phase composed of single-wall carbon nanotubes. *Physical Review B*, 65(3), 033408

Qin, X., Wang, H., Wang, X., Miao, Z., Chen, L., Zhao, W., Shan, M. & Chen, Q. (2010). Amperometric biosensors based on gold nanoparticles-decorated multiwalled carbon nanotubes poly(diallyldimethylammonium chloride) biocomposite for the determination of choline, *Sensors and Actuators B,* 147, 593-598.

Reed, J.S. (1994). Principles of Ceramic Processing, Wiley-Interscience, New York.

Ren, Z.F., Huang, Z.P., Xu, J.W., Wang, J.H., Bush, P., Siegal, M.P., Provencio, P.N. (1998). Synthesis of Large Arrays of Well-Aligned Carbon Nanotubes on Glass. *Science*, 282(5391), 1105–1107

Saito, R, Fujita, M., *et al.* (1992). Electronic structure of graphene tubules based on C60. *Physical Review B.* 46(3), 1804-1811

Saito, Y., Inagaki, M. & Shinohara, H. (1992). Yield of fullerenes generated by contact arc method under He and Ar: dependence on gas pressure. *Chemical Physics Letters*, 200, 643-648

Salvetat, J.P., Briggs, G.A.D., Bonard, J.M., Bacsa, R.R., Kulik, A.J., Stockli, T. *et al.* (1999). Elastic and shear moduli of single-walled carbon nanotube ropes. *Physical Review Letters*, 82(5), 944–947.

Samani, M.K., Khosravian, N., Chen, G.C.K., Shakerzadeh, M., Baillargeat, D. & Tay, B.K. (2012). Thermal conductivity of individual multiwalled carbon nanotubes, *International Journal of Thermal Science*, 62, 40-43.

Sanchez-Portal, D., Artacho, E., Solar, J.M., Rubio, A. & Ordejon, P. (1999). Ab initio structural, elastic, and vibrational properties of carbon nanotubes. *Physical Review B*, 59(19), 12678–12688

Scott, C.D., Arepalli, S., Nikolaev, P. & Smalley R.E. (2001). Growth mechanisms for single-wall carbon nanotubes in a laser-ablation process. *Applied Physics A*, 72, 573-580

Singh, C., Shaffer, M., Kinloch, I. & Windle, A. (2002). Production of aligned carbon nanotubes by the

Sinha, S., Barjami, S., Iannacchione, G., Schwab, A. & Muench, G. (2005). Off-axis thermal properties of carbon nanotube films. *Journal of Nanoparticle Research*, 7(6), 651–657

Sun, L., Yan, C., Chen, Y., Wang, H. & Wang, Q. (2012). Preparation of amorphous carbon nanotubes using attapulgite as template and furfuryl alcohol as carbon source. *Journal of Non-Crystalline Solids*, 358, 2723-2726

Tang, Z.K., Zhang, L., Wang, N., Zhang, X.X., Wen, G.H., Li, G.D., Wang, J.N., Chan, C.T. *et al.* (2001). Superconductivity in 4 Angstrom Single-Walled Carbon Nanotubes. *Science* 292(5526): 2462–2465

Tello, A., Cardenas, G. & Haberle, P. 2008. The synthesis of hybrid nanostructures of gold nanoparticles and carbon nanotubes and their transformation to solid carbon nanorods. *Carbon* 46: 884-889.

Thostenson, E., Li, C. & Chou, T. (2005). Nanocomposites in context. *Composites Science and Technology*, 65(3–4), 491–516

Tombler, T.W., Zhou, C., Alexseyev, L., *et al.* (2000). Reversible electromechanical

characteristics of carbon nanotubes under local-probe manipulation. *Nature*, 405, 769-772.

Treacy, M.M.J., Ebbesen, T.W. & Gibson, J.M. (1996). Exceptionally high Young's modulus observed for individual carbon nanotubes. *Nature*, 381(6584), 678–680.

Tsai, S.H., Chiang, F.K., Tsai, T.G., Shieu, F.S. & Shih, H.C. (2000). Synthesis and characterization of the aligned hydrogenated amorphous carbon nanotubes by electron cyclotron resonance excitation. *Thin Solid Films*, 366, 11-15

Waldorff, E.L., Waas, A.M., Friedmann, P.P. & Keidar, M. (2004). Characterization of carbon nanotubes produced by arc discharge: Effect of the background pressure. *Journal of Applied Physics*, 95(5), 2749-2754.

Walt, A.H., Chatelain, A. & Ugarte, D. A. (1995). Carbon Nanotube Field-Emission Electron Source. *Science*, 270(5239), 1179-1180

Wang, W., Huang, J.Y., Wang, D.Z. & Ren, Z.F. (2004). Low-temperature hydrothermal synthesis of multiwall carbon nanotubes. *Carbon*, 43, 1317-1339.

Wiltshire, J.G., Khlobystov, A.N., Li, L.J., Lyapin, S.G., Briggs, G.A.D. & Nicholas, R.J. (2004). Comparative studies on acid and thermal based selective purification of HiPCO produced single-walled carbon nanotubes. *Chemical Physics Letters*, 386(4-6), 239-243.

Wu, Y. & Hu, H. (2005). The fabrication of a colloidal gold–carbon nanotubes composite film on a gold electrode and its application for the determination of cytochrome c. *Colloids and Surfaces B*, 41, 299-304.

Xia, W., Wang, Y., Bergstra, R., Kundu, S. & Muhler, M. (2007). Surface characterization of oxygen-functionalized multi-walled carbon nanotubes by high-resolution X-ray photoelectron spectroscopy and temperature-programmed desorption, *Applied Surface Science*, 254, 247–250.

Xiao, L., Liu, P., Liu, L., Jiang, K., Feng, X., Wei, Y., *et al.* (2008). Barium functionalized multiwalled carbon nanotube yarns as low work-function thermionic cathodes. *Applied Physics Letters*, 92, 153108–153110.

Yang, Y., Hu, Z., Wu, Q., Lu, Y.N., Wang, X.Z. & Chen, Y. (2003). Template-confined growth and structural characterization of amorphous carbon nanotubes, *Chemical Physics Letters*, 373(5-6), 580-585

Yosida, Y., Oguro, I. 1999. Variable range hopping conduction in bulk samples

Yosida, Y., Oguro, I. 1999. Variable range hopping conduction in bulk samples composed of single-walled carbon nanotubes. *Journal of Applied Physics*. 86(2), 71-73

Yu, G., Gong, J., Wang, S., Zhu, D., He, S. & Zhu, Z. 2006. Etching effects of ethanol on multi-walled carbon nanotubes. *Carbon* 44: 1218-1224.

Yu, M.F., Lourie, O., Dyer, M.J., Moloni, K., Kelly, T.F. & Ruoff, R.S. (2000). Strength and Breaking Mechanism of Multiwalled Carbon Nanotubes Under Tensile Load. *Science*, 287(5453), 637–640.

Zhang, M., Yudasaka, M., Nihey, F. & Iijima, S. 2000. Effect of ultrafine gold particles and cationic surfactant on burning as-grown single-wall carbon nanotubes. *Chemical Physics Letters* 328: 350-354.

Zhang, R., Wang, Q., Zhang, L., Yang, S., Yang, Z. and Ding, B. (2008). The growth of uncoated gold nanoparticles on multiwalled carbon nanotubes. *Colloids and Surfaces A: Physicochemistry Engineering Aspects*, 312, 136-141

Zhang, Y., Gu, H. & Iijima, S. (1998). Production of SWNTs in presence of nitrogen atmosphere, *Applied Physics Letters*. 73, 3827

Zhao, J., Chen, X. & Xie, J.R.H. (2006). Optical properties and photonic devices of doped carbon nanotubes. *Analytica Chimica Acta* 568, 161-170

Zhao, N.H., Zhang, P., Yang, L.C., Fu, L.J., Wang, B. & Wu, Y.P. (2009). Tunable amorphous carbon nanotubes prepared by simple template, *Materials Letters*, 63(22), 1955-1957.

Zhao, N.Q., He, C.N., Du, X.W., Shi, C.S., Li, J.J. & Cui, L. (2006). Amorphous carbon nanotubes fabricated by low-temperature chemical vapor deposition. *Carbon*, 44, 1845-1869

Zhao, T., Liu, Y. & Zhu, J. (2005). Temperature and catalysts effects on the production of amorphous carbon nanotubes by a modified arc discharge, *Carbon*, 43(14), 2907-2912.

Zheng, L.X., O'Connell, M.J., Doorn, S.K., et. al. (2004). Ultralong single-wall carbon nanotubes. *Nature Materials 3, 673-676*

Zhu, J., Wei, S., Yadaz, A. & Guo, Z. 2010. Rheological behaviors and electrical conductivity of epoxy resin nanocomposites suspended with in-situ stabilized carbon nanofibers. *Polymer,* 51:2345-2350.